

We are IntechOpen, the world's leading publisher of Open Access books Built by scientists, for scientists

6,900

Open access books available

186,000

International authors and editors

200M

Downloads

Our authors are among the

154

Countries delivered to

TOP 1%

most cited scientists

12.2%

Contributors from top 500 universities



WEB OF SCIENCE™

Selection of our books indexed in the Book Citation Index
in Web of Science™ Core Collection (BKCI)

Interested in publishing with us?
Contact book.department@intechopen.com

Numbers displayed above are based on latest data collected.
For more information visit www.intechopen.com



Late to Post-Orogenic Brasiliano-Pan-African Volcano-Sedimentary Basins in the Dom Feliciano Belt, Southernmost Brazil

Delia del Pilar Montecinos de Almeida¹,
Farid Chemale Jr.² and Adriane Machado³

¹*Universidade Federal do Pampa (UNIPAMPA)*

²*Universidade de Brasília (UnB)*

³*Centro de Geofísica da Universidade de Coimbra (CGUC)*

^{1,2}*Brazil*

³*Portugal*

1. Introduction

The Neoproterozoic/Early Paleozoic transition in Southern Brazil was marked by the last phases of the Brasiliano/Pan-African Cycle (900-540 Ma, Chemale Jr., 2000). These include the development of a trough series related to the different Brasiliano Orogenesis phases, which occupied one preferential subsiding locus called Camaquã Basin (Paim et al., 2000). This basin is located in the Sul-Riograndense Shield (Rio Grande do Sul State, Southernmost Brazil, Fig. 2). The Camaquã Basin is a northeast-southwest elongated basin positioned along the Dom Feliciano Belt limits (to the east) and the Rio de la Plata Craton (to the west). The basin was filled with a thick (ca. 11 km) sedimentary rocks package deposited in marine (at the base) and continental (at the top) environments, and a volcanic rocks series interbedded with the sediments. At least three volcanic events were recognized and related to the Hilário and Acampamento Velho Formations, and Rodeio Velho Member, from the base to the top (Fig. 1).

Paim et al. (2000) divided the Camaquã Basin into four sub-basins named as Taquarembó-Ramada, Santa Bárbara, Guaritas and Piquiri-Arroio Boici, from West to East (Fig.1). Each sub-basin showed a partial independent evolution, and consequently, the stratigraphic framework shows some differences in a regional scale. Santa Bárbara and Guaritas sub-basins show the most complete stratigraphic section. Paim et al. (2000) defined five major depositional cycles from tectonic origin separated by unconformities. Every cycle corresponds to a unit ranking as group or allogroup. From the base to the top, there are the following groups: Maricá, Bom Jardim, Cerro do Bugio, Santa Bárbara and Guaritas (Table 1).

This chapter aims to make the characterization of the two last volcanic events associated to the filling of Camaquã Basin, named as Acampamento Velho Formation and Rodeio Velho Member in Rio Grande do Sul, Brazil. The book chapter will be composed of an introduction. After the introduction, it will be presented the Camaquã Basin stratigraphy and evolution compilation, aiming to introduce the reader to the volcanic events

characterization. We also present a compilation of geochronological data from different units that fill the Camaquã Basin as well as the U-Pb ages obtained by us for Rodeio Velho, Acampamento Velho, Hilário volcanic events and Maricá Formation (in sandstone). The mineralogy, petrography, geochemistry (major, trace and rare-earth elements) and isotope data will be presented to the Acampamento Velho Formation and Rodeio Velho Member.

2. Camaquã Basin stratigraphy and evolution

2.1 Camaquã Basin tectonic evolution

Camaquã Basin is related to a system of late to post tectonic basins associated with the Pan African Brasileiro Orogeny. In the late stages of the Brasileiro Orogenic phase (700-500 Ma); the depressions formed received sediments from the erosion of mountain areas still undergoing active uplifting (Almeida, 1969). Almeida (1969) and Almeida et al. (1976, 1981) subdivided the deposits of these basins in lower and upper molasse. The lower molasse sequence is folded and associated with volcanism, whereas the upper molasse is horizontal or tilted, associated with magmatism. Almeida (1969) attributed the configuration of these molassic basins to reactivation processes of the deep faults. Wernick et al. (1978) related their genesis to strike-slip movements. Other authors suggested that these basins were formed in depressions generated by synforms developed during the Brasileiro Orogenic event (Fragoso Cesar et al., 1982). According to Fragoso Cesar et al. (2000), Camaquã Basin is a Neoproterozoic - Early Cambrian extensional, post orogenic and pre-cratonic rift system. Paim et al. (2000) interpreted this basin as a depositional locus in which different basins succeeded one another, each of them with their own lithological record and distinctive subsidence mechanisms. These authors admitted a connection between the evolution of the Camaquã Basin and the final tectonic stages of the Pan-African Brasileiro Orogeny in Southern Brazil. They also mentioned the continentalization that took place in later stages, even as the clear tectonic control in the stratigraphic arrangement of the allogroups, thus suggesting, a residual tendency of crustal uplifting during the final stages of the Pan-African-Brasileiro Orogeny.

According to Chemale Jr. (2000), the subsidence of the Neoproterozoic Rio de la Plata Plate beneath the Kalahari Plate led to the formation of oceanic crust around 700 Ma. Rifting of the Kalahari Plate resulted in the formation of the Encantadas Microcontinent (or microplate), with a converging margin to the west and a diverging one to the east. The proto-ocean Adamastor was formed between 700 and 650 Ma. Between 650 and 540 Ma, it started to subside to the west, beneath the Encantadas Microplate. The calc-alkaline orogenic magmatism occurred between 630-610 Ma, and the later to post orogenic around 600-540 Ma (Phase III). The closing of this proto-ocean was achieved initially through transgression, changing to transcurrence in the final stages. The last deformational pulses related to the Brasileiro Event (Dom Feliciano) took place around 540 Ma. The deposition in the Camaquã Basin formed in the retroarc region, initially preceded through the accumulation of sedimentary sequences and associated to the magmatism at 620 Ma. There is evidence for progressive continentalization and alkaline signatures toward the top of the rock record about 500 Ma, when the final accretion of west Gondwana took place. Thus, these events marked the beginning of the stabilization of Gondwana Supercontinent and the initiation of erosional processes in the Brasileiro mountain ranges. Subsidence of the Paraná Basin occurred from 500 Ma onwards, with the accumulation of basal sediments in a rift

environment. In the Sul-Riograndense Shield, this is probably represented by the Guaritas Group (Fig. 2).

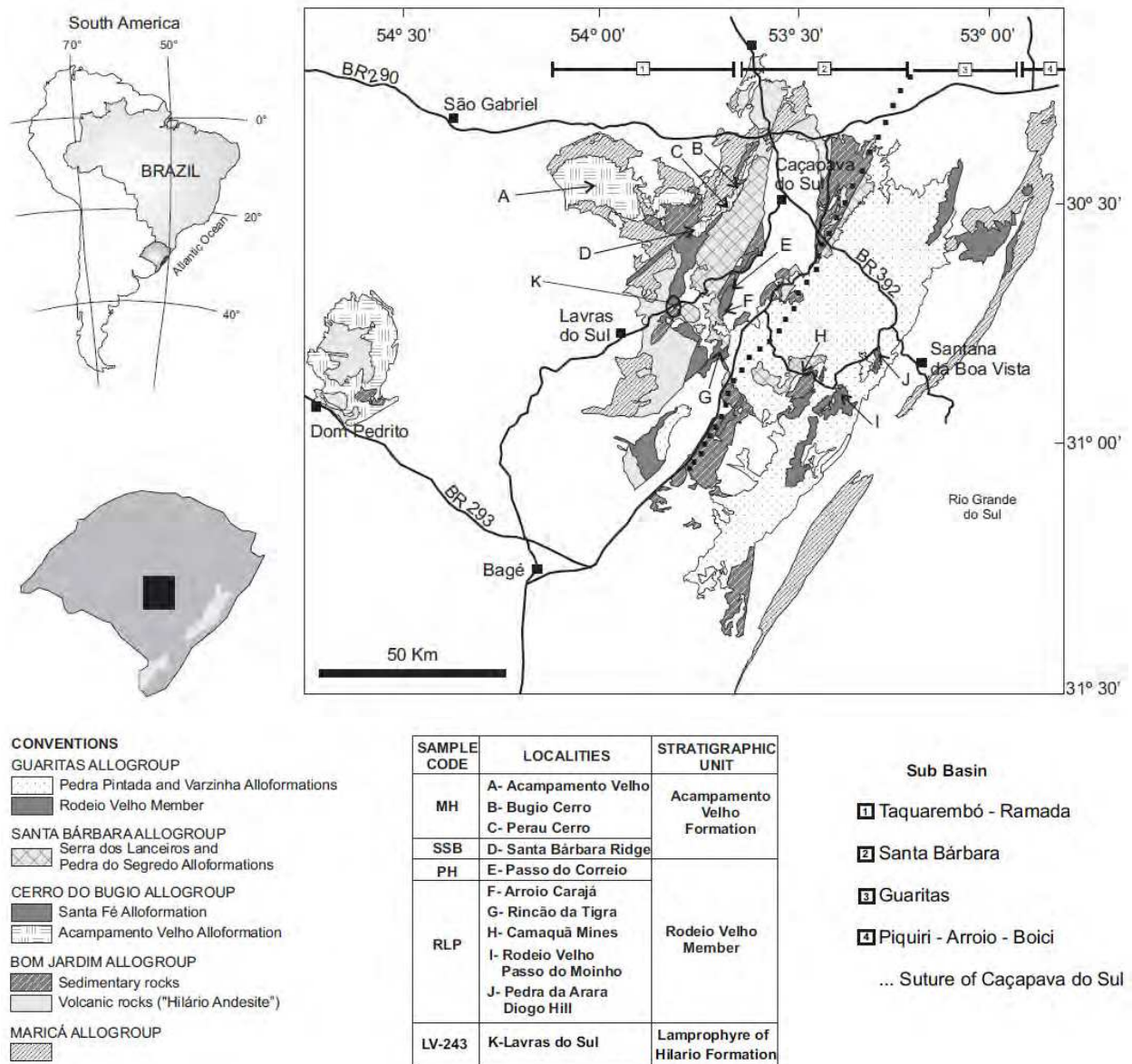


Fig. 1. Geological map showing the main Camaquã Basin stratigraphic units (modified from Paim et al, 2000) and the localization of the main regions.

According to Basei et al. (2000), the magmatic, metamorphic structural and geotectonic features in Southeastern South America recorded the superposition of two Neoproterozoic-Eopaleozoic orogenies: Brasiliano (700-620 Ma) and Rio Doce (620-530 Ma) orogenies. The end of the extensional regime related to the Brasiliano cycle is marked by late magmatism (600±10 Ma), conspicuous in Southern Brazil. The foreland basins, with sedimentation around 560±20 Ma and deformation around 530 Ma, represent the main volcanic-sedimentary record of Rio Doce Orogeny in Southern Brazil. The Camaquã Basin is considered to represent this type of basin. Differently from the current thoughts, Fragoso-Cesar et al. (2001) suggested an intraplate evolution to this basin, detached from the

evolution of the Brasiliano Cycle. These authors related the development of the basin to the reactivation of the Brasiliano structures formed in the Neoproterozoic III to Eocambrian. They stated that the knowledge about the tectonic events and deformation of the sedimentary and volcanic rocks is still incipient, and there are no radiometric ages to position the deformation phases in time. They also ratify the connection between the Guaritas sedimentation and volcanics rocks from Rodeio Velho, and Paraná Basin. These units would be related to the development of SW-NE rifts during the initial stages of the evolution from Paraná Basin.

	Robertson (1966)	Ribeiro <i>et al.</i> (1966)	Santos <i>et al.</i> (1978)	Leites <i>et al.</i> (1990)	Beckel (1990)	Paim <i>et al.</i> (2000)
Camaquã Group	Coxilha Cong.	Coxilha Cong.	X	Volcano Sedimentary Sequence IV	(6) Santa Bárbara Formation	Guaritas
	Guaritas Formation	Guaritas Formation				Pedra Pintada
	(1) Santa Bárbara Formation	(2) Santa Bárbara Formation				Santa Bárbara
	Ramada Rhyolite	Crespos Form. (3)	Acampamento Velho Formation	Volcano-genic Sequence III	(3) Crespos Formation	Cerro do Bugio
	Hilário Andesite	Arroio dos Nobres Form. (4)	(5) Cerros dos Martins Formation	Volcano Sedimentary Sequence II		Bom Jardim
	Maricá Formation	Maricá Formation	Pessegueiro Formation	Volcano Sedimentary Sequence I	Maricá Formation	Maricá
					(7) Arroio dos Nobres Form.	

Modified after Paim *et al.* 2000.

Legend

—	Unconformity type not especificied
—	Erosive unconformity
—	Angular unconformity
---	Elongation surface
—	Transitional contact
←	Stratigraphic limits usually used
▲	Bimodal volcanics
▲	Basic to intermediary volcanics
△	Acid volcanics

Notes: Includes, at the base, the Martins Andesite Member. At the base, contains Rodeio Velho Member. Composed by lower (Hilário) and upper (Acampamento Velho) members. Comprise the Vargas and Mangueirão members. Made up by Hilário and Arroio dos Nobres members. Constituted by the Rodeio Velho, at the base, Lanceiros, Varzinha and Guaritas members. Composed by Passo dos Bravos at the base, Vargas and Mangueirão members.

Table 1. Stratigraphic concepts for Camaquã Basin.

Silva *et al.* (2005) as cited in Borba *et al.* (2008) focusing on the tectonic evolution of Brasiliano events in the Mantiqueira Province (South and Central Brazil and Uruguay, Fig. 3) revealed three main orogenic systems: (a) Brasiliano I, with juvenile island-arc accretion and collisional climaxes at ca. 790 Ma (Embu Domain, Southeastern Brazil) and 730-700Ma (São Gabriel Orogeny, Southern Brazil); (b) Brasiliano II, with dominance of crustal

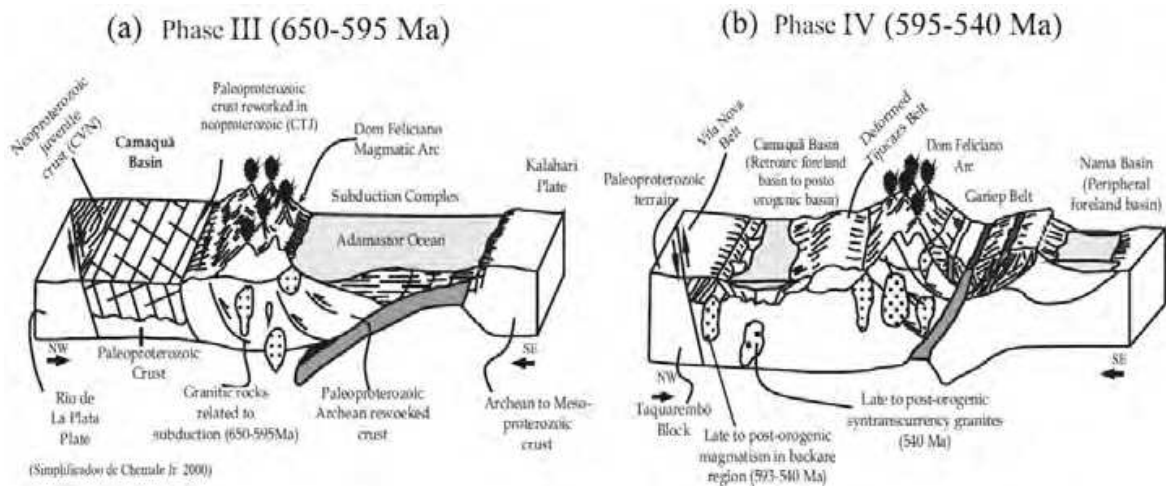


Fig. 2. Evolution model of the Sul-Riograndense Shield at the end of Neoproterozoic (Chemale Jr., 2000).

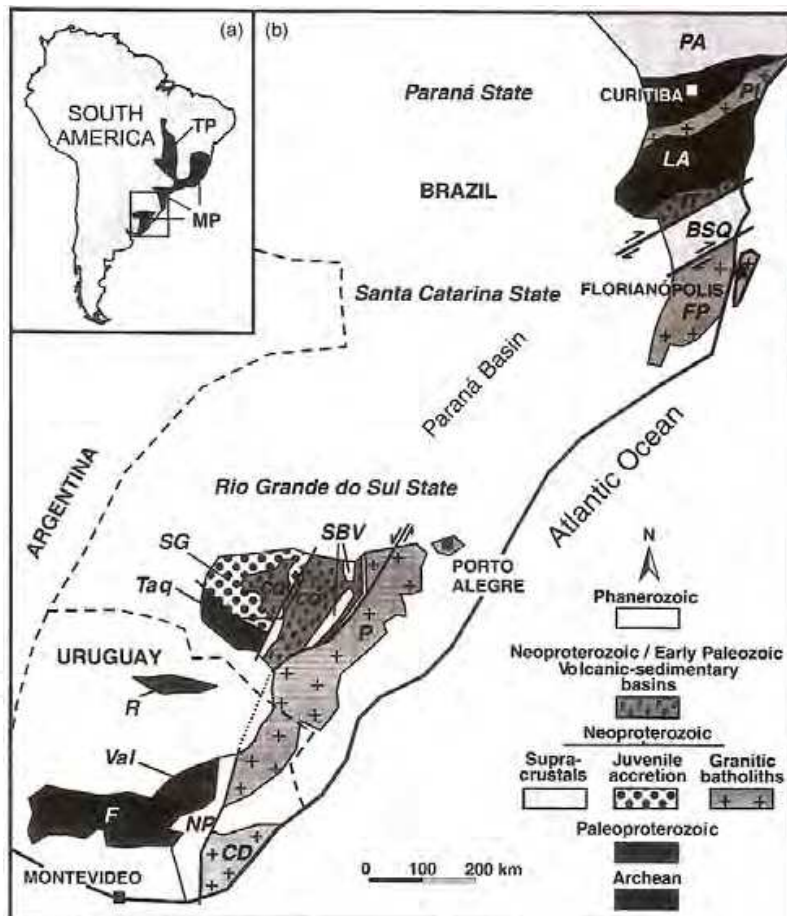


Fig. 3. Schematic geological map of the Southern portion of the Mantiqueira Province (b) located in Eastern South America (a); key to the terrains/blocks/belts/orogenies names: F= Florida; NP= Nico Perez; CD = Cuchilla Dionísio; Val= Valentines; R= Rivera; Taq=Taquarembó; SG= São Gabriel; SBV= Santana da Boa Vista; P= Pelotas; FP= Florianópolis; BSQ = Brusque; LA= Luiz Alves; PI = Piên; PA= Paranapiacaba; unmetamorphosed volcanic-sedimentary successions are named as Camaquã (CQ) and Itajaí (IT) (Silva et al., 2005, in Borba et al., 2008).

recycling and collisional climaxes at 640-620Ma (Dom Feliciano Orogeny, Southern Brazil and Uruguay) and 600Ma (Paranapiacaba and Rio Piên Orogenies, Southeastern Brazil); and (c) Brasiliano III, also characterized by crustal recycling and collisional climaxes between 590-560Ma (Araçuaí Orogeny) and 520-500Ma (Búzios Orogeny), recorded mainly in Eastern Brazil. Foreland basins associated with the Brasiliano II orogenic system comprise portions of volcanic-sedimentary (metamorphosed or unmetamorphosed) successions along the 3000 km of length from Mantiqueira Province.

2.2 Stratigraphy

Thick accumulations of sedimentary and volcanogenic rocks are present in the Camaquã and Itajaí basins of Southern Brazil, considered to be the “molassic fore deep of the Dom Feliciano Belt” by Fragoso-Cesar et al. (1984). These sedimentary successions evolved from marine to alluvial-aeolian continental strata and have been considered to be foreland basins along with their African counterparts (Gresse et al., 1996). Recent research considers the Camaquã Basin to be a series of the different basins (foreland, strike-slip and rift) with a shared locus of subsidence (Paim et al., 2000). In terms of stratigraphy, five major unconformity bounded units (Allogroups) have been defined by Paim et al. (2000): the Maricá, Bom Jardim, Cerro do Bugio, Santa Bárbara and Guaritas Allogroups (Table 1). They reflect the progressive continentalization of the Camaquã Basin. These units can be interpreted as the evolution of temporally and spatially restricted basins, evolved from a foreland retroarc into a rift (or hemigraben) tectonic setting. In this more recent interpretation, only the Maricá Formation was deposited in a foreland basin.

The Maricá Formation was defined by Leinz et al. (1941) as a basal unit of Camaquã Basin. This Formation is a ± 2500 m-thick sedimentary package with coastal deposits, including fluvial to shallow marine sediments with scarce volcanic contribution (Leites et al., 1990). The nature of the basal contact of this unit with the Neoproterozoic juvenile terrain is difficult to be defined, either an unconformity or a thrust plane, due to low relief, thick soil profiles and vegetation, and widespread younger intrusive bodies. According to Borba (2004), the Maricá formation can be divided into three major packages: the lower, intermediate and upper successions. The lower succession comprises conglomeratic and coarse-grained sandstones with very well rounded granite-gneiss pebbles and cobbles either marking the stratification planes or dispersed through the beds. The intermediate succession is made up of indurated siltstones and shales, either massive or showing plane-parallel lamination, wave and climbing ripples, and lenticular lamination, as well as hummocky sandstones, suggesting a marine origin. The upper succession is very similar to the lower one, with the sandstones featuring large-scale troughcross and low-angle stratifications. Well-rounded granite-gneiss and rare volcanic, rhyolitic pebbles and cobbles are also present within the sandstone beds. The lower and upper successions correspond to braided fluvial deposits, while the intermediate package is related to a shallow marine depositional environment. The strata of the Maricá Formation were strongly affected by subsequent events of volcanism, intrusion, sedimentation and uplift. Volcanic rocks of the Bom Jardim Group (andesite Hilário) and the Acampamento Velho Formation (rhyolitic flow, rhyolitic pyroclastic rocks and basic flow) caused metamorphism contact in the Maricá Formation. The unit is unconformably overlain by the alluvial, fluvial and eolian deposits of the Santa Bárbara and Guaritas formations (Borba & Mizusaki, 2003). A syn-depositional volcanic event (Santos et al., 1978) has been recognized in the rock record of the Maricá Formation, evidenced by the occurrence of

volcanogenic beds interlayered with sedimentary rocks of the lower succession. Circular structures resembling degassing pipes also suggest the activity of volcanic hot springs (Borba et al., 2004). According to Paim et al (2000), in terms of deformation at the Taquarembó/Ramada sub-basin, are recognized reverse rupture faults and weak folds, while the Piquiri/Boici sub-basin is dominated by structures associated to the transcurrent processes in rupture to ductile-rupture structural level.

The Bom Jardim Group (Paim et al, 2000), is a volcano-sedimentary sequence that shows a lithostratigraphic complexity in its area-type and similarity lithological of some its units with others from Camaquã Supergroup units (Table 1). Bom Jardim Group, in its area-type (Janikian et al., 2003), shows approximately 4,000 thicknesses and constituted of andesitic volcanic rocks, pyroclastic rocks (lapilli tuffs, lithic tuffs and thick vitreous tuffs - Hilário Formation) and sedimentary rocks. These rocks were generated in an active tectonic lacustrine basin. Robertson (1966) made the first attempted correlation among the volcano-sedimentary units from Bom Jardim area and others expositions from Camaquã Supergroup. Ribeiro et al. (1966) and Tessari & Picada (1966) correlated the outcropping units from Bom Jardim and Vale Piquiri (Piquiri Sub-basin) areas, covering the Arroio dos Nobres Formation.

The Hilário term was first used by Robertson (1966) to designate a variety of rock types composed of mainly andesitic to dacitic composition (flows, tuffs, volcanic conglomerates, mudflows, dykes and intrusive mafic rocks). Ribeiro et al. (1966) formalized this unit as a member of Crespos Formation - Bom Jardim Group. Santos et al. (1978) used the Hilário term to refer a member of Cerro dos Martins Formation, while Horbach et al. (1986) upgraded these rocks to the formation level. Several studies have been carried out Hilário Formation rocks. Nardi & Lima (1985), Porcher et al. (1995), Lima & Nardi (1998) works are especially relevant. Thus, Lima & Nardi (1998) defined the Lavras do Sul Shoshonitic Association, which comprises a wide compositional range of intrusive and extrusive basic to acid rocks. The extrusive rock includes the Hilário Formation and the spessartitic lamprophyres. In the Bom Jardim Group, the volcanic rocks are mostly in the lower stratigraphic levels, as lava flows or small shallow intrusion.

In the Santa Bárbara Sub-basin (Paim et al., 2000) toward the Guaritas Sub-basin, the volcanic rocks of this group are replaced gradational by alluvial conglomerates rich in volcanic clasts from basic to intermediate composition, and more distally, by sandy and silty related to the bottom flows (turbidites), which are bounded to underwater deltaic systems. Next to the high topographic that today subdivides the Santa Bárbara and Guaritas sub-basins (e.g. Alto Caçapava), is common the occurrence of the erratic conglomerates containing local derivation clasts (shales and marble), indicating that the partitioning of the Camaquã Basin in several sub-basins occurred prior to the deposition of this unit.

Cerro do Bugio Allogroup (or Group) is composed of volcanic rocks at the base (Acampamento Velho Alloformation or Formation) and alluvial conglomerate deposits from Santa Fé Alloformation (ou Formation). According Paim (2000), Cerro do Bugio is limited by two angular unconformity that delineate its contact with the lower (Bom Jardim Allogroup) and upper (Santa Bárbara Allogroup) units. Cerro do Bugio Unit shows approximately 500 m thick and is composed of, from the base to the top, Acampamento Velho (volcanic) and Santa Fé (alluvial conglomerates, and secondarily, by sand-pelitic rhythmites and pelites), separated by an erosive unconformity. The Santa Fé Formation consists mainly of alluvial conglomerates rich in volcanic and plutonic clasts of the acid composition, which vary vertically to sand-pelitic rhythmites. These lithologies represent the alluvial systems

interlaced, considering the transversal (deltaic fans, conglomeratic with paleocurrents for SE) and longitudinal (fans of the interlaced plain) characters. This allogroup was affected by dip-slip and transcurrent faults generated in crustal to ductile-ruptile level. Considering the field work observations, the Acampamento Velho Formation volcanic rocks are often interdigitated with rocks from Santa Fé Formation, suggesting the contemporaneity between both units.

Acampamento Velho Formation (*sensu* Cordani et al., 1974) is the basal unit of the Santa Bárbara Group and crops out mainly in the Santa Bárbara and Taquarembó-Ramada sub-basins. The basal contact of the Acampamento Velho Formation is unconformable with the Maricá and Bom Jardim Groups. According to Almeida et al. (2002), in the Cerro do Bugio, Perau and Serra de Santa Bárbara (Fig. 1), the volcanic rocks (basaltic and rhyolitic compositions) upper contact is a disconformity by the alluvial conglomerates, and locally, by deltaic-lacustrine sandstones and mudstones from Santa Fé Formation.

The Santa Bárbara Group, defined by Robertson (1966), Ribeiro et al., (1966) and Ribeiro & Fantinel (1978) as Santa Bárbara Formation, comprises red-colored, sandstones and siltstones, and includes the Acampamento Velho and Santa Bárbara formations. It was named as Santa Bárbara Allogroup by Paim et al. (2000). This group is composed of Acampamento Velho, Santa Fé, Lanceiros and Segredo Formations, from the base to the top (Table 1). According to the same authors, the Lanceiros Formation is related to the progradation of an interlaced and sandy deltaic system of the longitudinal character, and the Pedra do Segredo Formation can be bounded to the progradation of an interlaced and sandy-conglomeratic of transversal nature. Borba & Mizusaki (2003) organized the Santa Bárbara Formation rocks in three depositional sequences named as, from the base to the top: Sequence I, Sequence II and Sequence III. The two basal sequences (I and II) represent a coherent depositional pattern, with axial fluvial and deltaic fan systems, which deposit North-Eastward with lateral contribution from alluvial fans. Such coarse deposits are composed mainly of metamorphic clasts derived from Alto Caçapava and Eastern steep Santa Bárbara Basin. The Sequence I shows a dip ranging from 32° to 40° NE in the Northern outcrops and 10° to 16° NE in the South, and the Sequence II from 28° to 30° SE. The Sequence III lies unconformable over basal subunits and reflects the axial system inversion, in that the gravel bed deposits paleocurrents systematically point South/South-Westward. The alluvial fan deposits of the Sequence III also suggest a tectonic rearrangement basin, with partial erosion from basal sequences, and the presence of granitic composition fragments, which reflects the deeper denudation stage of the Alto Caçapava and possibly a significant hiatus at the Sequence III base. The third dip sequence is between 23° to 26° ENE. The Acampamento Velho Formation is not included in the Santa Bárbara Formation (Borba & Misuzaki, 2003).

The Guaritas was defined by Goñi et al. (1962), Ribeiro et al (1966), Robertson (1966) and Ribeiro & Fantinel (1978) and is lithologically similar to the Santa Bárbara Group. This unit represents the last great depositional event preserved in Camaquã Basin and is above unconformity of the previous units. It was denominated Guaritas Allogroup (Paim et al., 2000) and is composed of two alloformations or formations, from the base to the top: Pedra Pintada and Varzinha (Table 1). These units are bounded by an erosive unconformity. The Guaritas Group shows around 800 m thick and represents the last depositional episode preserved within of the Camaquã Basin. The Pedra Pintada Formation is temporal and spatially related to the volcanic rocks named as Rodeio Velho Member. It was originated in a desert environment with crescent eolian dunes, in an inter-dune area that describes

interchange of dry and wet periods, and basal level plains that comprehend dry seasons during wetter periods (Paim et al., 2000). It is characterized by fine to medium sandstone, well selected, with large to very-large size cross-stratification and bulk sandstones, and occurs secondarily mudstones and fine to medium sandstones with crossed lamination by stream and waves (Paim et al., 2000). The rocks that belong to this formation are found in the Santa Bárbara and Guaritas sub-basins (Fig. 1). The Varzinha Alloformation is composed of sedimentary faces that represent a braided fluvial system at the West Guaritas Sub-basin portion, and a fanlike alluvial system at the East portion. According to Paim et al. (2000), analyzing the paleocurrents data of this unit, we detect a lateral association of two different alluvial systems: (1) interlaced fluvial system, West side of the Guaritas sub-basin; (2) alluvial fans represented by, at the least two lobes, at the East side of the Guaritas Sub-basin (Paim, 1995). The Varzinha Alloformation upper levels correspond to the several sets of the progradacional parasequences from deltaic source. They were developed de within a shallow lacustrine basin. The deltaic deposits were associated to a tributary deltaic fan system (lateral contribution) at the East edge of the Guaritas Sub-basin, and an interlaced plain delta system (longitudinal contribution), which shows progradation to the SW, at the East edge of the Guaritas Sub-basin. Almeida et al. (2003a) described the Varzinha Alloformation as a covering of the area that present four cones (Rodeio Velho Member) at Santa Bárbara Sub-basin (see item 5). According to Takehara et al (2010), the Guaritas Group, which comprises the aeolian and alluvial plain as well as fan deposits, is covering the Santa Bárbara Group rocks in Santa Bárbara Sub-Basin.

Rodeio Velho Member (*sensu* Ribeiro et al., 1966) has been described as being at least three vesicular andesite flows, with thickness estimated at 100 m and no evidence of explosive activity. Silva Filho (1996) showed the intrusive character of the magmatism, rejecting to form ideas of an exclusively volcanic event. Fragoso Cesar et al. (2000) named these rocks as Rodeio Velho Intrusive Suite, which is represented by tabular intrusions within the sub-horizontal continental deposits of the Guaritas Group. Almeida et al. (2000, 2003a) stated that the before mentioned event has a basaltic andesitic composition with alkaline affinity and the rocks cropped out as lava flows, pyroclastic deposits and shallow intrusions.

3. Geochronological data

We present a synthesis of geochronological ages for the different lithologies mentioned in the literature as well as new U-Pb ages obtained by us in samples from Maricá Formation (sandstone), Hilário Formation (lamprophyre), Acampamento Velho base (andesitic basalt) and Rodeio Velho Member (alkaline basalt).

3.1 Analytical procedures used for new U-Pb ages

All zircons were mounted in epoxy with 2.5 cm diameter and polished until the zircons were just revealed. Images of zircons were obtained using the optical microscope (Leica MZ 12₅) and back-scatter electron microscope (Jeol JSM 5800). Zircon grains were dated with laser ablation microprobe (New Wave UP213) coupled to a MC-ICP-MS (Neptune) at the Isotope Geology Laboratory from UFRGS. Isotope data were acquired using static mode with spot size of 25 and 40 μm . Laser-induced elemental fractional and instrumental mass discrimination were corrected by the reference zircon (GJ-1) (Simon et al., 2004), following the measurement of two GJ-1 analyses to every ten sample zircon spots. The external error is calculated after propagation error of the GJ-1 mean and the individual sample zircon (or spot).

Laser operating conditos	
<p>Laser type New Wave UP213</p> <ul style="list-style-type: none"> • Laser output power 6 J/cm² • Shot repetition rate 10 Hz • Laser spot 25 and 40 μm 	<p>MC-ICP-MS Neptune</p> <ul style="list-style-type: none"> • Cup configuration: Faradays ²⁰⁶Pb, ²⁰⁸Pb, ²³²Th, ²³⁸U MIC's ²⁰²Hg, ²⁰⁴Hg + ²⁰⁴Pb, ²⁰⁷Pb • Gas input: Coolant flow (Ar) 15 l/min Auxiliary flow (Ar) 0.8 l/min Carrier flow 0.75 l/min (Ar) + 0.45 l/min (He) Acquisition 50 cycles of 1.048 s

The common ²⁰⁴Pb, after Hg correction based on ²⁰²Hg simultaneously measured, is insignificant in most situations. For instance, typical signal intensity due to ²⁰⁴Hg during a laser ablation on standard Zircon is 600-1000 cps range, while the calculated count rate for ²⁰⁴Pb is less than statistical error of ca. 25-33 cps. We assume that the ²⁰⁴Pb values obtained from zircons have common Pb composition, assuming concordant age of ²⁰⁶Pb/²³⁸Pb and ²⁰⁷Pb/²⁰⁶Pb (as estimated age). In this case, we estimate the radiogenic composition of ²⁰⁶Pb and Pb²⁰⁷ using the equation as fraction of non radiogenic ²⁰⁶Pb (Williams, 1998):

$$f_{206} = [^{206}\text{Pb}/^{204}\text{Pb}]_c / [^{206}\text{Pb}/^{204}\text{Pb}]_s$$

$$f_{207} = [^{207}\text{Pb}/^{204}\text{Pb}]_c / [^{207}/^{204}]_s$$

For common lead isotope composition, we assumed an isotope composition evolution proposed by Stacey and Kramers (1975), which is required to attribute an initial estimated age.

3.2 Geochronological data for different units

Soliani Jr. et al. (1984) presented a synthesis of all the radio-chronological determinations obtained for the crystalline and sedimentary rocks from Sul-Riograndense Shield meridional portion, including part of the Santa Catarina, the whole Rio Grande do Sul and Uruguay, thus preserving the Cordani et al (1974) and Teixeira (1982) proposal, which says that the West Sul-Riograndense Shield region would have had an Transamazonian evolution, and the meridional portion would have been generated in the Brasiliano Cycle. Sartori & Kawashita (1985) obtained the age of 550 Ma for Caçapava do Sul Granitic Batholith using 21 Rb-Sr isotope analyses on total-rock.

According to Soliani et al. (2000), the first work of the regional integration and geochronological synthesis was made by Cordani et al (1974). The authors relate the K-Ar and Rb-Sr radiometric data to the Eopaleozoic rocks, which fill the Camaquã Basin. Thus, the Rb-Sr data of the Eastern portion with syntectonic characteristics (granites and migmatites) and post-tectonic (isotropic granites) show respectively, values from 650-600 Ma. K-Ar ages of the same region are in the same coherent interval characteristics of the Brasiliano Cycle. For the Midwest region of the shield were found radiometric values that suggest an older age, although a significant data percentage show Brasiliano ages for the granitic massive such as the Caçapava do Sul and Lavras do Sul among others. In the same way was confirmed that the volcanic rocks (Hilário and Acampamento Velho formations) were generated at the end of the Pre-Cambrian or at the beginning of the Phanerozoic, exactly as has been commented by Minioli & Kawashite (1971).

Leite et al. (1995, 1998) and Leite (1997) mentioned for the Rio Grande do Sul region, the first U-Pb data obtained in zircons using the sensitive high mass-resolution ion microprobe

method, being the isotope data for the Caçapava do Sul granitic massives of the 561 ± 6 Ma and 541 ± 11 Ma. The first age is considered as corresponding to the igneous protolith that generated the Caçapava Granite. The second age is related to a magmatic event that generated the granite. Remus et al. (1996, 1997) used sensitive high mass-resolution ion microprobe method to obtain the U-Pb ages in zircons for the Lavras do Sul Granite core and edge, respectively: 592 ± 5 and 580 ± 5 Ma. The age of 565 ± 14 Ma was obtained for the Caçapava do Sul Granite.

3.2.1 Maricá Formation

The first geochronological investigation in Maricá Formation was performed by Borba et al. (2008). These authors made analysis of zircons from pyroclastic cobbles, which yielded an age of 630.2 ± 3.4 Ma (2σ), interpreted as the age of syn-sedimentary volcanism, and thus of the deposition itself. This result indicates, according to Borba et al. (2008), that Maricá Formation was deposited during the main collisional phase (640–620 Ma) of the Brasiliano II Orogenic system from Silva classification (2005). Paim et al (2000) suggested a depositional age between 620 and 600 Ma in a foreland basin.

Spot number	Isotope ratios ^{2,3}						Age (Ma)						²³² Th/ ²³⁸ U ¹	% of Conc ⁵	Apparent age		
	²⁰⁷ Pb/ ²³⁵ U		²⁰⁶ Pb/ ²³⁸ U		²⁰⁷ Pb/ ²⁰⁶ Pb	²⁰⁶ Pb/ ²³⁸ U		²⁰⁷ Pb/ ²³⁵ U		²⁰⁷ Pb/ ²⁰⁶ Pb	±	±			±	±	
	1s	1s	1s	1s	Rho ⁴	1s	±	±	±	±							
156-A-I-01	0,88525	3,2	0,1064	2,3	0,73	0,0604	2,2	652	15	644	20	616	13	1,18	106	616	13
156-A-I-02	0,79543	6,5	0,0965	4,8	0,74	0,0598	4,3	594	28	594	38	596	26	0,67	100	596	26
156-A-I-07	0,81604	2,4	0,0988	1,4	0,59	0,0599	2	607	9	606	15	600	12	1,49	101	600	12
156-A-I-10	0,85889	2,7	0,1028	1,5	0,55	0,0606	2,2	631	9	630	17	626	14	1,08	101	626	14
156-A-I-11	0,78707	3,7	0,0949	2,4	0,65	0,0601	2,8	585	14	590	22	608	17	1,02	96	608	17
156-A-I-14	0,76104	4,1	0,0904	3,9	0,96	0,0611	1,1	558	22	575	23	642	7	0,11	87	642	7
156-A-I-25	0,77688	3,4	0,0925	2,3	0,69	0,0609	2,4	570	13	584	20	636	16	0,60	90	636	16
156-A-I-37	0,84301	2,8	0,1007	1,6	0,56	0,0607	2,3	619	10	621	17	629	15	0,86	98	629	15
156-A-I-09	4,67403	2,02	0,31130	0,74	0,37	0,1089	1,9	1747	25	1763	42	1781	34	0,61	98	1781	34
156-A-I-03	5,9604	2,5	0,3495	2,2	0,88	0,1237	1,2	1932	43	1970	50	2010	24	0,38	96	2010	24
156-A-I-18	6,07717	2,5	0,3555	1,9	0,74	0,124	1,7	1961	37	1987	50	2014	34	1,54	97	2014	34
156-A-I-19	6,47889	1,4	0,3709	1,1	0,75	0,1267	0,9	2033	22	2043	29	2053	19	0,08	99	2053	19
156-A-I-28	10,3139	2,5	0,4624	1,7	0,71	0,1618	1,7	2450	42	2463	60	2474	43	0,90	99	2474	43
156-A-I-33	9,85995	1,5	0,4457	1,1	0,72	0,1604	1	2376	26	2422	36	2460	25	0,32	97	2460	25
156-A-I-36	10,2057	2,6	0,4624	1	0,37	0,1601	2,4	2450	24	2454	63	2457	59	0,53	100	2457	59
156-A-I-13	9,68137	1,4	0,4187	0,9	0,62	0,1677	1,1	2255	19	2405	33	2535	27	0,42	89	2535	37
156-A-I-06	11,4312	1,9	0,4747	1,5	0,77	0,1747	1,2	2504	37	2559	49	2603	32	0,73	96	2603	32
156-A-I-23	11,371	2,3	0,4715	0,9	0,4	0,1749	2,1	2490	23	2554	58	2605	54	0,43	96	2605	54
156-A-I-27	11,4641	2,6	0,4738	1,9	0,71	0,1755	1,9	2500	47	2562	68	2611	49	0,73	96	2610	49

Table 2. U/Pb zircon data of the sandstone sample (CK-239D) for Maricá Formation obtained by in situ LAM-ICPMS-MC.

One sandstone sample (CK-239-D) used in the U-Pb analysis was collected at North of the Estância 3 Estradas (UTM 771863- 6576404) in Coxilha do Tabuleiro Sheet (1:50.000). Twenty zircon crystals from sample CK-239-D were dated. Based on the dating results, we detected the presence of follow age set: 2606 Ma (4 zircons), 2473 Ma (3 zircons), 2050 Ma (3 zircons) and 1790 Ma (one zircon - Table 2, Fig. 4). The 601 ± 13 Ma age (based on eight zircons - Table 2, Fig. 4 - Early Ediacaran) was considered as the age older from Maricá Formation (Fig. 6). All the zircons that showed older ages were considered xenocrystal zircons. Thus, the magma would have assimilated Neoproterozoic (NA), Paleoproterozoic (Siderian, Rhyacian and Statherian) material during its ascension. The selected zircons that allowed the Maricá age setting (Fig. 5), in general are colorless and dirty, all grains are between $175 \mu\text{m}$ and $344 \mu\text{m}$ in size and show diffuse zonation and subrounded contours. The zircons do not have impurities and inclusions, but show few fractures. In the A-I-02 zircon (Fig. 5) is observed an incomplete concentric fracturing at the edge of the crystal.

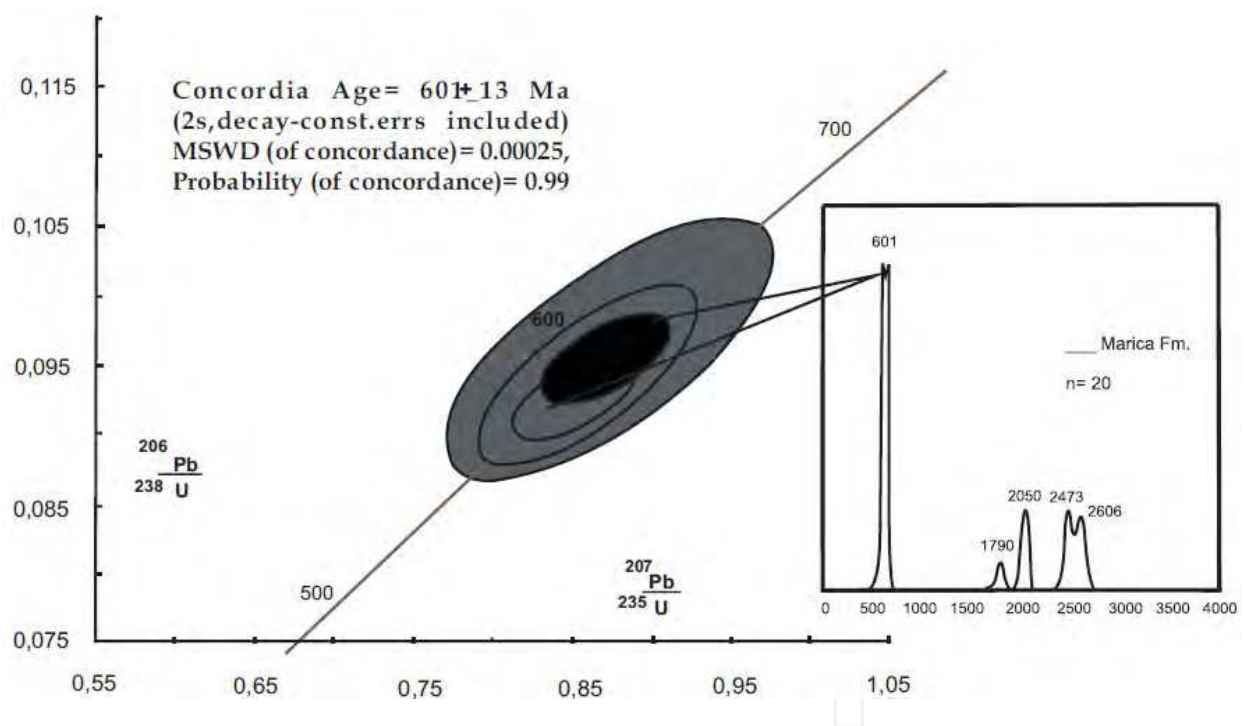


Fig. 4. U-Pb concordia data diagram with tracing considering only the younger zircon ages from Maricá Formation sandstone sample. a: U-Pb age histogram considering all the obtained ages (table 2). We detected the presence of five ages: 2606 Ma, 2473 Ma, 2050 Ma, 1790 Ma and 601 Ma. The 601 Ma age is considered as the older from Maricá Formation.

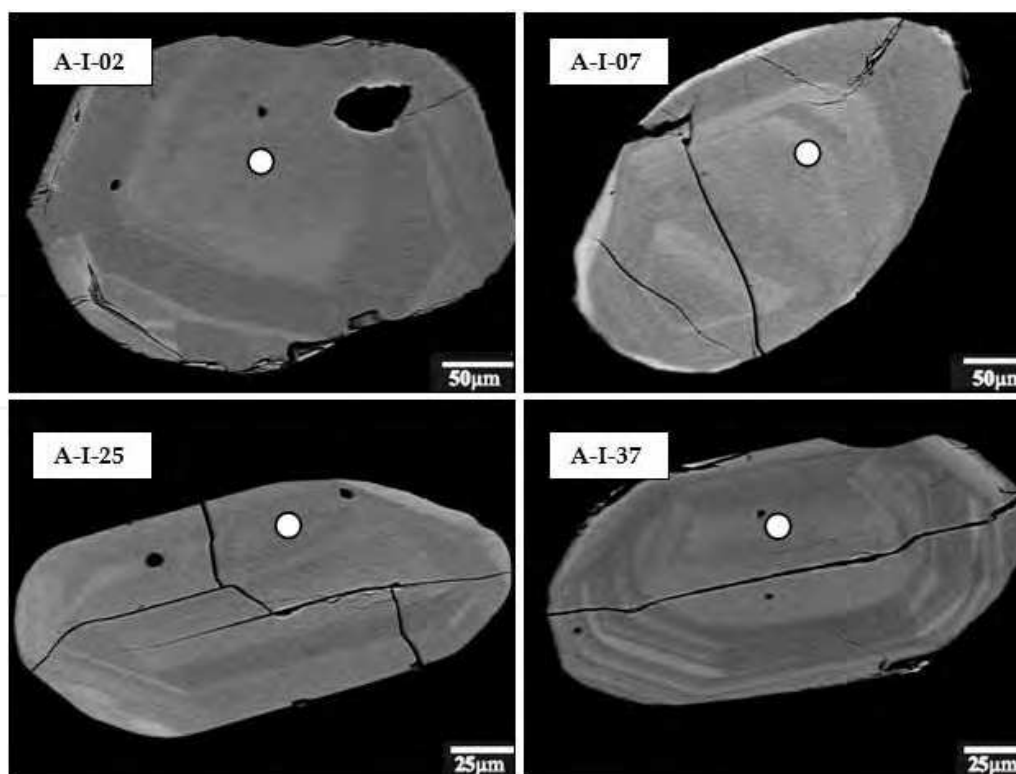


Fig. 5. Zircons microphotographies that defined the 601 ± 13 Ma age from CK239D sample for Maricá Formation sandstone. A-I-02 = sample number, o = spot showing the place where the analyses were obtained in each zircon. Data showed in table 2.

3.2.2 Hilário Formation

Ribeiro & Teixeira (1970) mentioned values between 510-535 Ma for Hilário Andesite. These values were obtained through the K-Ar method. Cordani et al. (1974) obtained ages of 510 and 535 Ma using the Rb/Sr method. $^{206}\text{Pb}/^{238}\text{U}$ data (sensitive high mass resolution ion microprobe) were obtained for Hilário Andesite by Remus et al. (1999) and gave an age of 580 Ma. Janikian et al (2008) mentioned ages from 590 to 585 Ma, which are interpreted for us as representative of Hilário Formation extrusion, being U-Pb age of 590 ± 5.7 Ma obtained in the Hilário Andesite as the most representative. The ages obtained by Remus et al. (2000) using the U-Pb (sensitive high mass-resolution ion microprobe) for Lavras Granite (592 ± 5 Ma, 597 ± 5 Ma, 580 ± 7 Ma) and Caçapava do Sul (589 ± 5 Ma) are considered as comagmatic to the Bom Jardim volcanism. Chemale Jr. et al. (2000) reported an age of 592 Ma for Andesite Hilário.

The LV- 243 sample (alkaline basalt) dated using the U-Pb method by us was collected 15 km away from the Lavras do Sul, following by RS 357 road toward Caçapava do Sul (Fig.1). Lima & Nardi (1998) said that the out crop is a dome with size around 0.5 km^2 and a circular shape. It shows a marked columnar disjunction with hexagons of variable diameter, but no exceeding 15 cm diameter. Nine zircon crystals (sample LV- 243) were dated (Table 3). The obtained age of 591.8 ± 3.0 Ma was calculated based on individual zircon ages from Table 3. This age defines the lamprophyre age (Fig. 6), which belong to the Hilário volcanism manifestation. The selected zircons that allowed the lamprophyres ages setting, in general, are colorless and clean, all grains are between $150 \mu\text{m}$ and $333 \mu\text{m}$ in size and the most show very clear zoning. The grains also show prismatic and pyramidal shapes, incomplete and partially serrulated contours and few fractures (Fig. 7).

Spot number	Concordia 1					Age (Ma)						% Disc	f206	
	$^{207}\text{Pb}/^{235}\text{U}$	error	$^{206}\text{Pb}/^{238}\text{U}$	error	Rho 1	$^{206}\text{Pb}/^{238}\text{U}$	error	$^{207}\text{Pb}/^{235}\text{U}$	error	$^{207}\text{Pb}/^{206}\text{Pb}$	error			$^{232}\text{Th}/^{238}\text{U}$
072-B-II-1	0,80351	3,22	0,09732	1,80	0,56	599	11	599	19	599	16	0,34	0	0,0010
072-B-II-2a	0,80971	3,22	0,09779	1,47	0,46	601	9	602	19	605	17	0,53	1	0,0005
072-B-II-2b	0,81989	3,00	0,09891	1,46	0,49	608	9	608	18	608	16	0,33	0	0,0009
072-B-II-3	0,80923	3,56	0,09799	1,58	0,44	603	10	602	21	600	19	0,34	0	0,0012
072-B-II-4	0,78691	3,08	0,09534	1,37	0,45	587	8	589	18	599	17	0,34	2	0,0004
072-B-II-7	0,78269	3,54	0,10586	1,80	0,51	649	12	638	23	602	18	0,41	-8	0,0004
072-B-II-9	0,76140	3,95	0,09280	1,59	0,40	572	9	575	23	586	21	0,41	2	0,0003
072-B-II-16a	0,74234	4,22	0,08980	3,22	0,76	554	18	564	24	602	16	0,45	8	0,0002
072-B-II-16b	0,79361	3,39	0,09618	1,57	0,46	592	9	593	20	598	18	0,34	1	0,0007

Table 3. U/Pb zircon data of the lamprophyre sample (LV-243) for Hilário Formation obtained by in situ LAM-ICPMS-MC.

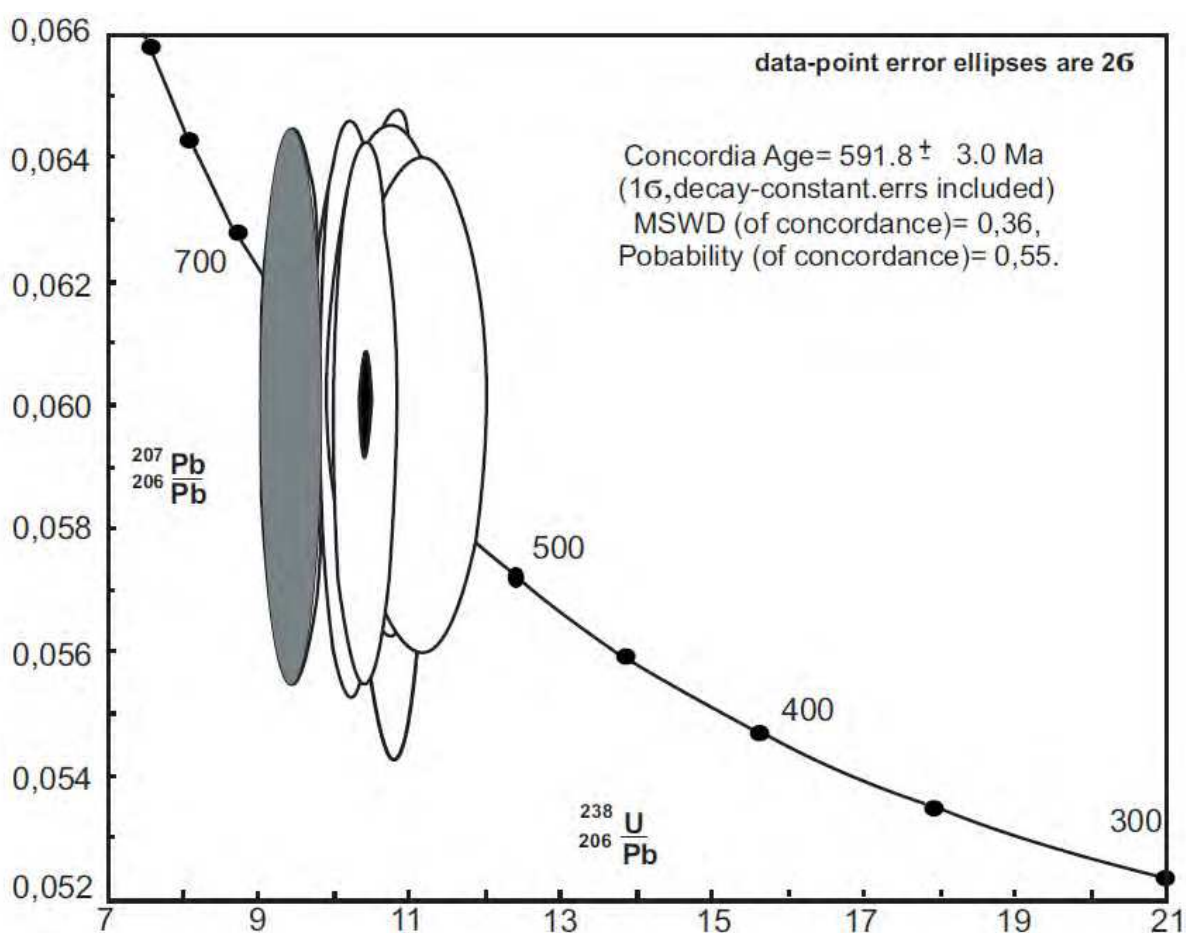


Fig. 6. U-Pb concordia data diagram with tracing considering the zircon ages for Hilário Formation lamprophyre (LV-243 sample). Gray ellipse cores represent the single analysis from zircons of the table 3. Black ellipse represents the concordia age for LV-243 sample, calculated from single zircon ages of the table 3.

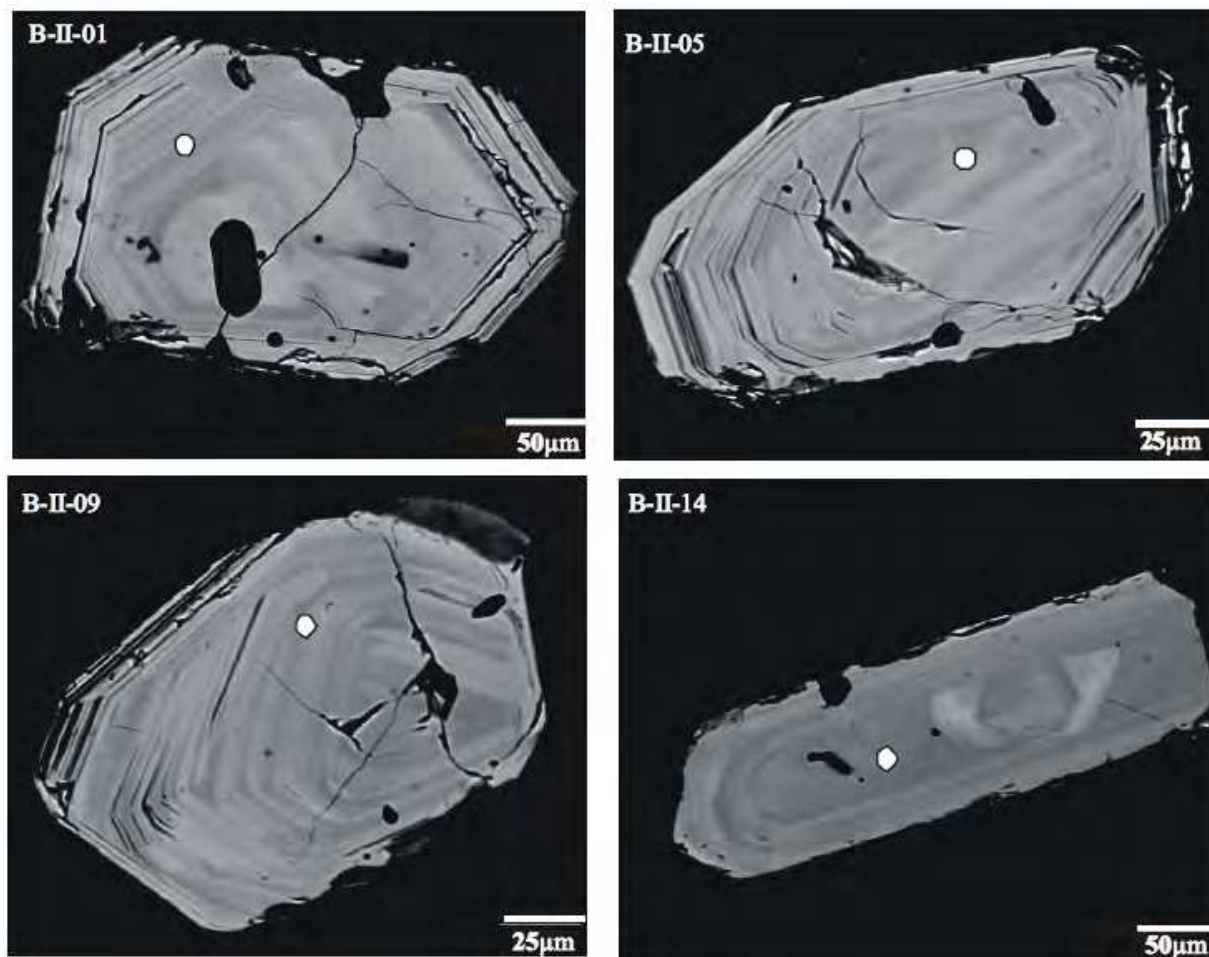


Fig. 7. Zircons microphotographies that defined the 553 ± 5.4 Ma age for lamprophyric rock from Hilário Formation (LV-243 sample). A-I-02 = sample number, o = spot showing the place where the analyses were realized in each zircon. Data showed in table 3.

3.2.3 Acampamento Velho Formation

The first geochronological investigation of the rhyolites was performed by Cordani et al. (1974) followed by Sartori (1978) and Teixeira (1982). Soliani Jr. (2000) compiled their data and obtained an age of 529 ± 4 Ma and $R_0 = 0,706$ (Rb-Sr whole rock). Another Rb-Sr dating was performed by Almeida et al. (2002), who studied the rhyolitic flows from Cerro do Bugio area and the dykes intruding the Maricá Formation. These authors obtained two whole rock isochrons: 545.1 ± 12.7 Ma ($R_0 = 0.709$) and 546 ± 12.9 Ma ($R_0 = 0.714$). However, Sommer et al. (2005) presented U-Pb data (sensitive high mass-resolution ion microprobe) using eleven zircon crystals from rhyolites of Vila Nova do Sul area (Ramada Plateau), obtaining an age of 549.3 ± 5 Ma, which is more reliable. Therefore, all the obtained ages indicate that the rocks from Acampamento Velho Formation upper felsic association belong to the Early Neoproterozoic III (NP₃).

The MH-13 sample (andesitic basalt) was selected to obtain the absolute age from lower mafic association of Acampamento Velho Formation base. Nineteen zircons crystals were dated (Table 4). Based on the dating results, we detected the presence of four age group: 2799 ± 21 Ma (one zircon); 2182 ± 55 Ma (one zircon), 612.6 ± 15 Ma (seven zircons) apart

from anchored age, that corresponds to intersection at 2442 ± 54 Ma (three zircons) (Table 4, Fig. 8a). The 553 ± 5.4 Ma age (based on six zircons – Table 4, Fig. 8b) was considered as the lower mafic association age. All the zircons that showed older ages were considered xenocrystal zircons. Thus, the magma would have assimilated Neoproterozoic (NA), Paleoproterozoic (Siderian and Rhyacian) and older Neoproterozoic material during its ascension.

The selected zircons that allowed the Acampamento Velho Formation base age setting, in general are colorless and dirty, all grains are between $87 \mu\text{m}$ and $158 \mu\text{m}$ in size and show diffuse zonation, prismatic and pyramidal shapes, incomplete and partially serrulated contours, few fractures and inclusions (Fig. 9). The faint and broad zoning suggest that it may have been formed by very slow and complex crystallization of a magma body with prolonged residence time in the lower crust. The crystallization velocity appears to be the major controlling factor of the elongation ratio to the zircon. Skeletal zircon crystals are the most extreme form of rapid growth. It is relevant to point out that the Acampamento Velho Formation mafic flow dated zircons show morphologic characteristics of a slow generation in the magmatic chamber.

Spot number	Concordia 1					Age (Ma)						Dis.	F206	
	$^{207}\text{Pb}/^{235}\text{U}$		$^{206}\text{Pb}/^{238}\text{U}$		Rho1	$^{206}\text{Pb}/^{238}\text{U}$		$^{207}\text{Pb}/^{235}\text{U}$		$^{207}\text{Pb}/^{206}\text{Pb}$				$^{232}\text{Th}/^{238}\text{U}$
119-A-I-02	0,73099	4,86	0,09051	2,05	0,42	559	11	557	27	551	24	0,62	-1	0,0007
119-A-I-12	0,71742	5,44	0,08906	2,96	0,54	550	16	549	30	546	25	0,51	-1	0,0008
119-A-I-24	0,71164	4,02	0,09119	3,43	0,85	563	19	546	22	476	10	0,69	-18	0,0000
119-A-I-28	0,71175	2,90	0,08921	1,89	0,65	551	10	546	16	525	12	0,99	-5	0,0000
119-A-I-32	0,72048	4,18	0,08986	2,12	0,51	555	12	551	23	535	19	0,66	-4	0,0000
119-A-I-26	0,68233	4,88	0,08835	4,35	0,89	546	24	528	26	453	10	1,06	-21	0,0000
119-A-I-05	0,77464	3,54	0,09524	1,96	0,55	586	11	582	21	567	17	0,52	-3	0,0003
119-A-I-07	0,83567	4,54	0,10066	2,19	0,48	618	14	617	28	611	24	1,32	-1	0,0005
119-A-I-16	0,79403	4,41	0,09638	1,88	0,43	593	11	593	26	595	24	0,96	0	0,0009
119-A-I-19	0,81080	3,32	0,09729	2,50	0,75	599	15	603	20	619	14	0,50	3	0,0000
119-A-I-22	0,84916	5,93	0,10603	2,60	0,44	650	17	624	37	533	28	0,49	-22	0,0001
119-A-I-23	0,83998	3,39	0,10432	1,63	0,48	640	10	619	21	545	16	0,65	-17	0,0000
119-A-I-29	0,77999	4,20	0,09460	3,70	0,88	583	22	585	25	596	12	0,66	2	0,0002
119-A-I-20	14,70031	2,19	0,54875	1,28	0,58	2820	36	2796	61	2779	49	0,72	-1	0,0001
119-A-I-01	10,30577	2,14	0,46719	1,94	0,90	2471	48	2463	53	2456	22	0,23	-1	0,0011
119-A-I-10	10,20802	2,51	0,46490	1,98	0,79	2461	49	2454	62	2448	38	0,34	-1	0,0005
119-A-I-18	9,37569	1,89	0,43936	0,99	0,52	2348	23	2375	45	2399	39	1,07	2	0,0018
119-A-I-17	4,33522	2,14	0,28940	1,58	0,74	1639	26	1700	36	1777	26	0,73	8	0,0010
119-A-I-01	7,59979	6,12	0,40841	4,51	0,74	2820	36	2185	134	2163	89	0,41	-2	0,0017

Table 4. U/Pb zircon data of the andesitic basalt sample (MH-13) for Acampamento Velho Formation base obtained by in situ LAM-ICPMS-MC.

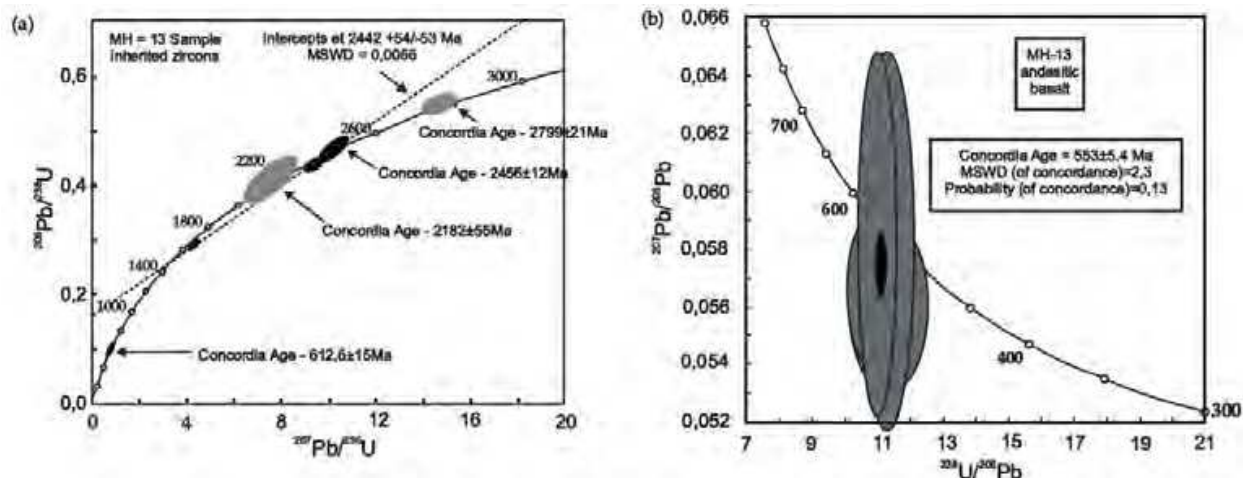


Fig. 8. Concordia diagram from Acampamento Velho Formation lower mafic association: (a) U-Pb data diagram with tracing considering only the older zircon ages of the 553 Ma (table 4). We detected the presence of four ages: 2799 ± 21 Ma, 612.6 ± 15 Ma, 612.6 ± 15 Ma and 2442 ± 54 Ma. (b) U-Pb data diagram with tracing considering only the younger zircon ages from Acampamento Velho Formation lower mafic association (MH-13 sample). Gray ellipse cores represent the single zircon analysis (table 4). Black ellipse represents the concordia age of the MH-13 sample calculated from single zircon ages (table 4).

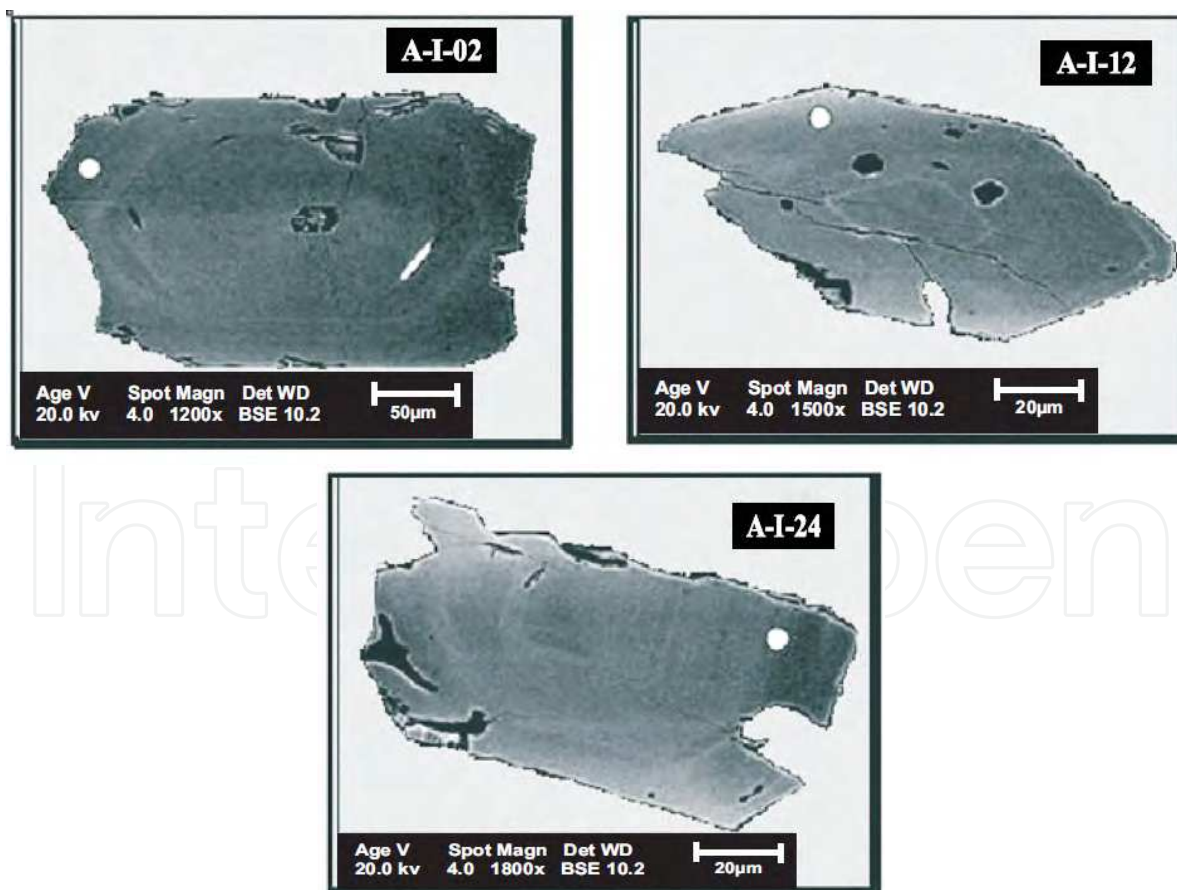


Fig. 9. Zircons microphotographies that defined the 553 ± 5.4 Ma age for Acampamento Velho Formation base. A-I-02 sample number, \bigcirc = spot showing the place where the analysis were realized in each zircon. Data showed in table 4.

3.2.4 Rodeio Velho Member

Hartmann et al. (1998) determined the U-Pb age of 470 ± 19 Ma (sensitive high mass-resolution ion microprobe method) for this event (Middle-Ordovician), which suggest that Rodeio Velho Member is related to the beginning of the Paraná Basin formation. On the other hand, Chemale Jr. (2000) obtained Sm-Nd model ages (T_{DM}) from 1.6 to 1.9 Ga, suggesting a modified mantle origin for these rocks. Rodeio Velho Member was probably the source of heat and hydrothermal solutions for Cu (Ag, Au), Pb and Zn (Cu, Ag) mineralizations in the Camaquã Mines (Lima et al., 2001). Hydrothermal illites collected in those mines also yielded K-Ar ages around 465 Ma (Bonhomme & Ribeiro, 1983).

We used the sample RLP-20 (alkaline basalt) to date Rodeio Velho event using U-Pb method. The sample was collected between Rodeio Velho and Pedra de Arara area (Fig. 1). At this area, the volcanic rocks show two lava flows, being the lower flow more vesiculated (flow top) than the upper, which is massive. This is related to the sandstones with great cross-stratification, suggesting the eolian character of this rock and it would correspond to the Pedra Pintada Formation from Guaritas Group. We dated sixteen zircon crystals from sample RLP-20. Based on these dating results, we detected the presence of 4 age groups: 2190 ± 18 Ma (one zircon); 1079 ± 12 Ma (six zircons); 658 ± 8.3 Ma (two zircons) and 547 ± 6.3 Ma (based on five zircons), (Table 5, figs. 10a and 10b). The younger obtained age, that was calculated based on individual zircon ages from Table 5, defined the Rodeio Velho Member age (Fig. 10a). All the zircons that showed older ages were considered xenocrystal inherited zircons. Thus, the magma would have assimilated Paleoproterozoic (PP₂), Mesoproterozoic (MP₃) and Neoproterozoic (NP₂) rocks during its ascension. The selected zircons used to obtain the Rodeio Velho Member age are in general (Fig. 11) colorless and transparent, the

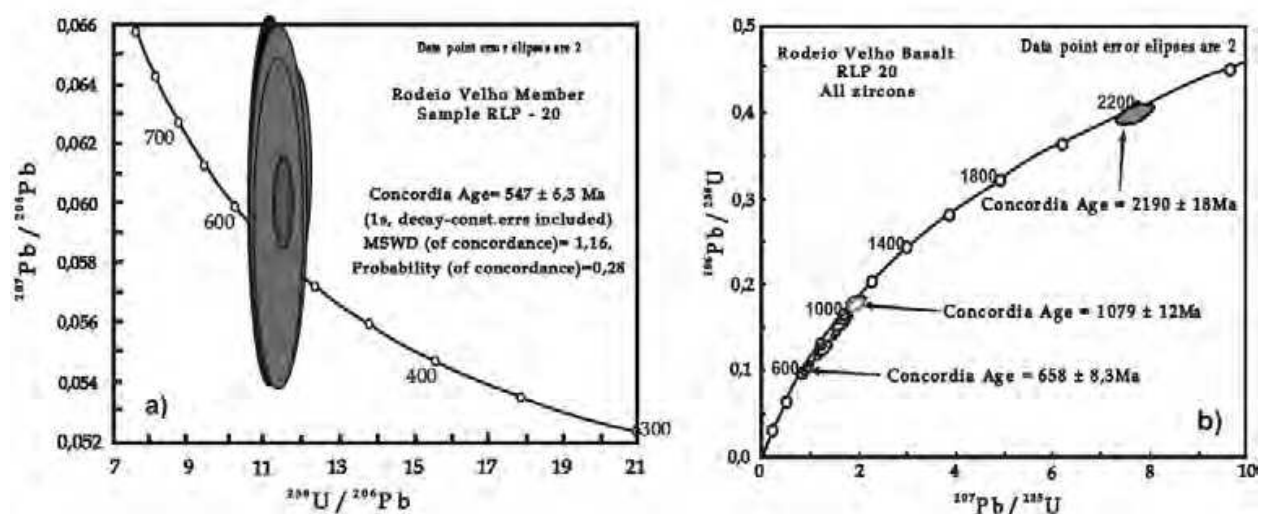


Fig. 10. U-Pb concordia data diagram for Rodeio Velho Member. (a) - U-Pb concordia data diagram with tracing considering only the younger zircon ages. Gray ellipse cores represent the single zircon analysis, with exception of A-I-02 zircon (black ellipse). Dark gray ellipse represents the concordia age calculated from single zircon ages (Table 5). The A-I-02 zircon sample shows high percentage of discordance and was not included in the calculating data (black ellipse). (b) - U-Pb concordia data diagram with tracing considering only the older zircon ages of the 547 Ma (table 5).

size varies between 202 μm and 321 μm , the crystals show zonation, euhedral to subhedral shape, contours partially serrulated, few fractures, impurities and inclusions. They are very small and occupy the crystal rims. The A-I-19 zircon (Fig. 11d) is constituted by an older core with age between 983 Ma and 1000 Ma (spot a, figure 11d) and 545 to 554 Ma rims (spot b, figure 11d).

Spot number	Concordia 1					Age (Ma)						%		F206
	$^{207}\text{Pb}/^{235}\text{U}$		$^{206}\text{Pb}/^{238}\text{U}$		Rho 1	$^{206}\text{Pb}/^{238}\text{U}$		$^{207}\text{Pb}/^{235}\text{U}$		$^{207}\text{Pb}/^{206}\text{Pb}$		$^{232}\text{Th}/^{238}\text{U}$	Dis	
072-A-I-02	0,72563	3,62	0,08724	2,32	0,64	539	12	554	20	615	17	1,60	12	0,0010
072-A-I-04	0,7353	4,74	0,08913	2,67	0,56	550	15	560	27	598	23	0,63	8	0,0005
072-A-I-09	0,72257	4,60	0,08907	2,48	0,54	550	14	552	25	561	22	0,68	2	0,0009
072-A-I-15	0,75070	4,76	0,09133	2,09	0,44	563	12	569	27	590	25	1,06	4	0,0012
072-A-I-19b	0,71359	4,29	0,08823	2,36	0,55	545	13	547	23	554	20	0,00	2	0,0004
072-A-I-01	0,93941	2,94	0,11007	2,01	0,68	673	14	673	20	671	14	0,95	0	0,0004
072-A-I-16	0,88815	4,07	0,10494	1,85	0,45	643	12	645	26	653	24	0,86	1	0,0003
072-A-I-21	1,18814	3,86	0,13100	1,65	0,43	794	13	795	31	799	28	0,30	1	0,0002
072-A-I-05	1,13452	2,71	0,12177	1,49	0,55	741	11	770	21	855	19	0,62	13	0,0007
072-A-I-07	1,51559	2,95	0,14998	2,26	0,77	901	20	937	28	1022	19	0,37	12	0,0004
072-A-I-11	1,89571	4,13	0,18311	1,92	0,46	1084	21	1080	45	1071	39	0,56	-1	0,0013
072-A-I-12	1,91441	3,36	0,18097	1,66	0,50	1072	18	1086	36	1114	32	0,29	4	0,0000
072-A-I-13	1,25790	4,45	0,13097	2,39	0,54	793	19	827	37	918	34	0,27	14	0,0082
072-A-I-18	1,60946	4,10	0,15956	2,17	0,53	954	21	974	40	1018	35	0,53	6	0,0003
072-A-I-19 ^a	1,67807	3,58	0,16466	1,60	0,45	983	16	1000	36	1039	33	0,48	5	0,0004
												0,37	12	0,0004
072-A-I-10	7,66631	2,05	0,40217	1,25	0,61	2179	27	2193	45	2205	36	0,56	-1	0,0013

Table 5. U/Pb zircon data of the alkaline basalt sample (RLP-20) for Rodeio Velho Member obtained by in situ LAM-ICPMS-MC.

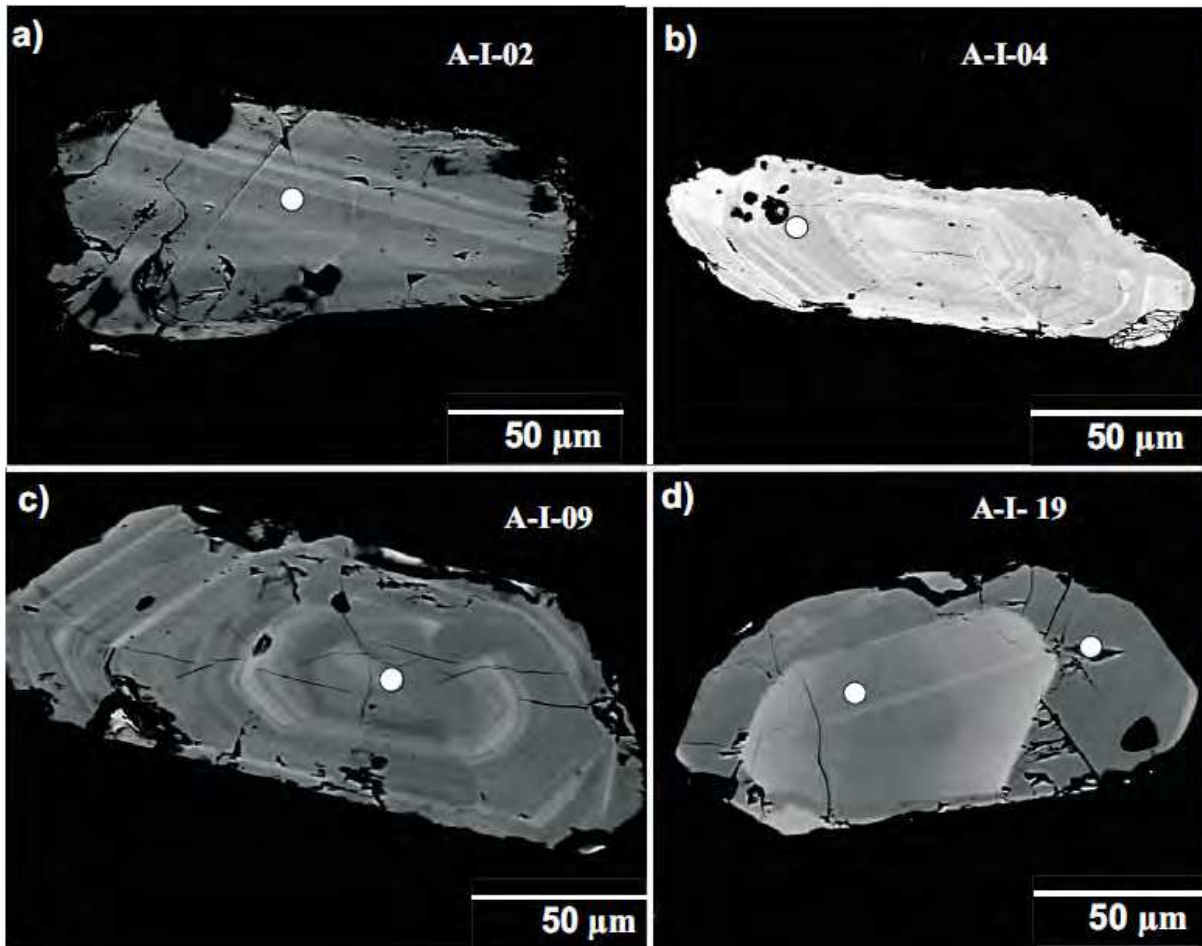


Fig. 11. Zircons microphotographies that defined the 547 ± 6.3 Ma age for Rodeio Velho Member. A-I-09 sample, o = spot showing the place where the analyses were realized in each zircon.

4. Acampamento Velho Formation: geological context, petrography and geochemistry

The earliest references to acid volcanic rocks in Southern Brazil are made by Leinz et al. (1941), who described tuffs, vitrophyres, feldsites and quartz-porphyrries, which unconformably overlying the Maricá Formation. This unit was named as Ramada Rhyolite by Robertson (1966) and as Acampamento Velho Formation by Cordani et al. (1974). However, Leites et al. (1990) considered the Acampamento Velho Group as Volcanogenic Sequence III. Paim et al. (2000) named the unit as Acampamento Velho Formation (from Cerro do Bugio Allogroup), and this set of volcanic rocks were considered as an unit limited on the top and base by discontinuities, which marked a special period in the evolution of the basin. It has been traditionally considered as exclusively acid in composition, but detailed geological mapping in the Cerro do Bugio, Cerro do Perau and Serra de Santa Bárbara area (West of Caçapava do Sul town) revealed the existence of a basaltic/andesitic unit at the base and a felsic unit at the top (Zerfass & Almeida 1997, Zerfass et al. 2000, Almeida et al. 2002). This observation leads to the existence of a bimodal alkaline volcanism, mafic at the base and a felsic at the top. Sommer (2000) described the existence of an effusive sequence, pyroclastic and volcanic comenditic rocks at Taquarembó Plateau. In the same area, Wildner

et al. (1999) verified that the rocks are alkaline, saturated in silica, and have post-collisional characteristics. Sommer et al. (2005) recognized the existence of a bimodal mildly alkaline magmatism related to post-collisional events at Ramada Plateau.

The four main areas of occurrence of the volcanism Acampamento Velho are Santa Bárbara Sub-Basin, Guaritas Sub-Basin and Taquarembó-Ramada Sub-Basin from Camaquã Basin (Paim et al. terminology, 2000 - Fig. 1). At Santa Bárbara and Guaritas sub-basins, the volcanic package is limited at the top and base by sedimentary rocks from own Camaquã Basin, while at Taquarembó-Ramada Basin, the volcanic rocks maintains the relief, sat down on rocks from Sul-Riograndense Shield.

4.1 Geological setting

In the Santa Bárbara area Sub-basin, the area is a long narrow N20°E ridge formed by Acampamento Velho Formation volcanic rocks, where the main elevations are Cerro do Bugio (419 m), Cerro do Perau (331 m) and Serra de Santa Bárbara (440 m), from North to South (Fig. 12). In this area, an unconformity marks the lower contact of the Acampamento Velho Formation over the sedimentary rocks from Maricá or Bom Jardim allogroups (sensu Paim et al. 2000). The upper contact with Santa Fé or Lanceiros alloformations is delineated by a disconformity. The Acampamento Velho Formation is composed of a Lower Mafic Association and an Upper Felsic Association (Fig. 12). The Lower Mafic Association is composed of basaltic and andesitic basalt flows, as well as subordinate andesitic breccias that occur as a continuous bed, with thickness between 10 m and 350 m. It is usually massive, with rare stratification, dipping about 20° to the E or SE (Fig. 12). These rocks show porphyritic texture with plagioclase phenocrysts (Almeida et al. 2002, 2003a).

The Upper Felsic Association is composed of rhyolitic rocks and comprises alternating pyroclastic rocks (lapilli-tuffs, tuffs, welded tuffs) at the base and flows at the top (Fig. 12). Its stratification is tilted, dipping about 20° to the E or SE. The lapilli-tuffs are preserved as discontinuous strata of thicknesses up to 40 m. The tuffs occur as lenses of variable thickness (up to 30 m) and internally consist of parallel layers, poorly sorted in general terms. The welded tuffs are also poorly sorted and present predominantly ash fraction, occurring as lenticular layers up to 350 m thick. The rhyolitic flows form a continuous layer of variable thickness from 20 m to 600 m. They display internally of flow foliation, which is frequently folded (Zerfass & Almeida, 1997, 2001). The lapilli-tuffs, tuffs and welded tuffs are interfingered and associated of pyroclastic flows generated during the rhyolitic eruptive phase, as a product of the eruptive column collapse. Pyroclastic fall processes are predominant in distal regions, as it is suggested by the well sorting of the finer tuff members. The rhyolitic flows overlie all of the previous facies, suggesting that the UFA is related to plinian volcanism (Zerfass et al., 2000).

4.2 Mineralogy and petrography

The basalts and andesitic basalts from lower mafic association show relict pilotaxitic texture and zoned plagioclase phenocrysts with diffuse appearance. Sericite, kaolinite, carbonate, chlorite and opaque minerals replace totally the pyroxene phenocrysts and sometimes, partially the plagioclase. Quartz, plagioclase and sanidine grains present on the top layers incipient "kidney-shaped" texture. The matrix is formed by plagioclase microliths, chlorite-carbonate, a ferro-magnesian pseudomorph (pyroxene?) and a large quantity of opaque minerals (Almeida et al., 2002, 2003a). Electron microprobe analyses show that plagioclase phenocrysts and microlites are sometimes totally albitized, with compositions between

Ab_{99,6} and Ab₉₈ (Table 6), which should be related to the interaction of late fluids on the plagioclase resulting in the albite formation. The smaller grains in the matrix are strongly altered to kaolinite. The pyroxene is altered to chlorite and generated opaque minerals. The late magmatic fluids rich in CO₂ used part of the Ca from plagioclase and/or pyroxene to form calcite. Albite and clay minerals are therefore product of late fluids relatively enriched in Na. Zircons show prismatic-pyramidal shapes and diffuse zonation (Fig. 9). They occur as inclusions in Ti-rich magnetite and pyroxene (Almeida et al., 2007).

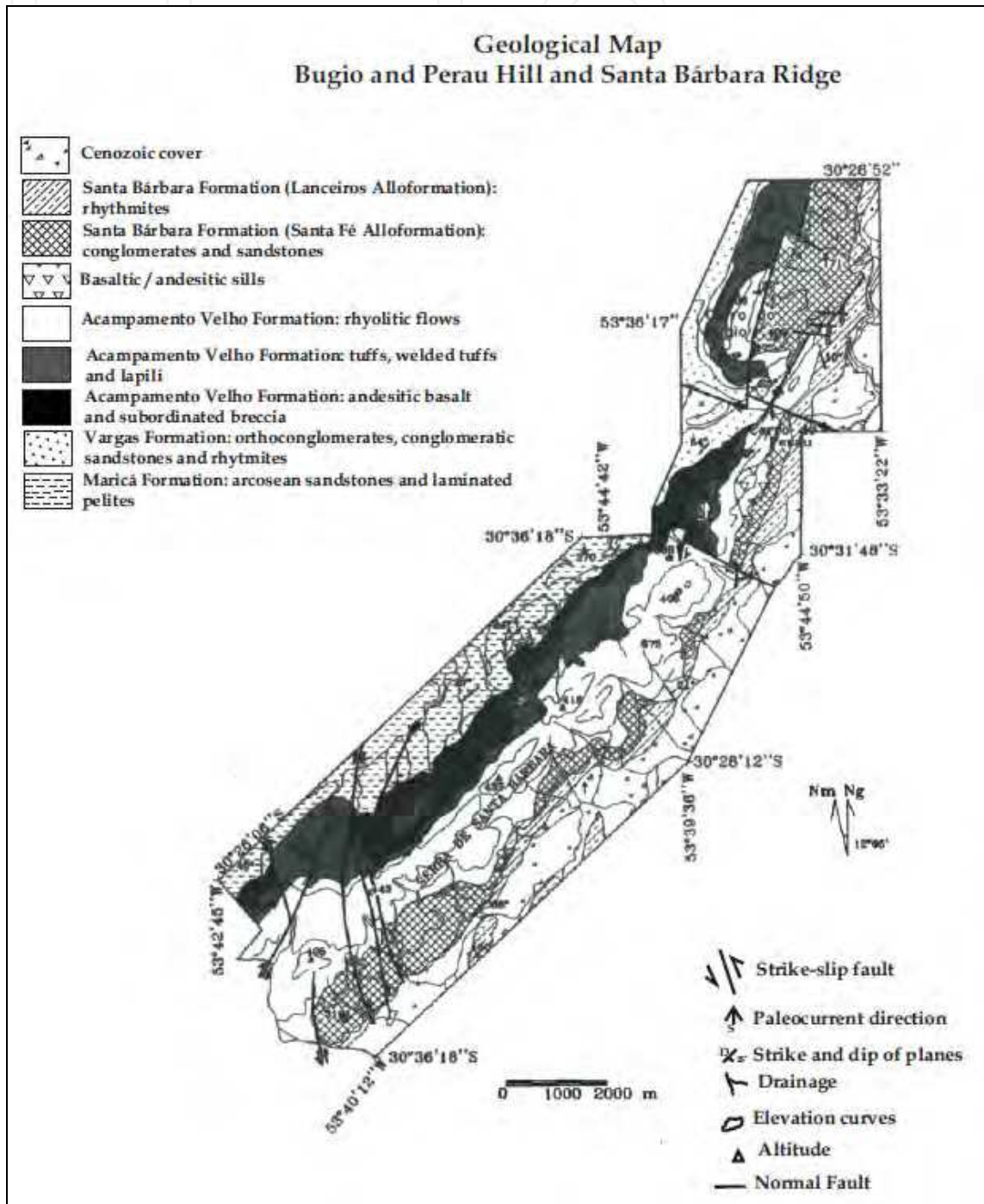


Fig. 12. Geological map of the Cerro Bugio, Cerro Perau and Sierra de Santa Bárbara areas (Almeida et al. 2002).

According to Almeida et al. (2007), for the lower mafic association, the crystallization sequence is: (1) zircon, (2) Ti-rich magnetite, (3) pyroxene, (4) plagioclase, (5) albite resulting from the late introduction of Na- and CO₂-rich fluids, which affected mainly the plagioclase and pyroxene (subordinate), (6) sericite, chlorite and calcite from late solutions that altered the pyroxene, and sericite-kaolinite that altered the plagioclase.

In the Upper Felsic Association, the lapilli-tuffs contain poorly sorted lithoclasts (3 to 40 mm in diameter); vitroclast pseudomorphs (cusped and platy shapes) substituted by silica and phyllosilicates, quartz crystalloclasts with corrosion gulfs, sanidine and heterogeneous alkali-feldspar (Fig. 13a). The latter is produced by the sodic metassomatic alteration of sanidine, forming heterogeneous pseudomorphs, where part of sanidine is transformed to albite. The lapilli-tuffs matrix is tuffaceous and microcrystalline. The tuffs and welded tuffs differ from each other on the welding degree. They contain crystalloclasts of euhedral quartz or with corrosion gulfs, heterogeneous alkali-feldspar, sanidine (altered to phyllosilicates) and magnetite. Eutaxitic flow structures, conchoidal fractures and perlitic textures are common (Fig. 13b). The tuffaceous matrix is composed of cusped and platy-shaped fragments (pseudomorphs of volcanic glass shards) and pumice shard-shaped fragments in the welded tuffs (fig. 13c), suggesting pumice pseudomorphs. Original glass is strongly devitrified. Spherical spherulitic structures occur subordinately.

Sample	phenocrysts			matrix		matrix		phenocrysts			matrix
	MH13-10	MH13-12	MH13-13	MH13-14	MH13-15	MH13-16a	MH13-16b	MH13-1a	MH13-6a	MH13-6b	MH13-8
Location	rim	core	core	core	rim	core	rim	core	core	rim	core
SiO ₂	71.05	71.65	70.52	71.24	71.23	70.42	71.60	71.37	71.20	70.77	71.51
Al ₂ O ₃	19.97	19.65	20.20	19.84	19.96	20.08	20.18	19.88	20.22	20.38	19.74
FeO	0.35	0.09	0.12	0.05	0.03	0.14	0.22	0.04	0.58	0.21	0.31
MgO	0.03	n.d.	n.d.	n.d.	n.d.	0.01	0.04	0.01	0.10	0.01	n.d.
BaO	0.06	0.08	0.07	n.d.	n.d.	n.d.	0.01	0.07	n.d.	0.03	0.17
CaO	0.13	0.04	0.08	0.09	0.07	0.03	0.06	0.04	0.05	0.25	0.07
Na ₂ O	10.25	10.34	10.43	10.45	10.09	9.99	10.35	10.64	10.40	9.89	10.14
K ₂ O	0.10	0.02	0.17	0.03	0.05	0.09	0.02	0.04	0.09	0.11	0.13
Total	101.94	101.87	101.59	101.70	101.43	100.76	102.48	102.09	102.64	101.65	102.07
Si	6.05	6.50	6.03	6.47	6.07	6.05	6.05	6.47	6.03	6.03	6.50
Al	2.00	2.10	2.03	2.12	2.00	2.03	2.01	2.12	2.02	2.05	2.11
Fe ₂	0.02	0.01	0.01	n.d.	n.d.	0.01	0.02	0.01	0.04	0.02	0.02
Mg	n.d.	n.d.	n.d.	n.d.	n.d.	n.d.	0.01	n.d.	0.01	n.d.	n.d.
Ba	n.d.	n.d.	n.d.	n.d.	n.d.	n.d.	n.d.	n.d.	n.d.	n.d.	0.01
Ca	0.01	n.d.	0.01	0.01	0.01	n.d.	0.01	n.d.	0.01	0.02	0.01
Na	1.69	1.82	1.73	1.84	1.67	1.66	1.70	1.87	1.71	1.64	1.78
K	0.01	n.d.	0.02	n.d.	0.01	0.01	n.d.	n.d.	0.01	0.01	0.02
Cations	9.80	10.43	9.83	10.45	9.76	9.77	9.79	10.47	9.82	9.77	10.43
X	8.05	8.59	8.06	8.59	8.08	8.08	8.06	8.59	8.05	8.08	8.59
Z	1.75	1.83	1.77	1.86	1.68	1.69	1.72	1.89	1.77	1.69	1.83
Ab	98.70	99.60	98.50	99.30	99.20	99.20	99.50	99.60	99.20	98.00	98.70
An	0.70	0.20	0.40	0.50	0.40	0.20	0.40	0.20	0.20	1.30	0.40
Or	0.64	0.16	1.08	0.22	0.36	0.60	0.12	0.21	0.58	0.72	0.89

Table 6. Albitized plagioclase analysis (electron microprobe) of the Lower Mafic Association from basaltic and andesitic basalt flows from Acampamento Velho Formation. n.d. = not detected. (Almeida et al., 2007).

Tuff analyses by electron microprobe (Table 7) show that the alkali-feldspar crystalloclasts are totally albitized ($Ab_{99,6}$ to $Ab_{98,9}$). Scanning electron microscope analysis show that alkali-feldspar is heterogeneous, contain albite and sanidine in the same crystals. Albite is the product of sanidine alteration. These tuffs display shard pseudomorphs devitrified to illite (Fig. 14a) and crystalloclasts of sanidine with illite pseudomorphs (Fig. 14b). Magnetite is Ti-rich (Table 8) and has inclusions of zircon grains, which are also located around the grain edges. Ti-rich magnetite is pseudomorphically replaced by sanidine and ilmenite along cleavages planes, and their edges are partially corroded by reaction with the matrix (Fig. 14c).

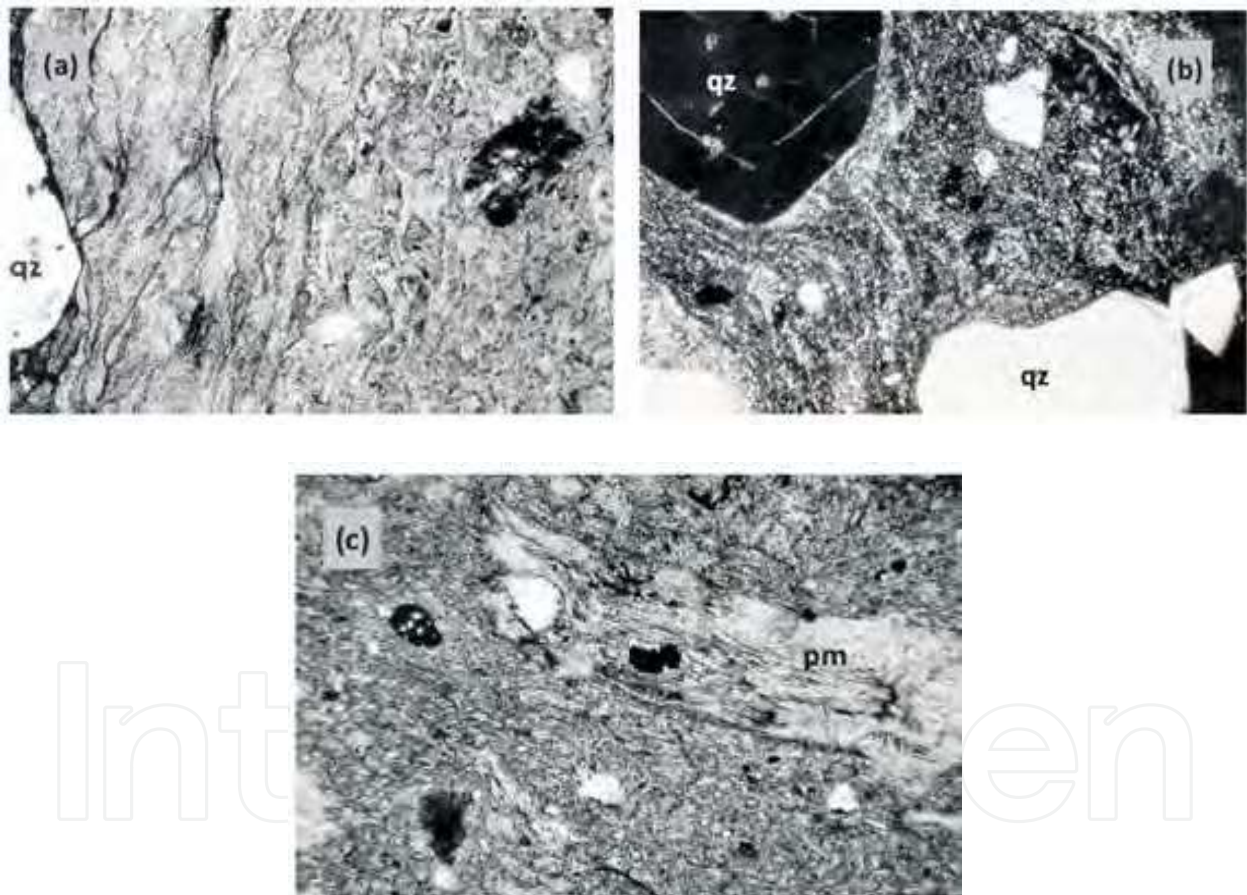


Fig. 13. Tuff photomicrography - 40x- optical microscope PL (a) - the tuff shows cusped and platy-shaped fragments, volcanic shards pseudomorphs, quartz (qz) and sanidine (sa) crystalloclasts; (b) - welded tuff with eutaxitic texture. qz = quartz crystalloclast; (c) - welded tuff with pumice lithoclasts (pm), fiammes and eutaxitic texture.

Sample	MH16-1a	MH16-1b	MH16-3a	MH16-3b	MH16-5 ^a	MH16-5b
Location	core	rim	core	rim	core	Rim
SiO ₂	71.10	71.80	70.85	71.63	71.06	71.06
Al ₂ O ₂	19.96	20.13	20.10	20.07	20.12	20.12
FeO	0.05	n.d	0.04	n.d	n.d	n.d
BaO	0.10	0.01	n.d	0.10	0.04	0.04
CaO	0.14	0.05	0.02	0.04	0.04	0.04
Na ₂ O	10.07	9.96	10.20	10.40	10.63	10.63
K ₂ O	0.06	0.11	0.03	0.06	0.04	0.04
Total	101.48	102.06	101.24	102.31	101.94	101.94
Si	6.066	6.08	6.05	6.06	6.04	6.04
Al	2.01	2.01	2.02	2.00	2.01	2.01
Fe ₂	n.d	n.d	n.d	n.d	n.d	n.d
Ba	n.d	n.d	n.d	n.d	n.d	n.d
Ca	0.01	n.d	n.d	n.d	n.d	n.d
Na	1.17	1.64	1.69	1.71	1.75	1.75
K	0.01	0.01	n.d	0.01	0.01	0.01
Cations	9.77	9.74	9.78	9.79	9.82	9.82
X	8.07	8.09	8.08	8.07	8.06	8.06
Z	1.69	1.65	1.70	1.72	1.76	1.76
Ab	98.90	99.00	99.60	99.40	99.50	99.50
An	0.70	0.20	0.10	0.20	0.20	0.20
Or	0.36	0.73	0.24	0.41	0.28	0.28

Table 7. Albite analyses (electron microprobe) of the Upper felsic Association - Acampamento Velho Alloformation rhyolitic tuffs. n.d. = not detected. (Almeida et al., 2007).

The analyses of welded tuffs by electron microprobe (Table 9) show that the alkali-feldspar crystalloclasts are composed predominantly by sanidine with variable amounts of albite and K-sanidine (Fig. 15a). The matrix contains predominantly K-sanidine and also sanidine Na-rich (Ab=32). Plagioclase crystalloclasts (andesine-labradorite) are present in some samples. The welded tuffs present pseudomorph pumices in fiammes, heterogeneous alkali-feldspar and sanidine crystalloclasts that are altered to illite and

sometimes corroded by matrix (Fig. 15b). The Ti-rich magnetite crystalloclasts are altered to ilmenite and rutile (Table 8), which are disposed according to twinning and/or cleavage planes (Fig. 15c), and sometimes replaced by sanidine. Homogeneous and zoned zircons usually occur as inclusions, similar to those observed in tuffs, in heterogeneous alkali-feldspar and quartz.

Sample	SSB-32-1	SSB-32-1	MH-32-2	MH-35-1	MH-35-2	SSB-23a
rocks	tuff		welded tuff			flow
Mineral	Mt	Mt	Mt	Il	Ru	Mt
SiO ₂	9.80	9.21	n.d.	17.58	4.12	0.99
TiO ₂	N.d.	n.d.	7.45	35.81	89.83	15.44
Al ₂ O ₃	1.61	1.12	0.47	11.63	2.04	n.d.
Fe ₂ O ₃	87.94	89.10	92.08	33.35	1.73	83.57
MgO	n.d.	n.d.	n.d.	0.26	1.48	n.d.
K ₂ O	n.d.	n.d.	n.d.	1.36	0.80	n.d.
total1	100.00	99.99	100.00	99.99	100.00	100.00
Total	99.35	99.43	100.00	99.99	100.00	100.00
Cl	0.65	0.56	n.d.	n.d.	n.d.	n.d.
Si	4.85	0.13	n.d.	8.22	1.93	0.46
Al	0.85	0.11	0.25	6.16	1.08	n.d.
Ti	n.d.	n.d.	4.47	35.81	53.58	9.26
Fe ₃	61.51	62.32	64.40	23.32	1.21	58.45
Mg	n.d.	n.d.	n.d.	0.16	n.d.	n.d.
K	n.d.	n.d.	n.d.	1.13	0.66	
Cations	67.21	62.56	69.12	74.80	58.73	68.17

Table 8. Oxides analysis (scanning electron microscope) of the Upper Felsic Association – Acampamento Velho Formation tuffs, welded tuffs and flows. Mt = magnetite; Il = ilmenite; Ru = rutile. n.d. = not detected. The Si and Al detected is due probably the sanidine contamination that is inside the Ti-enriched magnetite. (Almeida et al, 2007).

The rhyolitic flows are homogeneous or banded. Relict structures of perlitic devitrification and conchoidal fractures are common in the microfelsitic matrix. Sanidine, heterogeneous alkali-feldspar and quartz phenocrysts display corrosion gulfs and conchoidal fractures (Figs. 16a). Iron oxide/hydroxide and sericite are also present as alteration products. Rhyolitic flows, when banded, show an intercalation of thick spherical spherulites, product of devitrification, and microcrystalline bands of quartz and feldspar. Electron microprobe analyses of spherulites show heterogeneous composition with fine aggregates of anorthoclase and albite grains (Fig. 16b). Analyses of rhyolitic flows by electron microprobe (Table 10) show that the alkali-feldspar phenocrysts consist of sanidine, albite and heterogeneous alkali-feldspar (Figs. 16c and d). Scanning electron microscope analyses

indicate that Ti-rich magnetite (Table 8) and zircon are similar to those described before. The Ti-rich magnetite crystalloclasts are pseudomorphically replaced by sanidine, rutile and ilmenite, which upon interaction with a late fluid altered to TiO_2 , probably rutile and hematite, according to the reaction: $4\text{FeTiO}_3 + \text{O}_2 \rightarrow 4\text{TiO}_2 + 2\text{Fe}_2\text{O}_3$. The interaction with this late fluid also promoted the migration of Ti into cleavage planes and the crystallization of ilmenite and rutile.

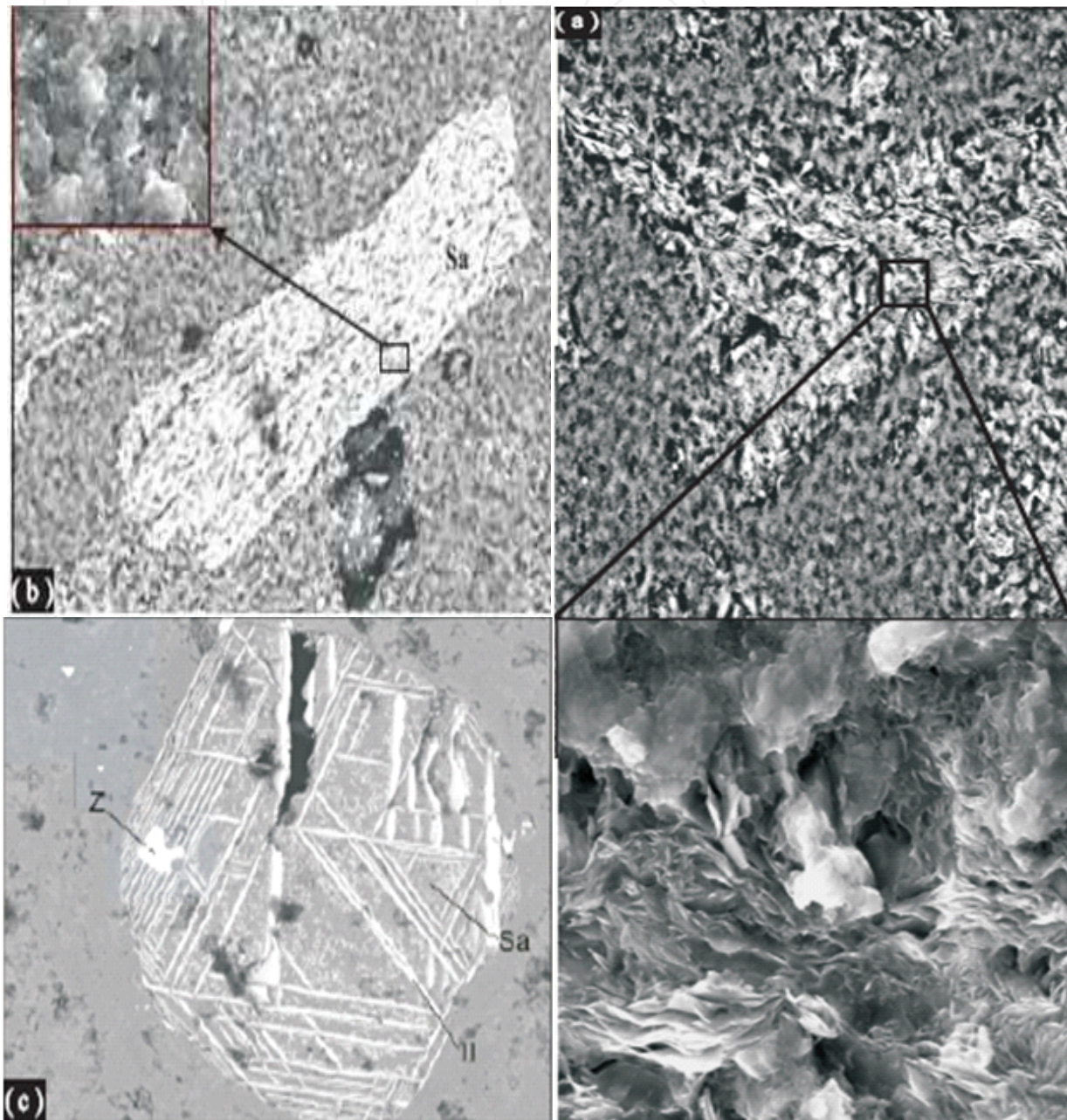


Fig. 14. Tuff: (a) glass shard photomicrography with pseudomorphic substitution by illite (scanning electron microscope); (b) photomicrography of the sanidine altered to illite crystalloclast (scanning electron microscope); (c) Ti-rich magnetite crystalloclast pseudomorphically replaced by ilmenite and sanidine with zircon inclusions (scanning electron microscope).

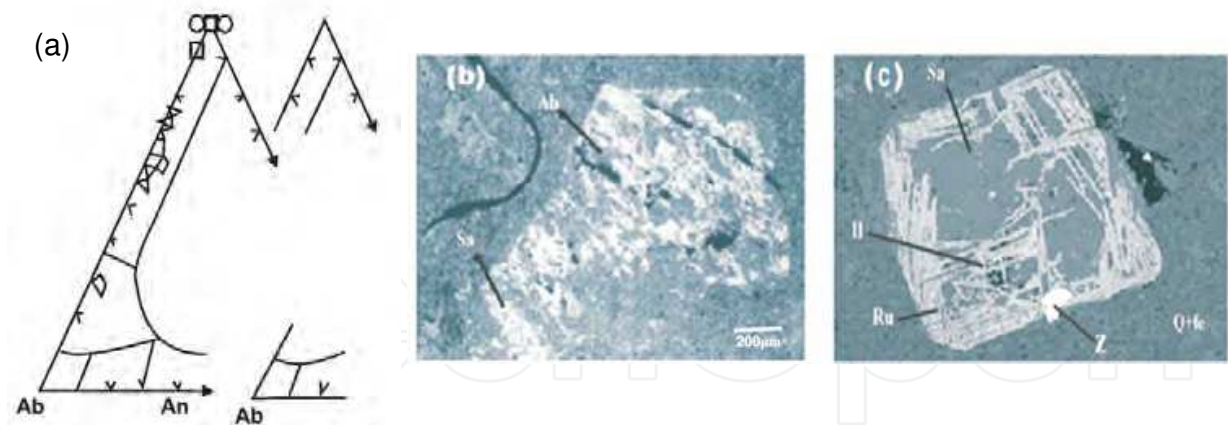


Fig. 15. Welded tuff: (a) diagram Ab-Or-An (electron microprobe and scanning electron microscope) = matrix, ♦ = rim, Δ = inter, ▽ = core, + = bright, x = dark, O = in Mt. (b) Photomicrography of the heterogeneous alkali feldspar crystalloclast corroded by the matrix (analyzed through the electron microprobe); (c) Photomicrography of the Ti-rich magnetite crystalloclast altered to ilmenite (Il), rutile (Ru) disposed according to twinning and/or cleavages with zircon inclusions (Z) and replaced by sanidine (Sa) (scanning electron microscope).

Sample	MH21-21	MH37-32bb	MH37-35b	MH 37-35c	MH37-38	MH37-44b	MH37-44c	MH37-47b	MH37-49	heterogeneous alkaline feldspars			MH32-p1*	MH35-1*	MH35-2*
Location	matrix	rim	rim	inter	core	rim	inter	rim	core	brigh	dark	brigh	matrix	In Mt	In Mt
SiO ₂	93.40	84.78	88.03	86.09	95.48	85.10	90.06	97.38	89.14	59.73	68.16	52.01	45.12	67.70	55.12
TiO ₂	n.d.	n.d.	n.d.	n.d.	n.d.	n.d.	n.d.	n.d.	n.d.	n.d.	n.d.	n.d.	n.d.	n.d.	0.58
Al ₂ O ₃	3.64	8.92	7.66	7.45	0.18	9.32	6.02	1.16	6.74	14.48	16.30	28.17	23.46	18.57	27.23
Fe ₂ O ₃	n.d.	n.d.	n.d.	n.d.	n.d.	n.d.	n.d.	n.d.	n.d.	n.d.	n.d.	n.d.	n.d.	n.d.	3.75
FeO	0.07	0.12	0.23	0.74	0.15	0.39	0.714	0.05	0.12	n.d.	n.d.	n.d.	19.25	n.d.	n.d.
MgO	0.01	n.d.	0.01	n.d.	0.02	0.01	0.01	n.d.	n.d.	n.d.	n.d.	n.d.	n.d.	0.90	0.950
BaO	n.d.	0.10	0.02	0.03	n.d.	n.d.	0.01	n.d.	0.04	n.d.	n.d.	n.d.	n.d.	n.d.	n.d.
CaO	n.d.	0.06	0.02	0.08	0.01	0.12	0.14	0.01	0.09	n.d.	n.d.	n.d.	n.d.	n.d.	n.d.
Na ₂ O	0.15	3.84	1.49	1.05	0.35	1.78	1.57	0.11	1.17	7.38	6.85	7.29	n.d.	n.d.	n.d.
K ₂ O	2.21	2.41	3.80	4.13	1.49	4.96	3.34	0.34	3.25	18.41	8.69	11.65	12.18	9.07	11.82
Total	99.48	100.29	101.26	99.57	100.68	101.68	101.86	99.05	100.55	100.00	100.00	99.12	100.01	99.99	100.01
Si	15.82	14.66	15.00	14.94	15.91	14.64	15.23	16.30	15.19	27.92	31.86	24.31	21.09	31.65	25.76
Al	0.73	1.82	1.54	1.53	0.62	1.87	1.19	0.23	1.35	7.66	8.63	14.91	12.42	9.83	14.41
Fe ₃	n.d.	n.d.	n.d.	n.d.	n.d.	n.d.	n.d.	n.d.	n.d.	n.d.	n.d.	n.d.	n.d.	13.46	2.62
Ti	n.d.	n.d.	n.d.	n.d.	n.d.	n.d.	n.d.	n.d.	n.d.	n.d.	n.d.	n.d.	n.d.	n.d.	0.35
Fe ₂	0.01	0.12	0.03	0.11	0.02	0.05	0.10	0.01	0.02	n.d.	n.d.	n.d.	n.d.	n.d.	n.d.
Mg	n.d.	n.d.	n.d.	n.d.	n.d.	n.d.	n.d.	0.01	n.d.	n.d.	n.d.	0.53	n.d.	0.55	0.57
Ba	n.d.	0.01	n.d.	0.01	n.d.	n.d.	n.d.	n.d.	n.d.	n.d.	n.d.	n.d.	n.d.	n.d.	n.d.
Ca	n.d.	0.01	n.d.	0.02	n.d.	0.02	0.03	0.01	0.02	n.d.	n.d.	n.d.	n.d.	n.d.	n.d.
Na	0.05	1.29	0.49	0.35	0.11	0.59	0.51	0.04	0.39	n.d.	5.58	n.d.	n.d.	n.d.	n.d.
K	0.48	0.53	0.82	0.92	0.32	1.08	0.72	0.07	0.71	15.28	n.d.	9.67	10.11	7.53	9.81
Cations	17.08	18.34	17.82	17.90	16.99	18.26	17.78	16.64	17.68	50.86	45.57	49.42	57.08	52.18	53.91
X	16.54	16.48	16.53	16.50	16.53	16.51	16.42	16.52	16.55	35.58	40.49	39.22	46.97	44.10	43.53
Z	0.54	1.85	1.36	1.39	0.46	1.75	1.36	n.d.	1.13	15.28	5.08	10.20	10.11	8.08	10.38
Ab	9.30	70.30	37.20	27.50	26.20	34.90	40.80	32.40	35.00	n.d.	100.00	n.d.	n.d.	n.d.	n.d.
An	n.d.	0.60	0.30	1.20	0.70	1.30	2.10	2.70	1.40	n.d.	n.d.	n.d.	n.d.	n.d.	n.d.
Or	90.70	29.06	62.50	71.28	73.15	63.82	57.09	64.86	63.60	100.00	n.d.	100.00	100.00	100.00	100.00

Table 9. Sanidine and heterogeneous alkaline feldspar analysis from Upper felsic association – Acampamento Velho Formation welded tuffs. Data obtained through the electron microprobe and scanning electron microscope: inter = intermediary; In Mt = analyses made in magnetite that is substituted by sanidine of the matrix. n.d. = not detected. (Almeida et al., 2007).

Almeida et al. (2007) mentioned for felsic rocks the crystallization sequence: (1) zircon, (2) Ti-rich magnetite, (3) sanidine and (4) quartz. The introduction of late Na-rich fluids generated the formation of (5) heterogeneous alkali-feldspar, (6) ilmenite and rutile from the Ti-rich magnetite, (7) albite in the spherulites and finally generated, the alteration of sanidine, vitroclasts and pumice to (8) illite.

4.3 Geochemistry of major, trace and Rare-Earth elements

Almeida et al. (2002, 2003a) already published the Acampamento Velho Formation geochemical characteristics and the text above is a synthesis of mentioned papers.

Twenty samples were analyzed for major, trace and Rare-Earth elements using Argonium Plasma Spectrometry (ICP) at Activation Laboratories LTD (ACTLABS, Canada). The results shown in Table 11 correspond to four samples of the basalts and andesitic basalts, two of the tuffs, four of the welded tuffs and ten of the rhyolitic flows.

For the Lower Mafic Association group (Table 11), whole-rock analyses show a SiO₂ average content of 49.5 wt%; Na₂O = 4.3 wt%, K₂O = 0.8 wt% and CaO = 3.1 wt%. The REE behaviour points out to a moderate alkaline character with high La/Yb_N ratios (5.3 < La/Yb_N < 7.4, average of 6.2) and Eu/Sm_N ratios (0.7 < Eu/Sm_N < 0.8, average of 0.8). The LREE patterns show relatively low fractionation (2.2 < La/Sm_N < 3.1, average of 2.7) with a very slight negative Eu anomaly (0.9 < Eu_N/Eu* < 0.8, average of 0.9) (Table 11, Fig. 17a).

Sample	123a2a	123a2b	123a2c	123a2d	333b1a	333b1b	33b2a	333b2b	69.2-1a	69.2-1b	69.2-2a	69.2-2b	ps60-1a	ps60-3
Location	bright core	dark core	bright rim	dark rim	core	rim	core	core	core	rim	core	rim	core	matrix
	heterogeneous alkaline feldspars				sanidine		albita		albita		albita		sanidine	albita
SiO ₂	64.12	67.78	64.57	67.78	64.08	64.08	86.11	84.45	68.65	68.57	67.99	68.29	64.51	67.56
Al ₂ O ₃	18.31	19.72	18.47	19.10	18.26	18.43	8.36	9.58	19.54	19.77	19.52	19.35	18.40	19.45
FeO	n.d.	n.d.	n.d.	n.d.	n.d.	n.d.	n.d.	0.67	n.d.	n.d.	n.d.	n.d.	n.d.	0.67
Na ₂ O	0.35	11.71	0.28	11.21	0.45	0.25	4.33	4.68	11.60	12.10	11.77	11.64	n.d.	11.24
K ₂ O	16.36	0.18	16.6	1.11	16.32	16.73	0.43	1.39	n.d.	n.d.	n.d.	0.08	19.72	1.48
Total	99.14	99.39	99.92	99.20	99.11	99.49	99.23	100.43	99.79	100.35	99.28	99.36	99.63	100.37
Si	2.99	2.98	2.99	3.00	2.99	2.99	4.50	4.41	3.00	2.99	2.99	3.00	3.00	2.97
Al	1.01	1.02	1.01	1.00	1.01	1.01	0.52	0.59	1.01	1.02	1.01	1.00	1.01	1.01
Fe ₂	n.d.	n.d.	n.d.	n.d.	n.d.	n.d.	n.d.	0.02	n.d.	n.d.	n.d.	n.d.	n.d.	0.02
Na	0.03	1.00	0.03	0.98	0.04	0.02	0.44	0.47	0.98	1.01	1.00	0.99	n.d.	0.96
K	0.97	0.01	0.98	0.06	0.97	1.00	0.03	0.09	n.d.	n.d.	n.d.	n.d.	0.99	0.08
Cations	5.00	50.10	5.01	5.04	5.01	5.02	5.49	5.58	4.99	5.02	5.00	4.99	5.00	5.04
X	4.00	4.00	4.00	4.00	4.00	4.00	5.02	5.00	4.01	4.01	4.00	4.00	4.01	3.98
Z	1.00	1.01	1.01	1.04	1.01	1.02	0.47	0.58	0.98	1.01	1.00	0.99	0.99	1.06
Ab	3.00	99.00	3.00	94.20	4.00	2.00	93.60	83.90	100.00	100.00	100	100	n.d.	92.30
An	n.d.	n.d.	n.d.	n.d.	n.d.	n.d.	n.d.	n.d.	n.d.	n.d.	n.d.	n.d.	n.d.	n.d.
Or	97.00	0.99	97.03	5.77	96.04	98.04	6.38	16.07	n.d.	n.d.	n.d.	n.d.	100.00	7.69

Table 10. Sanidine (electron microprobe), albite and heterogeneous alkaline feldspar analysis from Upper Felsic Association – Acampamento Velho Formation rhyolitic lavas. n.d. = not detected. (Almeida et al., 2007).

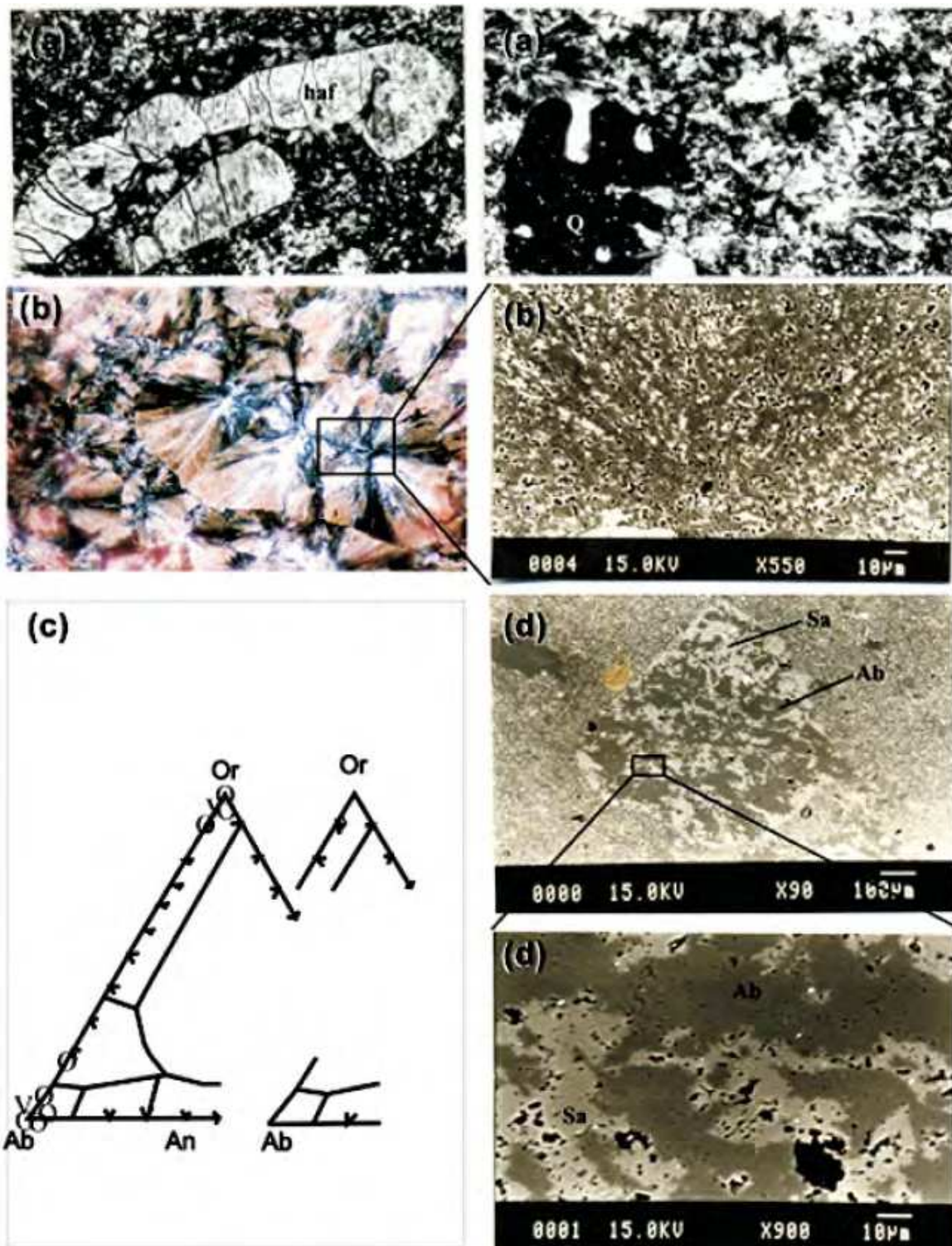


Fig. 16. Rhyolite flows: (a) Photomicrography of heterogeneous alkali-feldspar (haf) and quartz (Q) phenocrysts with gulfs of corrosion and conchoidal fractures (optical microscope PL, 40 x); (b) Photomicrography of spherulites (optical microscope) with fine aggregates of anorthoclase and albite grains as well as Fe oxides (electron microprobe); (c) Ab-Or-An diagram (electron microprobe), O = core, x = rim, + = matrix, \diamond = bright core, ∇ = dark core, \square = bright rim, Δ = dark rim; (d) Photomicrography of heterogeneous alkali-feldspar phenocryst and its detailed view (electron microprobe).

For the Upper Felsic Association, the tuff samples show a SiO₂ average of 73 wt%, with a low alkalinity (average of Na₂O = 1.5 wt% and K₂O = 3.9 wt%), and high CaO content (2.9 wt%). The light Rare Earth element pattern shows slight fractionation ($1.6 < La/Sm_N < 7.9$, average of 4.7), with a variable Eu negative anomaly ($Eu_N/Eu^* = 0.1$ to 0.3, average of 0.2). The welded tuffs are also highly siliceous with SiO₂ average of 78 wt%, low CaO content (average of 0.1 wt%) and the alkalinity higher than tuffs (Na₂O average = 1.7 wt% and K₂O = 5.7 wt%). The Rare Earth element behaviour is similar to the tuffs, although they present much more pronounced light Rare Earth element fractionation ($4.1 < La/Sm_N < 21.2$, average of 7.2) and an important Eu negative anomaly ($0.1 < Eu_N/Eu^* < 0.2$, average of 0.1) (Table 11, Fig. 17b).

Likewise, the rhyolitic flow samples are also siliceous, with SiO₂ average of 77 wt%, low CaO content (average of 0.2 wt%) and normal alkalinity, although these rocks are more sodic than the pyroclastic ones (Na₂O average = 2.2 wt% and K₂O = 5.3 wt%). The REE pattern is similar to the tuffs and welded tuffs, with LREE fractionation ($1.7 < La/Sm_N < 12.2$, average of 4.5) and Eu negative anomaly ($0.1 < Eu_N/Eu^* < 0.3$, average 0.1) (Table 11, Fig. 17b).

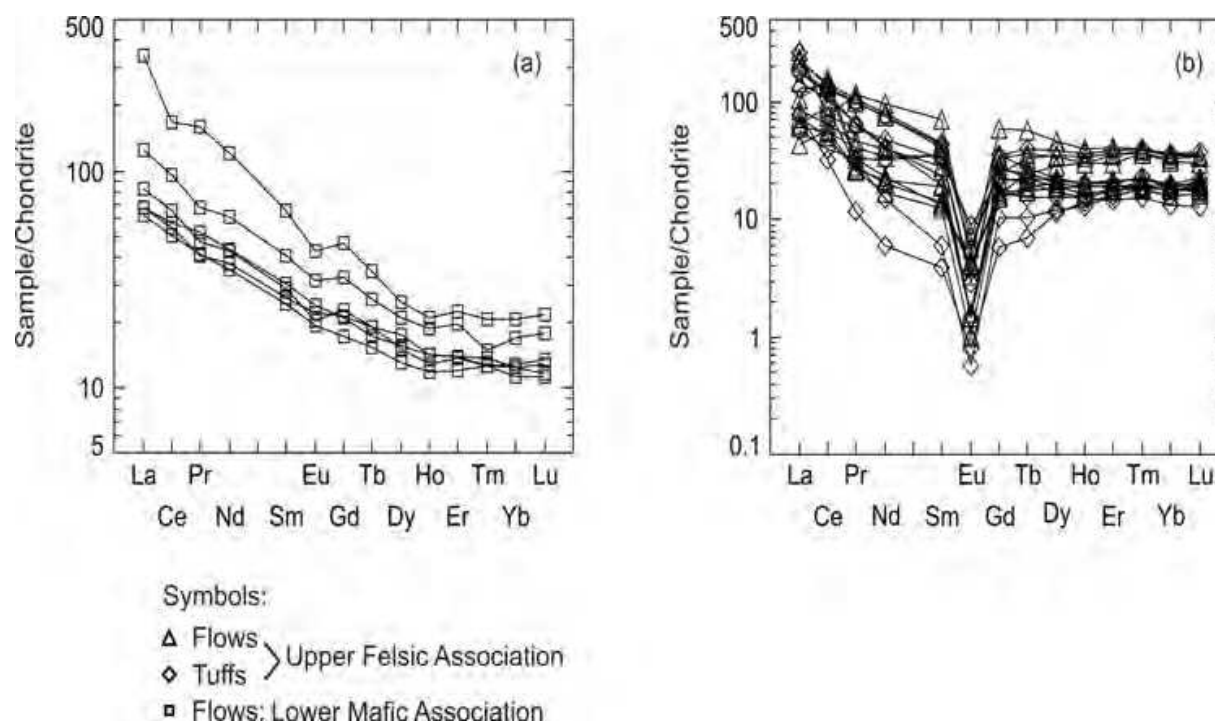


Fig. 17. Chondrite diagram normalized by Rare Earth element (Taylor and MacLennan, 1985) (Almeida *et al.* 2002) for the Acampamento Velho Formation showing a similar pattern for both associations, except for the strong negative Eu anomaly in the Upper Felsic Association rocks. (a) Lower Mafic Association; (b) Upper Felsic Association. (Almeida *et al.*, 2002, 2003a).

	Basalt – Andesitic basalt					Tuff		Welded tuff			
	MH9	MH13	MH14	SSB-7	SSB-32B	MH15	SSB-14	MH31	MH37	MH41	SSB-13
SiO ₂	47.05	51.48	54.31	48.84	45.72	78.54	67.64	77.46	77.05	76.59	81.73
TiO ₂	1.57	1.53	2.19	1.41	1.88	0.09	0.44	0.12	0.11	0.14	0.11
Al ₂ O ₃	16.49	15.59	12.12	15.19	14.75	9.39	11.45	11.3	11.47	11.49	9.08
Fe ₂ O ₃	8.84	9.13	6.44	9.73	10.63	0.95	3.29	1.87	1.56	2.22	2.08
MnO	0.12	0.07	0.17	0.15	0.15	0.03	0.07	0.01	0.01	0.01	0.01
MgO	5.57	4.23	2.14	4.2	6.19	0.28	0.95	0.08	0.09	0.13	0.03
vCaO	6.31	1.29	5.71	4.96	8.05	1.94	4.03	0.08	0.09	0.05	0.03
Na ₂ O	4.38	5	4.5	4.93	2.71	1.97	1.1	2.26	1.78	2.41	0.4
K ₂ O	0.77	0.63	1.2	1.34	0.35	3.74	4.18	5.56	5.5	5.54	6.42
P ₂ O ₅	0.27	0.28	0.41	0.26	0.41	0.01	0.1	0.02	0.02	0.04	0.04
LOI	8.84	7.62	9.29	8.84	9.58	2.81	6.26	1.07	1.34	1.31	1.04
Total	99.81	99.85	99.49	99.84	100.43	99.77	99.51	99.91	99.02	100.1	100.96
Ba	240	174.9	353.3	203	355	225	270	92.8	158.9	137.8	247
Rb	12.1	13.8	26	30	29	158.3	167	101.7	97.2	91.6	141
Sr	519	279.7	225.7	111	555	86.6	87	33.8	39.7	45.4	41
Ta	0.58	0.8	0.86	0.49	0.55	1.9	1.13	1.09	1.08	1.05	1.29
Nb	9.6	11.5	16.2	6	10	17.7	15	17.6	18	17.1	6
Hf	5	5.5	7.9	4.3	4.8	4.2	6.5	7.2	7.2	7.8	7.5
Zr	207.1	231.1	330.3	169	197	127.2	191	207.5	233	236.5	134
Y	31	32	42	28	32	91	38	30	35	36	13
Th	3.45	3.03	4.19	2.7	1.5	11.21	9.7	9.37	6.32	9.1	11
La	25.1	30.6	45.9	23	25	21.3	97	47.3	28.5	64	66
Ce	52.2	63	92.3	48	55	37.8	72	127.2	30.9	113.4	121
Pr	5.54	6.45	9.33	5.64	7.09	4.52	8.24	4.28	1.6	8.86	13.5
Nd	26.5	30.6	43.6	25	31	22.6	34	10.5	4.2	29.1	54
Sm	6	6.6	9.4	5.6	7	8.1	7.7	1.4	0.9	5.5	10
Eu	1.93	1.77	2.73	1.7	2.09	0.25	0.77	0.05	0.07	0.13	0.47
Gd	6.5	7	9.9	5.3	6.4	10.7	6.9	3.2	1.8	5.2	8.1
Tb	1.1	1.1	1.5	0.9	1	2.3	1.2	0.6	0.4	0.9	1.4
Dy	6.7	5.8	8	5	6	14.7	6.4	4.6	4.3	5.9	8.2
Ho	1.2	1.1	1.6	1	1.2	3.1	1.3	1.1	1.2	1.3	1.7
Er	3.5	3.4	4.9	3	3.5	9.6	3.6	3.9	4	4.4	5
Tm	0.45	0.45	0.53	0.45	0.49	1.42	0.55	0.63	0.82	0.67	0.82
Yb	3.2	3.1	4.2	2.8	3.1	9.1	3.3	4	4.4	4.4	4.9
Lu	0.51	0.49	0.68	0.43	0.44	1.41	0.49	0.84	0.69	0.71	0.77

Table 11. Acampamento Velho Formation. Geochemical analyses of the major, trace and Rare Earth elements (Almeida *et al.*, 2002). These analyses were performed at Activation Laboratories (ACTLAB), Canada, using the Argonium Plasma Spectrometry - ICP. MH = Cerro do Bugio and Perau samples; SSB = Serra de Santa Bárbara samples. Major elements values are in percent (wt%); trace and Rare Earth elements are in part per million (ppm).

	Rhyolitic Flows									
	MH20	MH21B	MH22	MH25	MH27	MH50	MH53	MH60	MH7	SSB-1B
SiO ₂	78.97	80.6	78.15	79.26	76.26	75.76	76.85	76.37	77.26	77.79
TiO ₂	0.07	0.07	0.09	0.09	0.09	0.12	0.13	0.13	0.12	0.14
Al ₂ O ₃	10.9	8.52	10.07	11.48	11.32	11.73	12.29	12.34	11.67	11.77
Fe ₂ O ₃	1.84	1.49	2.19	1.56	1.67	1.59	1.69	1.48	1.7	2.77
MnO	0.01	0.01	0	0.01	0.01	0.02	0.02	0.02	0.02	-0.01
MgO	0.08	0.02	0.01	0.11	0.06	0.11	0.08	0.1	0.1	0.06
vCaO	0.03	0.02	0.01	0.21	0.12	0.96	0.06	0.17	0.06	0.06
Na ₂ O	2.98	0.26	0.34	3.32	3.76	2.53	2.7	2.5	0.14	0.81
K ₂ O	4.18	6.41	7.87	3.9	4.75	5.26	5.49	5.36	5.01	5.37
P ₂ O ₅	0.01	0.02	0.01	0	0	0.01	0.02	0.01	0.03	0.02
LOI	0.68	0.94	0.76	0.75	0.41	1.45	1.12	1.33	2.8	1.9
Total	99.76	98.37	99.51	100.7	98.45	99.56	100.1	99	98.92	100.7
Ba	60.3	72.3	52	139.4	128.6	312.8	428.1	369.1	136.2	190
Rb	100.3	140.5	176.7	127.6	148.3	149	128.4	144.6	119.7	141
Sr	35.8	49.5	36.5	40.3	28	34.9	54.1	52.7	23.2	43
Ta	2.03	1.68	1.63	2.23	2.23	1.47	1.48	1.38	1.38	1.99
Nb	20	26	28.4	13	18	21	21.1	12	20	24
Hf	11.5	7.9	9.9	13.3	13.9	7.8	8.1	7.3	6.9	16
Zr	172	270	343.4	196	233	276	253.1	189.2	254	601
Y	45	55	85	114	35	57	46	42	46	75
Th	14.33	15.55	12	16.6	14.53	13.98	13.07	13.28	12.73	15
La	26.4	30.8	54.4	98.1	16	81.4	39	23.8	85.2	22
Ce	48.3	62.3	99.7	72.9	54.9	136	151.6	85.9	127.6	53
Pr	3.55	6.27	9.25	15.98	3.64	14.34	4.55	3.87	13.65	5.64
Nd	12	28.3	30.3	68	15.1	57.4	16.5	14.5	53.4	24
Sm	2.9	6.5	4.6	16.6	4.4	10.5	3.1	3.2	9.5	8
Eu	0.09	0.13	0.14	0.38	0.13	0.62	0.35	0.36	0.5	0.29
Gd	4.7	6.5	7.4	17.9	5	10.8	5.4	4.7	8.8	10
Tb	1.1	1.3	1.9	3.3	1.4	1.6	1	1	1.3	2.1
Dy	7.7	8.1	13.4	17.6	10.9	8.5	7.1	7	7.2	13
Ho	1.6	1.7	2.9	3.4	2.6	1.7	1.6	1.6	1.4	2.6
Er	4.8	5.2	9.1	10.1	8.8	5.4	4.8	4.8	4.5	7.5
Tm	0.65	0.79	1.3	1.42	1.36	0.76	0.7	0.68	0.64	1.28
Yb	4.4	4.9	8.2	8.9	8.6	5	4.7	4.4	4	7.6
Lu	0.68	0.78	1.28	1.35	1.31	0.84	0.73	0.66	0.62	1.14

Table 11. Continuation.

The light Rare Earth element fractionation in the rhyolitic flows is slighter than that observed at welded tuffs and very similar to the tuffs ($1.7 < La/Sm_N < 12.2$, average of 4.5). The Eu anomaly is similar to that of the welded tuffs (Fig. 17b). The Upper Felsic Association Rare Earth element diagram exhibits values corresponding to the evolved rocks, similar to those of Culler & Graf (1984). The rocks show moderate fractionation and clear

parallelism, especially of heavy Rare Earth element and confirm the alkaline character. The increasing values of Rare Earth element and the marked negative Eu anomaly are common in the felsic rocks associated with mafic one. According to Almeida *et al.* (2002, 2003a), the Acampamento Velho Formation bimodal volcanism is characterized by the presence of dominant acid and subordinated mafic rocks, with overall absence of rocks with SiO₂ content between 54 wt% and 67 wt%. The Nb x Zr and Y x Zr diagrams (Fig. 18) show different evolutionary trends for the mafic and felsic successions, reinforcing the bimodal character of this magmatism.

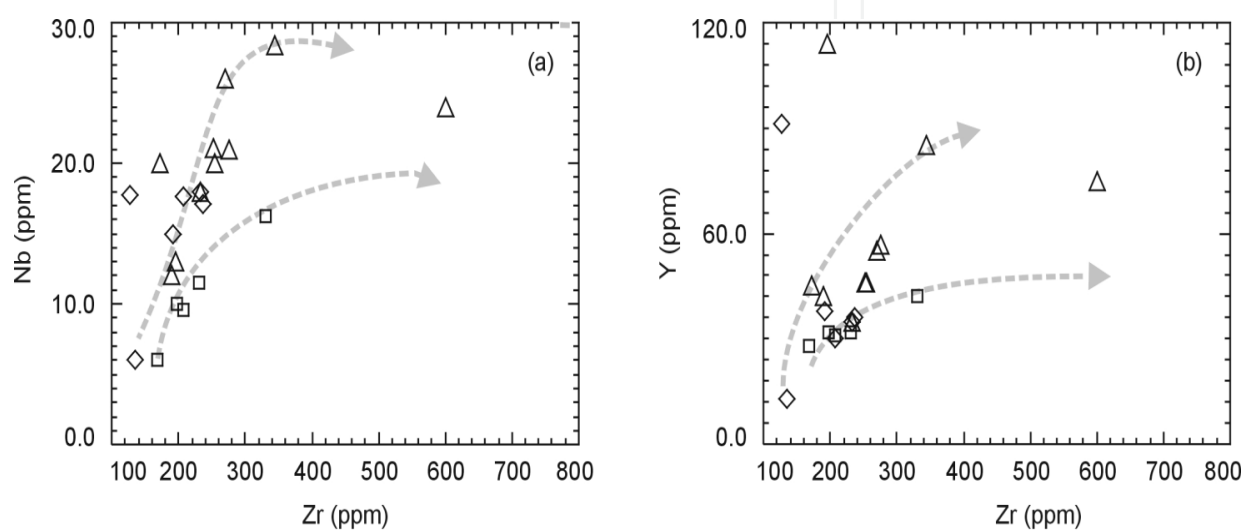


Fig. 18. Pearce and Norry (1979) plotting shows two distinct evolutionary trends for Lower Mafic Association and Upper Felsic Association from Acampamento Velho Formation (Almeida *et al.* 2002). (a) Zr versus Nb and (b) Zr versus Y. Symbols are the same as in figure 17.

5. Rodeio Velho Member: Geological context, petrography and geochemistry

The Rodeio Velho Formation (*sensu* Ribeiro *et al.*, 1966) has been described as bearing at least three vesicular andesite flows, with thickness estimated at 100 m and no evidence of explosive activity. However, it was observed that the Rodeio Velho Member manifested itself as flows, pyroclastic deposits and shallow intrusions. There are few petrographic and geochemical studies on the Rodeio Velho Member. Silva Filho (1996) showed the intrusive character of the magmatism, rejecting former ideas of an exclusively volcanic event. Fragozo Cesar *et al.* (2000) named these rocks as Rodeio Velho Intrusive Suite, which are represented by tabular intrusions within the sub-horizontal continental deposits of the Guaritas Group. Lopes *et al.* (1999) mentioned its occurrence in subsurface at the CQP-1-RS probing, North Camaquã Mines, where reach 119.50 thickness. Almeida *et al.* (2000, 2003) studied this event at the following areas within Camaquã Basin (Fig. 1): (i) Santa Bárbara Sub-basin: in the South-centre and North-centre portions from Arroio Santa Bárbara and Arroio Carajás, (ii)

Guaritas Sub-basin: at the Minas do Camaquã, Rodeio Velho, Passo do Moinho and Pedra da Arara regions and Arroio dos Neves drainage line.

5.1 Geological setting

The studied regions are localized in Southeast, South and Southwest Caçapava do Sul city (RS), in the Camaquã Basin (Fig.1). The text is a synthesis of Almeida et al. (2000, 2003a and 2003b).

5.1.1 Santa Bárbara sub-basin

The Rodeio Velho Member volcanic rocks are localized South-centre and North-centre portions from Arroio Santa Bárbara and Arroio Carajás (topographic map, respectively). This event presents four volcanic cones opens to SE and lined up NNE-SSW direction, parallels to the regional flow directions, evincing the structural control in the positing of these cones. Ejected bombs and blocks of vesicular basaltic andesitic rocks, local concentrations of jasper, chalcedony and geodes are present throughout the area. They probably represent the end of a strombolian-type event associated with the evolution of the cones. The preservation of this structure is regarded as due to the presence of younger sedimentary rocks across the region. These sedimentary rocks include arkosic sandstones, conglomeratic sandstones, and conglomerates. They correspond to the sedimentation named as Varzinha Alloformation (or Formation) from the Guaritas Allogroup (Table 1). An elliptical caldera that shows its longest axis about 7.2 km NNE-SSW and it is found in the surrounding of the cones. (Fig. 19).

To the West and South of the cones, Rodeio Velho Member basaltic dykes intrude the sediments building the Lanceiros Alloformation when they are solidified. These layers of the basaltic rocks, sub-vertical and preferentially aligned to N26°E, are massive in the centre and vesicular along the borders. They have been interpreted as a Rodeio Velho Member intrusive manifestation. However, considering that a dyke-sandstone contact was found in the sandstones vesicles, which was probably generated by gases coming from the magma and suggests that the sediment was still unconsolidated, so, the Rodeio Velho Member volcanism would be contemporary with the formation of the sandstone from Pedra Pintada Formation. 2 km to the South of the cones, in the Carajás Creek, the Rodeio Velho Member also crops out as lava flows, showing *aa* and *pahoehoe* structures with centimetric to decimetric hollow tubes, as well as amygdales and/or vesicles that are up to 5 mm long at the base and top of each flow (Fig. 20a). The sedimentary rocks layers are mainly composed of middle granulometry to fine sandstones and show crossed stratification of very low angle. Levels of pelites associated to this sandstone show feature of subaerial exposure with contraction cracks (Fig. 20b).

Rodeio Velho Member is positioned as a flow that went through the dunes, when the solidification occurs, the structure looks like an intrusion of the volcanic in the sedimentary rocks, but they correspond to a volcano-sedimentary interaction of the Rodeio Velho Member and Pedra Pintada Formation, and rhythmites from Guaritas Group (Fig. 21a). The volcano-sedimentary interaction features include also flow striation, xenoliths, clastic dykes, marks in increasing and peperites (Figs. 21 b, 21c and 21d). Based on field characteristics, it seems that the emitting centers would be exactly at the cones, which are 2 km North and open towards the South (Almeida et al., 2000).

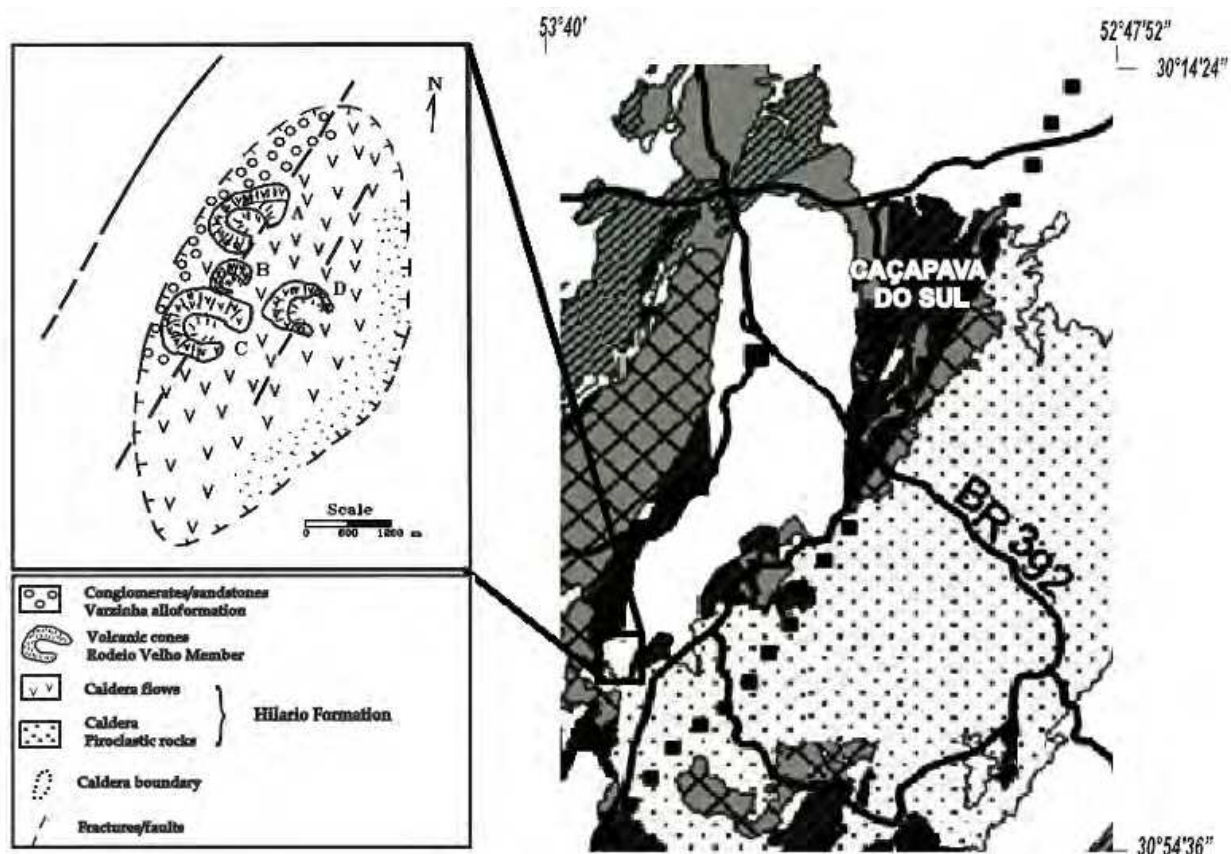


Fig. 19. Map for Camaquã Basin area showing the caldera and cones (Rodeio Velho volcanic rocks) location in the Camaquã Basin context. Modified from Almeida et al., 2003b.

5.1.2 Guaritas sub-basin

The Rodeio Velho Member are located at Minas do Camaquã, Rodeio Velho, Passo do Moinho and Pedra da Arara regions, and Arroio dos Neves drainage line (Fig. 1). These volcanic rocks show flows interdigitated in Pedra Pintada Alloformation rhythmites and the volcano-sedimentary interaction. Field observations indicate a contemporaneity between sedimentation and volcanism. The peperites, flux channels, clastic dykes and other features development suggest interaction between hot lava and wet poorly consolidated sediments. In Pedra de Arara area (Fig. 22a), it is observed the same structure found at Arroio Carajás region with volcanic rock positioned as the flow that went through the dunes, when the solidification occurred. The structure looks like an intrusion of the volcanic in the sedimentary rocks, but they correspond to an volcano-sedimentary interaction in this area with peperites in the sandstone-volcanic rock contact. Immediately above, at Passo do Moinho (South Pedra da Arara, Fig. 1), the sandstones are restricted to the enclaves and clastic dykes (Fig. 22b).

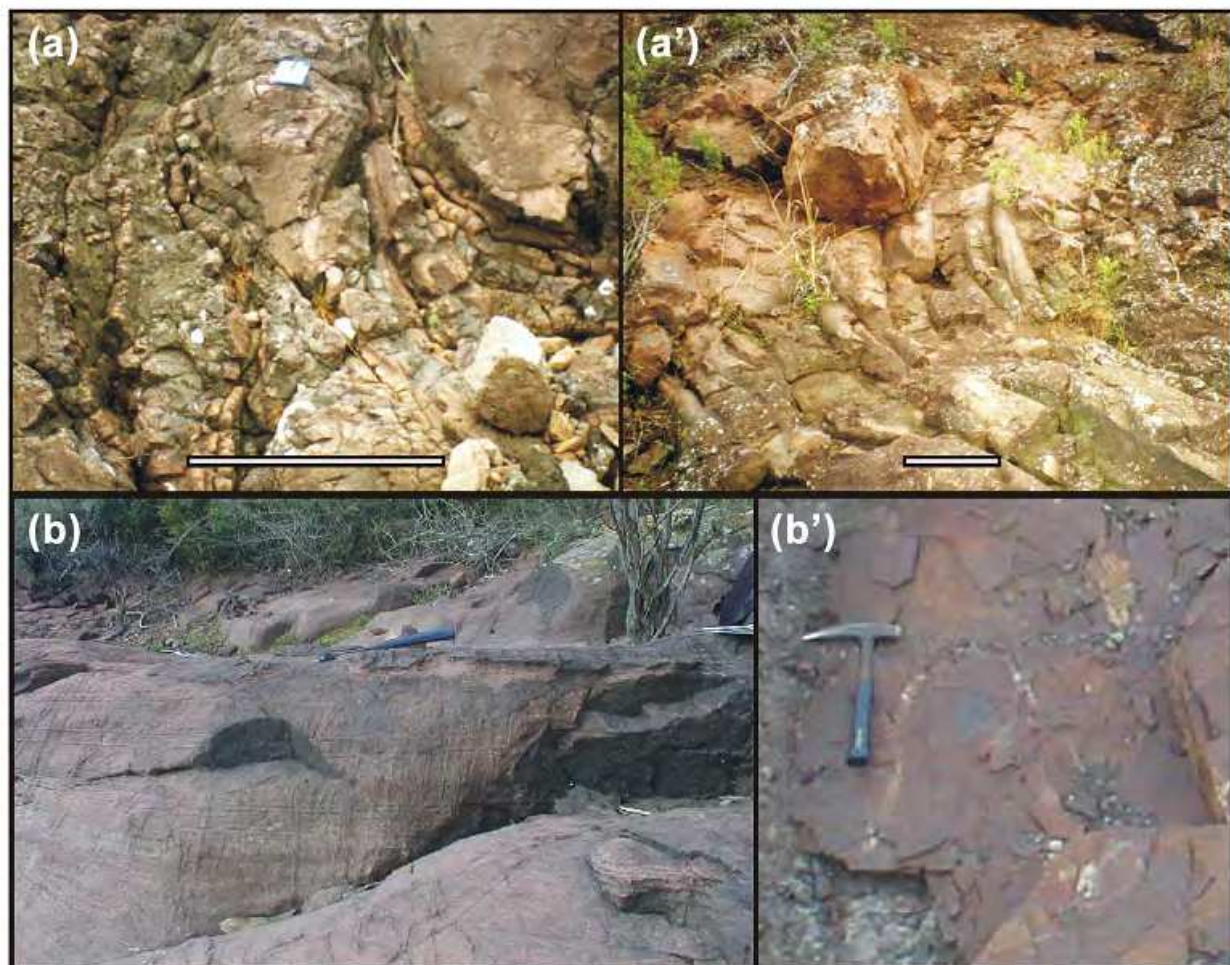


Fig. 20. Carajás Creek: (a) *pahoehoe* lavas downstream of the Arroio Carajás. The scale measures (a) 1 m and (a') 10 cm. (b) - sedimentary lithologies: sandstone with plane-parallel lamination masked by intense fracturing and (b') pelite with contraction cracks (in Petry, 2006).

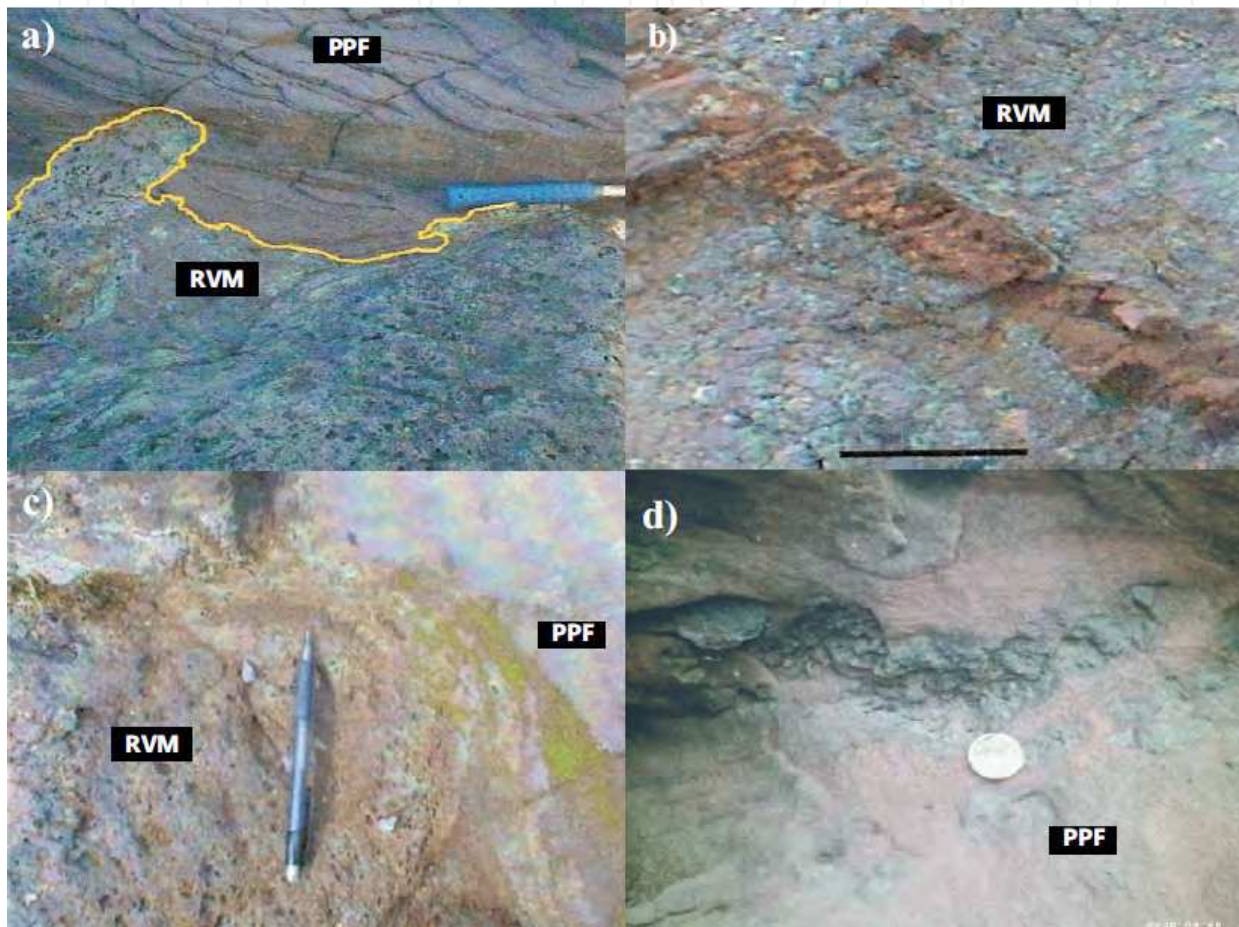


Fig. 21. Volcano-sedimentary interaction features found at Arroio Carajás outcrops – Santa Bárbara Sub-basin: a) volcanic rock (Rodeio Velho Member) and sandstone (Pedra Pintada Formation) positioned as a flow that went through the dunes; b) sandstone clastic dyke in amygdaloidal lava; c) marks in increasing; d) peperite with basaltic clasts evidencing the plasticity.

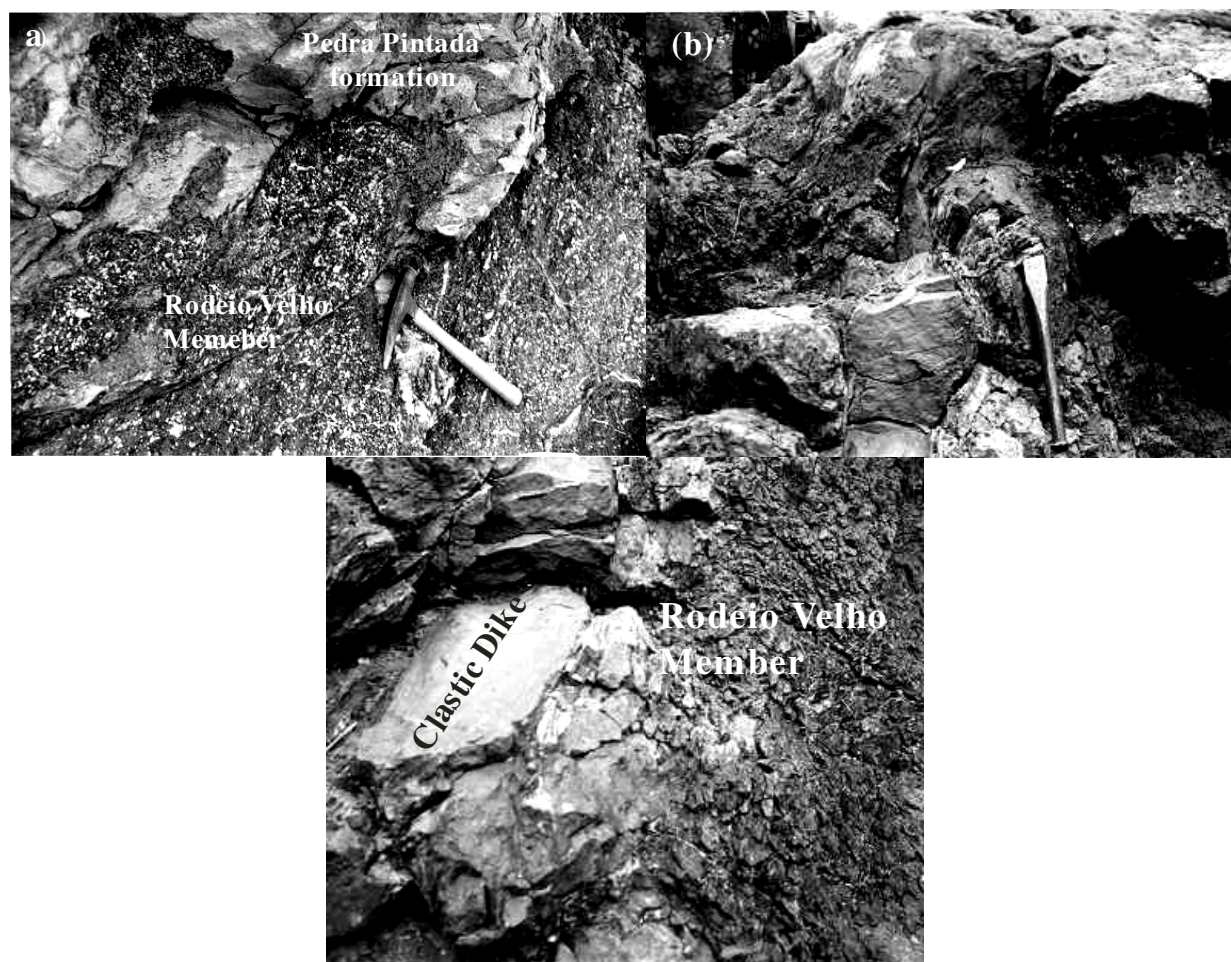


Fig. 22. Photos showing the several styles of the positioning from Rodeio Velho Member and the volcano-sedimentary interaction features found at Guaritas Sub-basin. a) – volcanic rock (Rodeio Velho Member) and sandstone (Pedra Pintada Formation) positioned as a flow that went through the dunes in Pedra da Arara area. (b) – Detail showing the clastic sandstone dike in amygdaloidal lava at Passo Moinho area.

5.2 Mineralogy and petrography

According to Almeida et al. (2000), the RVM is characterized by mafic and intermediate lava flows, pyroclastic deposits and intrusions. Petrographically, these rocks are andesites, subalkaline basalts and trachyandesites. The rocks show pyroclastic, vitrophyric or ophitic textures, with glomeroporphyritic euhedric to subhedric plagioclase phenocrysts. The plagioclase shows size around 0.5 mm, and is generally altered to carbonate and can be oriented within the matrix. Relics of euhedric pyroxene, olivine and opaques (Ti-magnetite and other Fe-Mn oxides) are present and show sizes that vary from 0.3 to 0.1 mm. Accessory minerals such as apatite and zircon are observed. Intersertal glass is recrystallized (forming spherulites) or altered. The presence of vesicles and amygdales is common and the sizes vary from 0.5 to 10 mm. The amygdales are filled with quartz and carbonate or both of them. The quartz precedes the carbonate. Pyroclastic rocks are stratified and vary from ash-flow tuffs to lapillites, brecciated and poorly sorted. Shards and fiammes attest to the pyroclastic character. Plagioclase and euhedral quartz crystalloclasts (<2%) are dispersed in the tuffaceous, partially glassy matrix.

5.3 Geochemistry

Almeida et al. (2000, 2003a and 2003b) already published the complete Rodeio Velho Member geochemical characteristics. The text above is a synthesis of mentioned papers.

The chemical analysis data are shown in Table 12. Considering the high alteration level present in the Rodeio Velho Member rocks, only trace and Rare earth elements were used in the diagrams.

Amostra	PH-3	PH-4	PH5	PM49	PM54	RLP1	RLP10	RLP12	RLP14	RLP15	PLR17
	1	2	3	4	5	6	7	8	9	10	11
SiO ₂	50.14	65.53	48.55	51.47	52.93	51.89	57.12	52.33	51.69	54.63	46.84
TiO ₂	2.15	1.82	1.71	2.71	2.13	1.66	2.24	1.83	1.856	1.807	2.099
Al ₂ O ₃	14.64	12.7	14.14	15.69	16.2	15.75	14.58	15.77	15.79	15.34	15.77
Fe ₂ O ₃	11.63	6.28	9.77	13.6	13.89	8.92	10.26	8.42	10.61	11.17	12.14
MnO	0.16	0.1	0.17	0.16	0.1	0.26	0.13	0.09	0.07	0.08	0.09
MgO	4.35	0.85	0.34	1.1	1.87	1.66	1.53	4.11	2.96	0	3.68
CaO	7.4	1.99	7.64	2.45	1.04	6.57	3.3	4.97	5.18	2.68	8.26
Na ₂ O	3.45	6.01	3.34	6.36	7.57	4.59	7.6	3.89	3.78	3.9	3.7
K ₂ O	1.24	1.06	6.27	1.95	0.88	2.75	0.26	2.24	2.2	5.56	1.43
P ₂ O ₅	1.18	1.2	0.91	1.41	0.36	1.05	1.4	1.08	1.1	1.08	0.85
LOI	3.22	1.42	5.95	2.14	2.35	4.57	1.73	3.89	3.59	2.05	4.51
total	99.56	98.94	98.78	99.05	99.32	99.68	100.15	98.62	98.83	98.83	99.37
Ba	1780	2695	2204	2093	344	1124	673	1150	1142	1560	1140
Rb	15.6	13.9	94.1	28	17	40	4.5	29	28	91	26
Sr	1186	276	222	824	328	558	454	775	808	387	805
Ta	1.36	1.18	1.18	2.1	0.94	1.03	1.67	1.2	1.3	1.2	1.2
Nb	30.2	25.5	27.9	36	19	19	25	27	27	25	20
Hf	7.4	2.5	3.4	8.5	3.3	8	7.8	8.3	7.9	7.5	3.8
Zr	461	399	360	380	185	383	369	395	384	367	164
Y	54	48	36	84	27	51	41	42	41	36	28
Th	3.47	2.61	3.41	3.7	1.4	2.9	3	3.2	3.2	3.1	1.6
La	102.7	86.9	84.5	104	40	136	104	76.6	77.1	80.6	42.8
Ce	204.7	164	168	186	76	217	201	148	145	151	91.3
Pr	20.13	16.53	16.65	23.8	11	26.6	23.8	19.5	19.6	19	11.8
Nd	91.7	75.2	72.7	95	45	108	97	70.4	70	66.8	45.1
Sm	16.2	13.7	12.2	17	8.5	17	16	12	11.7	10.6	8
Eu	4.81	4.02	3.52	4.81	2.52	4.45	4.46	3.58	3.43	3	2.88
Gd	14.5	12.8	11.2	15	6.8	12	11	10.1	9.7	8.7	6.8
Tb	2	1.8	1.4	2.2	1	1.7	1.6	1.5	1.4	1.3	1
Dy	10	8.9	6.8	12	5.5	8.9	7.6	8.1	7.7	6.8	5.8
Ho	1.9	1.8	1.3	2.4	1	1.6	1.4	1.5	1.5	1.3	1.1
Er	5.4	5.2	3.7	7.1	2.9	4.6	3.7	4.3	4	3.6	3
Tm	0.65	0.59	0.45	0.94	0.39	0.61	0.49	0.57	0.56	0.51	0.41
Yb	4.5	3.8	3	5.5	2.4	3.5	2.9	3.5	3.4	3.1	2.5
Lu	0.73	0.6	0.47	0.85	0.34	0.57	0.45	0.52	0.49	0.46	0.36

Table 12. Geochemical analysis of the major, trace and Rare Earth elements (Almeida *et al* 2000). These analysis were performed at Activation Laboratories (ACTLAB), Canada, using the Argonium Plasma Spectrometry - ICP. (1,2, 3) = volcanic cone samples (4, 5) Rodeio Velho flow sample; (6) = Rincão da Tigra flow sample; (7) = flow sample obtained South of Passo Moinho; (8) = Rincão da Tigra flow sample; (9, 10) = Arroio dos Carajás flow sample; (11) = Arroio dos Neves flow sample.

The Rodeio Velho Member rocks were plotted in the Nb/Y versus Zr/TiO₂ classificatory diagram (Winchester & Floyd, 1977 - Fig. 23a), which allowed classify the flows as sub-alkaline basalts, andesites, trachyandesites, alkaline basalts and basaltic andesites. The pyroclastic rocks were classified as trachyandesites, and the epizonal as trachyandesites and alkaline basalts.

The REE pattern normalized by the chondrite (Nakamura, 1977- Fig. 23b) shows a similar behavior to the alkaline basalts and the values correspond to the evolved rocks (Culler & Graf, 1984), displaying a marked fractionation and parallelism between all the rocks. According to the data and the REE distribution, the light Rare Earth elements (LREE) enrichment occurs under conditions of low partial melting, especially from a source that contains garnet, suggesting a great deep for genesis of these rocks.

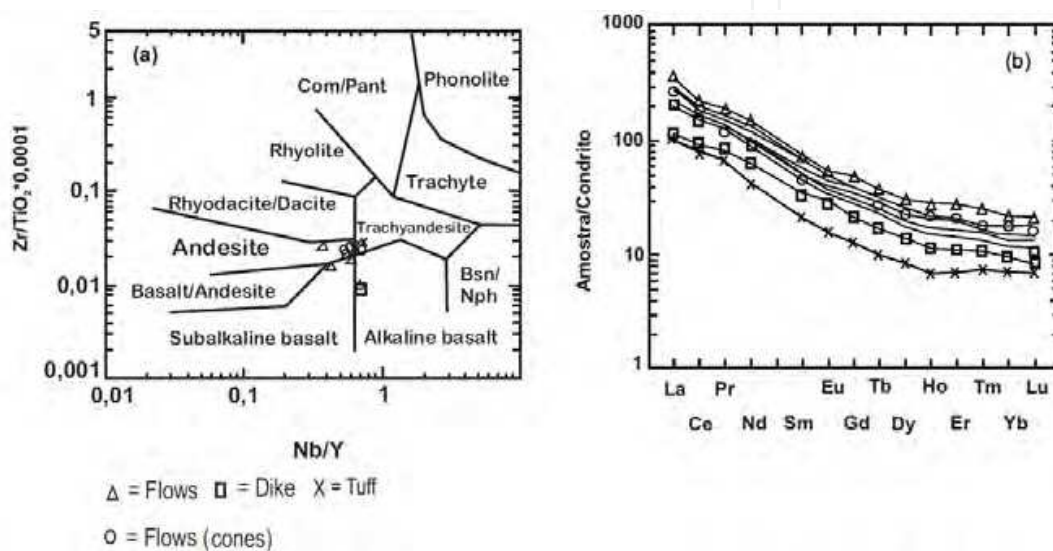


Fig. 23. (a) Zr/TiO₂ versus Nb/Y diagram (Winchester & Floyd, 1977) (b) Chondrite diagram normalized by REE (Nakamura 1977) (Almeida et al., 2000).

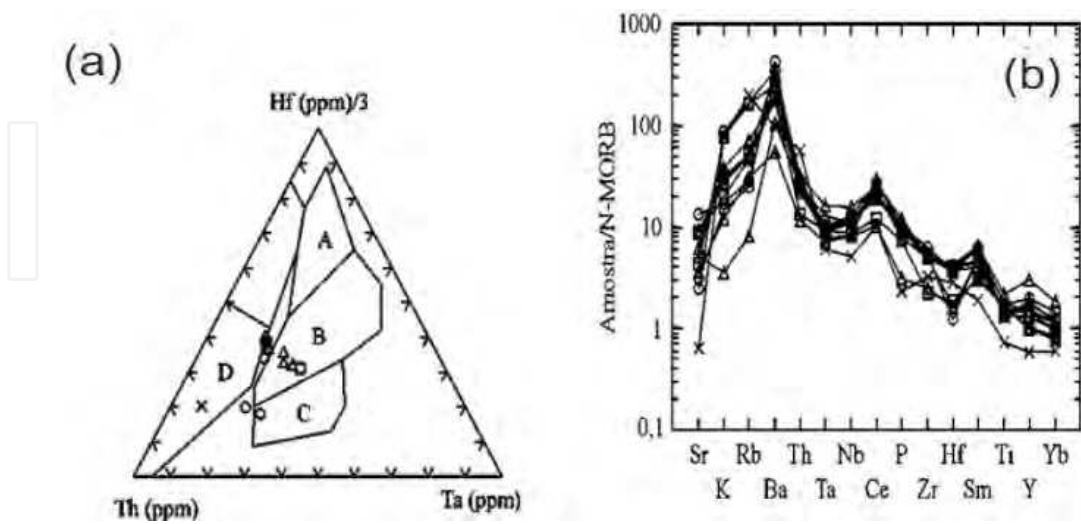


Fig. 24. (a) Tectonic discrimination diagram (Wood, 1980). A = MORB type N; B = MORB type E, tholeiitic WPB; C = alkaline WPB and differentiated; D = destructive continental margin basalts and differentiated. Legend for figure 23 (b) Multi-elements spiderdiagram normalized by Sun and McDonough (1989) values (Almeida et al., 2000).

Considering the chemical data, all the Rodeio Velho Member rocks are similar. Thus, the samples plotted on Hf/3 x Th x Nb/16 diagram (Wood, 1980 - Fig. 24a) show that the rocks were generated in a domain of intraplate continental basalts (alkaline and/or E-MORB type). This behavior is confirmed in the Zr/Y versus Zr diagram (Pearce & Norry, 1979) and in the spidergram normalized by N-MORB (Sun & McDonough, 1989 - Fig. 24b). These rocks probably were formed by fractionated crystallization, as indicated by the good correlation between the incompatible elements pairs, such as Ce versus Sm-La, and Zr versus Nb and Y.

6. Rb, Sr, Sm and Nd isotope data for Acampamento Velho Formation and Rodeio Velho Member

Almeida et al. (2005) already published the complete Acampamento Velho Formation and Rodeio Velho Member isotopic characteristics. The text above is a synthesis of the mentioned papers.

The isotopic results obtained in this study are shown in Table 13 and figures 25, 26, 27 and 28. The Acampamento Velho Formation lower mafic association samples show Rb contents between 12 and 83 ppm (average 32 ppm), and Sr contents vary from 23 to 703 ppm (average 309 ppm). Measured $^{87}\text{Sr}/^{86}\text{Sr}$ ratios in these rocks range from 0.707 to 0.731, while initial ratios, calculated for 550 Ma, are between 0.706 and 0.711. The Sm content varies from 5 to 13.7 ppm, and the Nd ranges between 22.9 and 78.2 ppm. Measured $^{143}\text{Nd}/^{144}\text{Nd}$ ratios are concentrated between 0.5116 and 0.5119, resulting on $\epsilon\text{Nd}_{(0)}$ from -9.3 to -16.6, and ϵNd ($t = 550$ Ma) of -2.9 to -10.3. TDM model ages lie between 1.11 and 1.78 Ga.

Tuffs and welded tuffs of the upper felsic association display Rb values of 91.6 to 167.0 ppm (average 126 ppm), and 36.2 to 98.8 ppm for Sr (average 55 ppm), compatible with acid volcanics. The measured $^{87}\text{Sr}/^{86}\text{Sr}$ ratios are high, between 0.745 and 0.771, while the initial values range from 0.701 to 0.713. They present low Sm and Nd contents (0.8 to 9.5 ppm and 4.1 to 43.8 ppm, respectively), and $^{143}\text{Nd}/^{144}\text{Nd}$ ratios from 0.511 to 0.512. The $\epsilon\text{Nd}_{(0)}$ lies between -11.9 and -16.4, while the ϵNd at the crystallization time ($t = 550$ Ma) ranges from -7.2 to -9.8. The TDM model ages for the pyroclastic rocks particulate fraction are 1.3 to 1.9 Ga. The rhyolitic lava flows of the upper felsic association show even higher Rb values (100 to 176 ppm, average 137 ppm) compared to Sr (13 to 55 ppm, average 39 ppm), with very high measured as well as initial $^{87}\text{Sr}/^{86}\text{Sr}$ ratios, respectively, 0.771 to 0.939 and 0.701 to 0.721. The $^{143}\text{Nd}/^{144}\text{Nd}$ ratios ranges from 0.511 to 0.512, corresponding to $\epsilon\text{Nd}_{(0)}$ values from -7.14 to -16.25, ϵNd (for $t = 550$ Ma) from -5.7 to -8.8 and T_{DM} ages between 1.3 and 2.1 Ga.

The Rodeio Velho Member rocks show low Rb (4.5 to 91 ppm, average 31 ppm) and high Sr contents 310 to 1203 ppm, (average 733 ppm), with low Sr isotopic ratios (0.705 to 0.710 measured, and 0.704 to 0.707 for initial $^{87}\text{Sr}/^{86}\text{Sr}$ calculated for 470 Ma.). The $^{143}\text{Nd}/^{144}\text{Nd}$ values concentrate between 0.51165 and 0.51193 correspond to strongly negative $\epsilon\text{Nd}_{(0)}$ from -13.89 to -19.36, ϵNd ($t = 470$ Ma) from -39 to -13.92, and T_{DM} model ages from 1.50 to 1.96 Ga. Plots of initial $^{87}\text{Sr}/^{86}\text{Sr}$ ratio against $^{143}\text{Nd}/^{144}\text{Nd}$ and ϵNd (Fig. 25) show different signatures for Rodeio Velho Member mafic lavas, Acampamento Velho Formation mafic lavas and felsic rocks. The Rodeio Velho Member mafic lavas show a variable radiogenic Nd and $\epsilon\text{Nd}(t)$ to a nearly constant radiogenic Sr (Fig. 25a). The opposite occurs with the Acampamento Velho Formation mafic lavas. The data in figure 25b show a negative correlation between radiogenic Sr and ϵNd for the Acampamento Velho Formation samples.

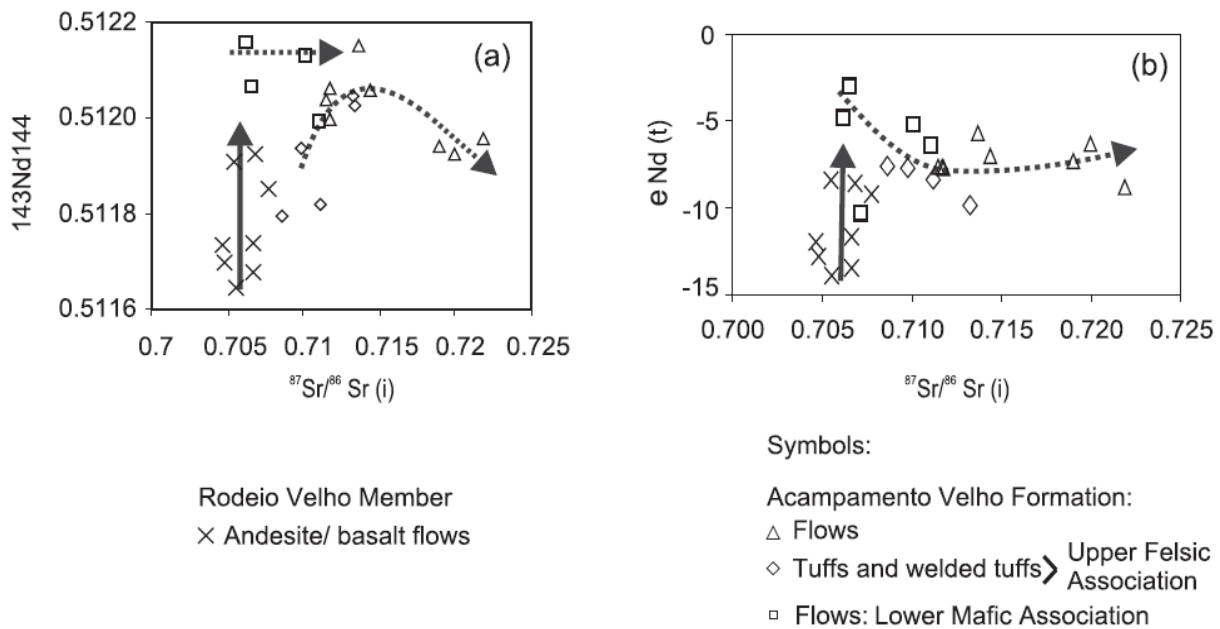


Fig. 25. (a) $^{144}\text{Nd}/^{143}\text{Nd}$ versus initial $^{87}\text{Sr}/^{86}\text{Sr}$ and (b) ϵNd versus initial $^{87}\text{Sr}/^{86}\text{Sr}$ isotope diagrams for Acampamento Velho Formation and Rodeio Velho Member (Almeida et al., 2005).

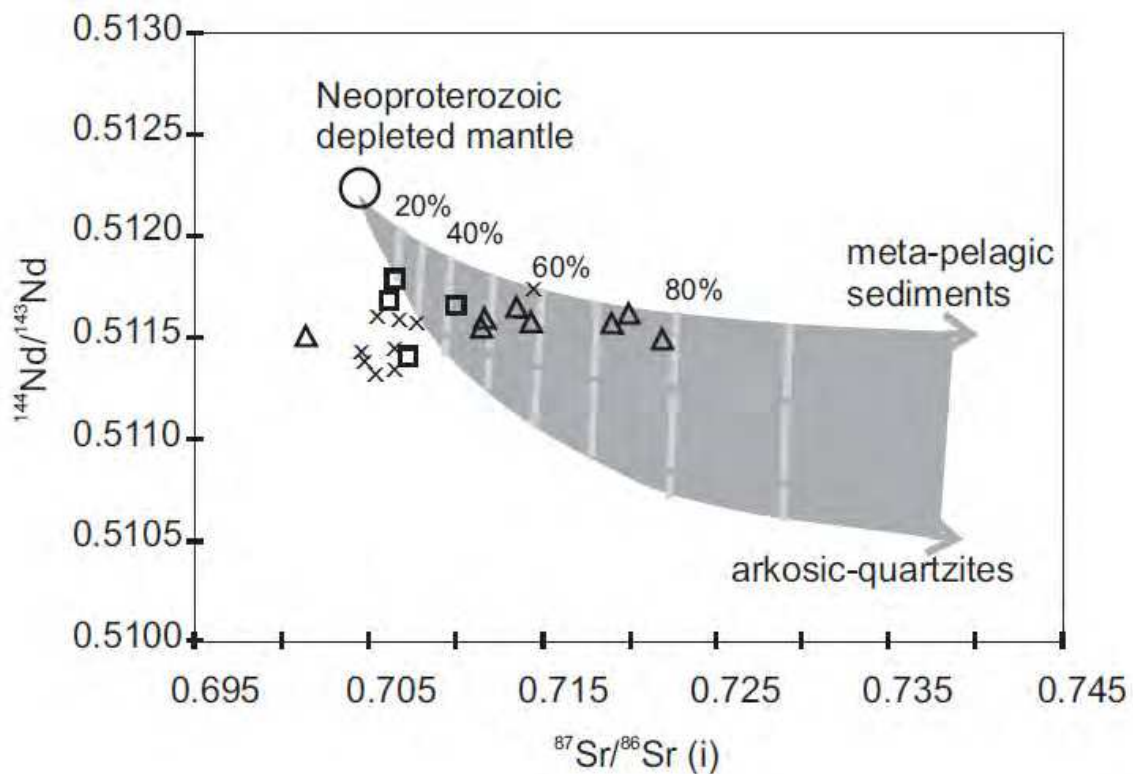


Fig. 26. $^{143}\text{Nd}/^{144}\text{Nd}$ versus initial $^{87}\text{Sr}/^{86}\text{Sr}$ diagram for the volcanic rocks from Rodeio Velho Member and Acampamento Velho Formation flows. The plotting shows the field for crustal contamination. Symbols are the same as in figure 25. (Almeida et al., 2005).

Acampamento Velho Formation - Upper Felsic Association									
Sample	SiO ₂	Al ₂ O ₃	Ba/Th	Sm (ppm)	Nd (ppm)	¹⁴³ Nd/ ¹⁴⁴ Nd	Erro ppm	εNd ₍₀₎	εNd _(t)
#MH-15	78.54	9.39	20.7	7.77	22.65	0.51205	14	-11.56	-12.32
#SSB-14	77.05	11.47	25.1	0.84	4.17	0.51194	15	-11.93	-7.51
##MH-31	77.46	11.3	9.9	1.36	11.44	0.51180	16	-16.44	-7.68
##MH-37	67.64	11.45	27.8	9.47	42.85	0.51203	14	-13.65	-8.36
##MH-41	76.59	11.49	15.1	5.17	28.59	0.51182	12	-16.00	-9.87
##SSB-13	81.73	9.08	22.4	8.35	43.85	0.51198	13	-12.91	-7.18
*MH-17	77.26	11.67	10.7	7.84	35.89	0.51195	12	-13.32	-8.80
*MH-20	78.97	10.9	4.2	2.98	12.40	0.51206	24	-11.24	-7.62
*MH-21b	80.6	8.52	4.6	6.5	28.69	0.51206	11	-11.29	-7.00
*MH-22	78.15	10.07	4.3	4.23	28.87	0.51193	15	-13.90	-6.30
*MH-25	79.26	11.48	8.4	17.27	73.33	0.51215	14	-9.50	-5.69
*MH-27	76.26	11.32	8.8	4.19	14.79	0.51227	18	-7.14	-5.36
*MH-50	75.76	11.73	22.3	10.71	60.40	0.51194	13	-13.57	-7.29
*MH-53	76.85	12.29	32.7	3.07	15.78	0.51200	14	-12.47	-7.72
*MH-60	76.37	12.34	27.7	3.00	13.13	0.51204	14	-11.71	-7.61
*SSB-1b	77.79	11.77	12.6	7.55	24.10	0.51217	13	-9.11	-8.61
(continuation)									
Sample	TDM	⁸⁷ Sr/ ⁸⁶ Sr _(m)	erro (SD bs)	⁸⁷ Sr/ ⁸⁶ Sr _(i)	Rb/Ba	⁸⁷ Rb/ ⁸⁶ Sr	erro (SDabs)	¹⁴⁷ Nd/ ¹⁴⁴ Nd	Erro ppm
#MH-15	---	0.75224	0.00107	0.71338	0.70355	4.95653	0.04957	0.20732	28
#SSB-14	1812.02	0.76577	0.00015	0.71107	0.61170	4.77399	0.04774	0.07200	24
##MH-31	1336.68	0.77196	0.00016	0.70983	1.09590	7.92374	0.07924	0.13358	32
##MH-37	1922.00	0.74597	0.00018	0.70854	0.61851	6.97588	0.06976	0.12139	28
##MH-41	1777.20	0.75648	0.00046	0.71327	0.66473	5.51066	0.05511	0.10928	26
##SSB-13	1638.2	0.7780	0.00038	0.70143	0.57085	9.77349	0.09773	0.11508	24
*MH-17	2021.17	0.77655	---	0.72188	0.87885	6.97300	0.06973	0.13211	48
*MH-20	2171.45	0.77186	0.00065	0.71169	1.66335	7.67411	0.07674	0.14515	22
*MH-21b	1906.70	0.78126	0.00015	0.71438	1.94329	8.52981	0.08530	0.13557	30
*MH-22	1354.44	0.82658	0.00015	0.71997	3.39807	13.59785	0.13598	0.08851	28
*MH-25	1893.04	0.78159	0.00019	0.71367	0.91535	8.6628	0.08663	0.14237	36
*MH-27	2799.16	---	0.00047	---	1.15318	---	---	0.17121	26
*MH-50	1566.44	0.81214	0.00018	0.71899	0.47634	11.88013	0.11880	0.10724	28
*MH-53	1642.65	0.76269	0.00026	0.71176	0.29993	6.49581	0.06496	0.11745	28
*MH-60	2018.02	0.77194	0.00015	0.71149	0.39176	7.71001	0.07710	0.13820	28
*SSB-1b	---	0.93947	0.00015	0.70140	0.74210	30.36370	0.030364	0.18943	26
Acampamento Velho Formation - Lower Mafic Association									
Sample	SiO ₂	Al ₂ O ₃	Ba/Th	Sm (ppm)	Nd (ppm)	¹⁴³ Nd/ ¹⁴⁴ Nd	Erro ppm	εNd ₍₀₎	εNd _(t)
*MH-15	47.05	16.49	69.5	13.74	78.23	0.5118	15	-16.66	-10.31
*MH-13	51.48	15.59	57.7	6.26	47.15	0.51207	37	-11.15	-2.97

*MH-14	54.31	12.12	84.3	8.3	40.58	0.51199	14	-12.55	-7.49
*SSB-7	48.84	15.19	75.1	5.02	22.94	0.51216	13	-9.34	-4.82
*SSB-32b	45.72	14.75	236.6	6.81	31.69	0.51213	13	-9.86	-5.17
(continuation)									
Sample	TDM	⁸⁷ Sr/ ⁸⁶ Sr (m)	erro (SDabs)	⁸⁷ Sr/ ⁸⁶ Sr (i)	Rb/Ba	⁸⁷ Rb/ ⁸⁶ Sr	erro (SDabs)	¹⁴⁷ Nd/ ¹⁴⁴ Nd	Erro ppm
*MH-15	1773.69	0.70755	0.00076	0.70716	0.05041	0.04859	0.04859	0.10617	30
*MH-13	1113.86	0.70765	0.00014	0.70656	0.07890	0.14012	0.14012	0.08029	74
*MH-14	1782.61	0.71012	0.00075	0.68567	0.07359	3.11922	3.11922	0.12468	28
*SSB-7	1642.67	0.71164	0.00026	0.70616	0.14778	0.69806	0.69806	0.13228	26
*SSB-32b	1643.06	0.71120	0.00360	0.71009	0.08169	0.14134	0.14134	0.12984	26
RODEIO VELHO MEMBER									
Sample	SiO ₂	Al ₂ O ₃	Ba/Th	Sm (ppm)	Nd (ppm)	¹⁴³ Nd/ ¹⁴⁴ Nd	Erro ppm	εNd ₍₀₎	εNd _(t)
*PH-	50.14	14.64	512.9	15.48	88.43	0.51165	14	-19.36	-13.92
*PH-4	65.53	12.7	1032.5	13.06	72.81	0.51168	14	-18.73	-13.45
*RLP-1	51.89	15.75	387.59	13.81	84.30	0.51191	14	-14.24	-8.39
*RLP-10	57.12	14.58	224.3	22.28	142.09	0.51185	13	-15.32	-9.21
*RPL-12	52.33	15.77	359.3	14.16	82.60	0.51170	13	-18.37	-12.80
*RLP-14	51.69	15.79	356.8	13.84	82.45	0.51173	16	-17.65	-11.95
*RLP-15	54.63	15.34	503.2	12.76	78.98	0.51174	9	-17.58	-11.65
*RLP-17	46.84	15.77	712.5	8.95	50.14		13	-17.58	-8.57
Sample	TDM	⁸⁷ Sr/ ⁸⁶ Sr (m)	erro (SD bs)	⁸⁷ Sr/ ⁸⁶ Sr (i)	Rb/Ba	⁸⁷ Rb/ ⁸⁶ Sr	erro SDabs	¹⁴⁷ Nd/ ¹⁴⁴ Nd	Erro ppm
*PH-3	1963.39	0.70579	0.00014	0.70555	0.00876	0.03662	0.00037	0.10581	28
*PH-4	1966.81	0.70750	0.00017	0.70665	0.00515	0.12658	0.00127	0.10848	28
*RLP-1	1500.53	0.70683	0.00021	0.70549	0.03558	0.20011	0.00200	0.09905	28
*RLP-10	1517.66	0.70788	0.00017	0.70774	0.00668	0.01975	0.00020	0.09481	26
*RPL-12	1854.20	0.70542	0.00017	0.70480	0.02521	0.092951	0.00093	0.10362	26
*RLP-14	1768.65	0.70526	0.00017	0.70467	0.02451	0.08756	0.00088	0.10149	32
*RLP-15	1705.90	0.71040	0.00016	0.70666	0.05833	0.55977	0.00560	0.09766	18
*RLP-17	1599.50	0.70739	0.00015	0.70685	0.02280	0.08146	0.00081	0.10791	26

Table 13. Geochemical analysis of the major and trace elements, Nd, Sr and Sm isotope results (modified from Almeida *et al* 2005). Major elements are in wt%; trace elements are in ppm. * = flows; ** = tuffs; # = welded tuffs. The analysis were performed at Activation Laboratories (ACTLAB), Canada, using the Argonium Plasma Spectrometry (ICP). The isotope analysis were carried out the Laboratory for Isotope Geology-LGI (Institute of Geosciences, Federal University of Rio Grande do Sul-UFRGS, Brazil).

All lavas, whichever unit they belong to, show a negative ϵNd in t or in the present time. The negative ϵNd values meaning in acid lavas is not always easily addressed. It could be related to crust derived lavas, basaltic lavas crustal contamination during differentiation, or mantle-derived, metasomatic lavas. However, negative ϵNd values in basalts are usually related to the latter two processes. Crustal contamination, either in acid or mafic lavas generally also affects the Rb/Sr system, increasing the radiogenic Sr amount and conferring to the rocks, a high initial $^{87}\text{Sr}/^{86}\text{Sr}$ ratio. Acampamento Velho Formation and Rodeio Velho Member mafic lavas display ϵNd ranging from -2.9 to -10.3 and from -8.4 to -13.9, respectively, and an initial $^{87}\text{Sr}/^{86}\text{Sr}$ ratio from 0.706 to 0.707 and from 0.704 to 0.707. These initial $^{87}\text{Sr}/^{86}\text{Sr}$ ratios are consistent with rocks derived from a Neoproterozoic depleted mantle, represented by the Cambaí Complex rocks (Babinski et al., 1996), plotted in figure 26. The negative correlation between initial $^{87}\text{Sr}/^{86}\text{Sr}$ ratio and SiO_2 content observed in figure 27a, along with the constancy of the SiO_2 content, despite ϵNd values (Fig. 27b) for Acampamento Velho Formation and Rodeio Velho Member mafic lavas ratify the idea that the crustal contamination was not significant during the differentiation of these rocks, in the early stages of differentiation (at least until these rocks have reached around 55 wt% of SiO_2 content). Crustal contamination or crustal origin is assumed for rocks with SiO_2 content higher than 55 wt%. It can also explain the occurrence of acid lavas and pyroclastic material in the Acampamento Velho Formation (Fig. 27a and b). A plot of initial $^{87}\text{Sr}/^{86}\text{Sr}$ against Ba/Th ratios (Fig. 28) shows strong enrichment in radiogenic Sr and Th in the acid rocks, which could be related to a crustal component. In order to better constrain the possible sources of the Acampamento Velho Formation and Rodeio Velho Member lavas, juvenile Neoproterozoic depleted mantle derived rocks (the Cambaí Complex) and Neoproterozoic crustal rocks (arkosic quartzites, taken as representative of the average composition of the crust and meta-pelagic sediments) were plotted with Acampamento Velho Formation and Rodeio Velho Member samples (Fig. 26). The isotopic ratios and compositions of these rocks were calculated for 550 Ma and mixture lines were calculated based on two-end-member models.

From the analysis of figure 26, the Acampamento Velho Formation mafic lavas could be regarded as a mixture of depleted mantle-derived basalt plus 20% to 30% of crustal contamination. The crustal material matches best Neoproterozoic arkosic quartzites rather than pelagic sediments. Acampamento Velho Formation felsic lavas evolution trend displays an increase in crustal contamination. However, Rodeio Velho Member mafic lavas can not be easily explained by crustal contamination of depleted mantle derived magma. The composition of these lavas request an end member highly enriched in radiogenic Nd, but impoverished in radiogenic Sr. An enriched mantle type I (EM I according to Zindler & Hart, 1986) is such a reservoir, well established for Phanerozoic rocks with the same trend as Rodeio Velho Member (Fig. 26).

The differences between Acampamento Velho Formation and Rodeio Velho Member mafic samples can be highlighted using Ba/Th ratio (Fig. 28). Both mafic lavas show preferential enrichment in Ba relative to Th. However, the mafic lavas of the RVM show distinctive enrichment in the Ba/Th ratio (due to its very high Ba content, up to 2695 ppm) without a change in the $^{87}\text{Sr}/^{86}\text{Sr}$ initial ratio. On the other hand, Acampamento Velho Formation mafic lavas show a weak enrichment in Ba/Th and $^{87}\text{Sr}/^{86}\text{Sr}$ initial ratios. Such behavior suggests that Rodeio Velho Member was originated from a depleted mantle, re-enriched in highly incompatible elements such as Ba.

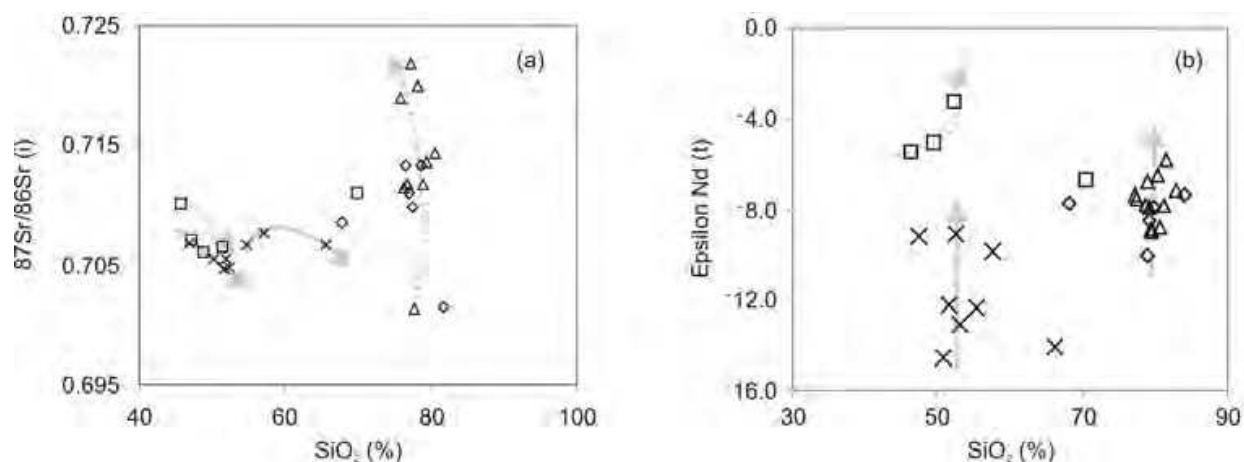


Fig. 27. (a) $^{87}\text{Sr}/^{86}\text{Sr}$ initial versus SiO_2 and (b) $\epsilon\text{Nd}(t)$ versus SiO_2 diagrams for the Acampamento Velho Formation and Rodeio Velho Member volcanic rocks. Symbols are the same as in figure 25 (Almeida et al., 2005).

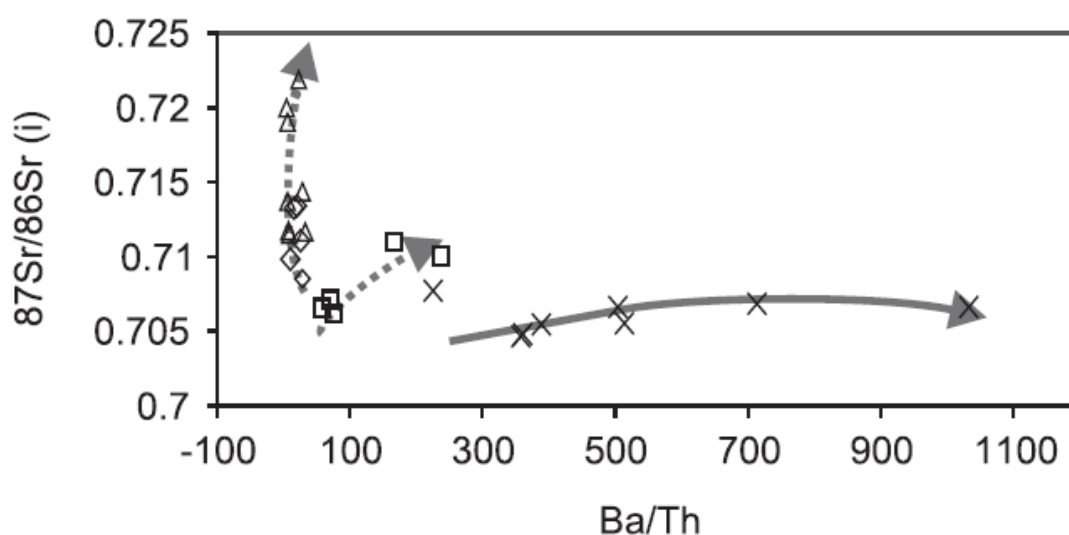


Fig. 28. Initial $^{87}\text{Sr}/^{86}\text{Sr}$ versus Ba/Th diagram for the isotope data obtained for the volcanic rocks from Acampamento Velho Formation and Rodeio Velho Member. Observe the different trends for these groups as well as the radiogenic Sr and Th enrichment in the Upper Felsic Association, and in a lesser degree for the mafic rocks of the Lower Mafic Association from Acampamento Velho Formation. Symbols are the same as in figure 25. (Almeida et al., 2005).

Regarding the Nd model ages (Table 13), we can see Acampamento Velho Formation and Rodeio Velho Member mafic associations with values ranging from 1.1 to 1.8 Ga and 1.5 to 2.0 Ga, respectively. These model ages point to also for a modified mantle at end of Brasiliano Cycle, in post-orogenic tectonic setting (during the Upper Neoproterozoic to Eopaleozoic). However, Acampamento Velho Formation has some juvenile component with already modified mantle since it displays somewhat younger model ages and lesser negative ϵNd values. On other side, the Acampamento Velho Formation felsic association Nd model age is from 1.3 to 2.8 Ga (Table 13). This information coupled with Acampamento Velho Formation felsic association lower ϵNd negative values, if compared to those of mafic

dominated by strike-slip tectonics with some transtensional/transpressional components in retroarc position. The Bom Jardim Group is limited by two angular discordances that are confined to the Maricá Group (base) and Acampamento Velho Formation volcanic rocks (top). The Acampamento Velho is a bi-modal magmatic association with some sedimentary contribution (as Santa Fé Member of Paim et al., 2000) and is the base of a volcano-sedimentary sequence, the Acampamento Velho/Santa Bárbara Group. This sequence begins with basic and acid volcanic magmatism of the alkaline signature, which is overlaid by the three Santa Bárbara Group sedimentary sequences. The lower and intermediate sedimentary sequences (Santa Fé and Lanceiros Formation) represent a fluvial-deltaic sedimentation, and the upper formation (Pedra do Segredo Formation), overlies in angular unconformity on Lanceiros Formation. Units are composed by a coarsening up alluvial-fluvial depositional sequence.

The U-Pb zircon data suggest that Acampamento Velho Rhyolites formed from 570 to 544 Ma, taking account the SHRIMP age obtained by Sommer (2005) for Ramada Plateau acid volcanic rocks of the is 549 ± 5 Ma and by Janikian et al. (2008) for acid volcanic rocks in the Caçapava region is 574 ± 7 Ma. However, we obtained the U-Pb zircon age of 553 ± 5 Ma for Acampamento Velho Formation using an andesitic basalt sample of the lower mafic association, which is close to that age of Ramada Plateau. In the Santa Bárbara (Fig. 29, west column) and Guaritas sub-basins (Fig. 29, east column), the basic flows from basal contact, pyroclastic manifestations and rhyolitic flows (from the base to the top) of the Acampamento Velho are in unconformity with the Bom Jardim Group, and the upper contact is made by unconformity with the Sequence I (or Santa Fé and Lanceiros Formation base from Santa Bárbara Group). The observed stratigraphic position in field – basalts and andesitic basalts on the base and felsic sequence on the top (Figs. 12 and 29), as well as the geochemical and isotopic behavior, show that the first phase formed the basalts and andesitic basalts, and later, the rhyolitic rocks, which confirm that the Acampamento Velho Formation is bimodal volcanism. The best estimated ages for the Acampamento Velho Formation and Santa Barbara Group are 553 and 549 Ma, during which, an extensional events controlled the deposition and magmatism.

The Santa Barbara Group units are overlaid in angular unconformity by the sediments of the Guaritas Group. At the base of this group, occurs the alkaline basalt lavas called as Rodeio Member. We obtained the age of 547 ± 6.3 Ma for the Rodeio Velho Member alkaline basalt, which can be interpreted the maximum age for the magmatism, therefore, the deposition of the Guaritas Formation. On other side, detrital zircon collected from the upper portion of the Guaritas Group is dated at 535 ± 10 Ma (Hartmann et al. 2008). The present data suggest a Cambrian age for the Rodeio Velho Formation, instead the U-Pb age of 470 ± 19 Ma (sensitive high mass-resolution ion microprobe - SHRIMP) obtained by Hartmann et al. (1998) for the Rodeio Velho Member. Santa Bárbara Sub-basin (Fig. 29 - west column), which is above the Rodeio Velho Member (Pedra Pintada Formation), is in contact by disconformity with the Sequence III (or Segredo Formation). Guaritas Sub-basin (Fig. 29 - east column), that is above the Rodeio Velho (and Pedra Pintada Formation), is in contact by disconformity and we can see the Santa Bárbara Group sedimentary rocks (Fambrini, 2005). Thus, beyond the U-Pb ages, the stratigraphic position showing the Rodeio Velho Member above Acampamento Velho Formation, allow us to postulate that first was generated the Acampamento Velho volcanism, and then, the Rodeio Velho volcanism. The Guaritas Group sedimentation occurred under more stable conditions in the retroarc region, and it is deposited under a transtensional tectonics.

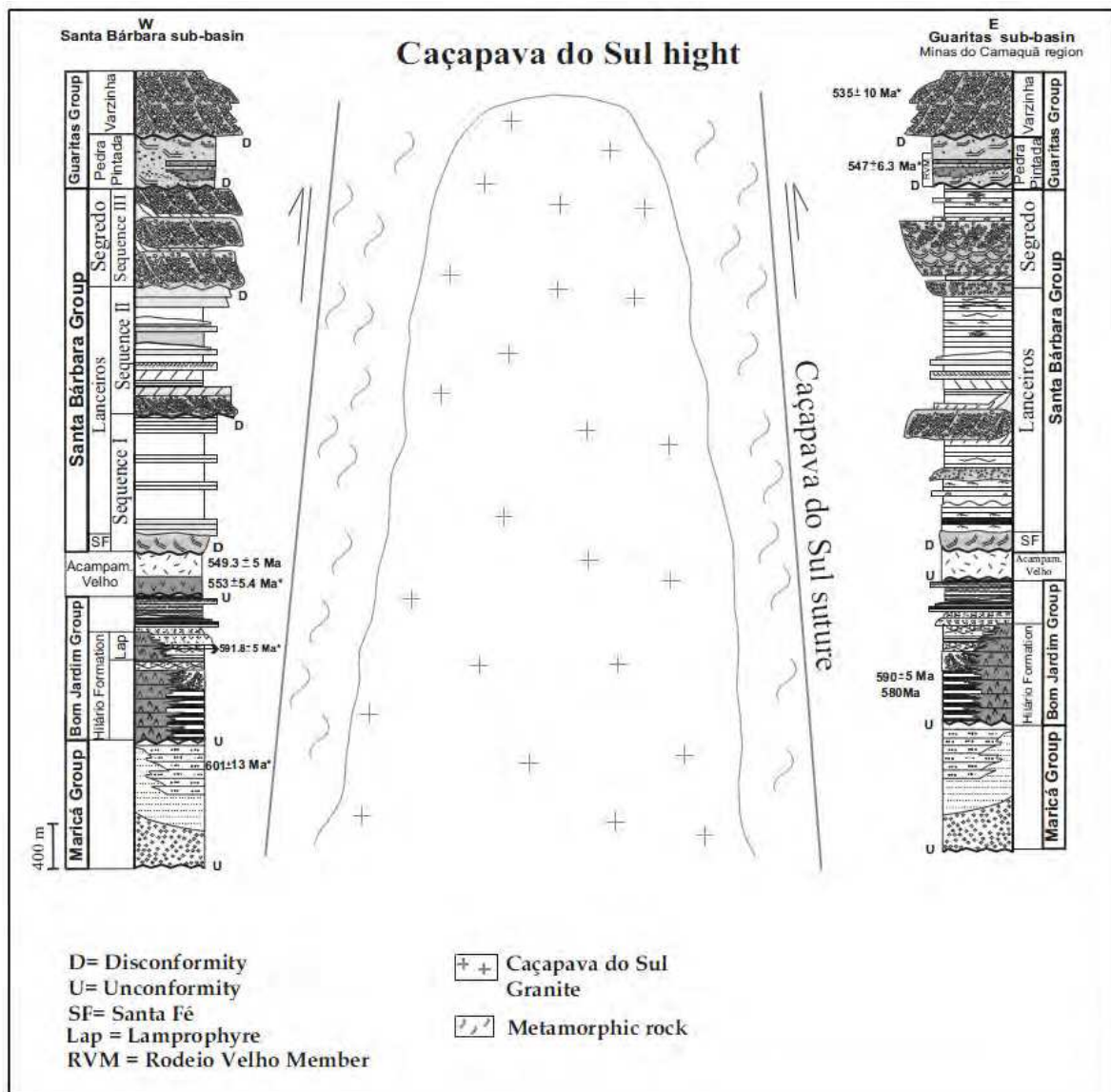


Fig. 29. Santa Bárbara and Guaritas sub-basin: stratigraphic columns including the main unconformity and disconformity, which bounds the Camaquã Basin unit. West column is modified from Paim et al (1995, 2000), Almeida et al (2002) and Borba & Misuzaki (2003). East column is modified from Paim et al. (1995), Wildner (2002), Fambrini et al. (2005) and Janikian et al. (2003, 2008).

The Rodeio Velho Member is interbedded or arranged in volcano-sedimentary features of the interaction (flow striation, xenoliths, clastic dykes, marks in increasing and peperites) with the Pedra Pintada Formation sedimentary rocks from Guaritas and Santa Bárbara sub-basins. We would like to point out that, between these two sub-basins, there is the Caçapava structural hill, the Caçapava Granite (average U-Pb age of 550 Ma) and the Caçapava do Sul Suture (Fig. 1 and Fig. 29). According to Nardi and Bitencour (1989), the Caçapava Granite was positioned in mesozone level, with microgranitiques and aplitiques rocks positioned at summit of the body and mainly associated to leucogranitiques. Considering these information, we may suggest that the granite together with the rocks above (more than 6 km thick) may have suffered uplift and denudation processes during a long time before the

granite emerge. These same authors mentioned that the Caçapava do Sul Granite Complex is a body composed of two contrasting blocks bounded by NW-trending structures. Borba et al. (2002) from the study about apatite fission-track (FT) thermochronology for samples of the Caçapava do Sul granites determined to the Northern block, an apparent FT ages of 293.5 and 274.8 Ma, and an estimated for the initial track recording an age of 366 Ma. These results are interpreted in the frame of the uplift and denudation history of the region during the Paleozoic-Mesozoic intraplate Parana' Basin evolution, as influenced by the convergent tectonic setting of Southwestern Gondwana. In the Southern block, where dioritic and gneissic portions crop out and apparent FT ages range from 252.1 to 245.5 Ma. A possible subsequent Upper Cretaceous uplift event can be inferred from the modeled thermal history curves and the apparent FT age of the Northernmost collected sample is 73.7 Ma. If it is considered the presence of aplites and microgranites at the summit of the body, then it can be said that it has suffered little denudation after have emerged. Costa (1997), based on geophysical data interpretations, mentioned that Caçapava do Sul Suture corresponds to a deep geophysical anomaly that separates two magnetic domains. Therefore, it is important to consider an independent basin evolution for each suture side and beyond that this sub-basin may have shown different subsidence degree. If we consider that Guaritas Sub-basin the Santa Bárbara Group rocks show marked dips, and the Guaritas Group rocks do not show this feature, while that in Santa Bárbara sub-basin, the rocks Guaritas Group's base (Pedra Pintada Formation) according to Almeida et al. (2003a), the layers exhibit latitudes $188^{\circ}/40^{\circ}$ NW, $194^{\circ}/23^{\circ}$ NW e $195^{\circ}/26^{\circ}$ NW, then, we could suggest that tilting would be produced by biggest Caçapava Suture influence (when reactivated), which is in direct contact with these rocks. Paim et al. (2000) attributed tilting of these rocks as a reflex of normal falls, and subordinately strike slip movements. Thus, these declivities can be formed due to basin different subsidences.

Almeida et al. (2002, 2003a, 2003b and 2005) based on Brazilian Orogeny evolution pattern from Chemale Jr. (2000); considered that the Acampamento Velho Formation was generated in an extensional regime preceding the Rio de la Plata and Kalahari continental plate collisions. The Rodeio Velho Member may correspond to the late magmatic manifestation and may have occurred after the collisional phase between Rio de la Plata (with Encantadas Microcontinent attached) and Kalahari Continental Plate. In the context of adopted pattern, it would correspond to the Phase IV of the same author (Fig. 2 and Fig. 30). Thus, we propose that between 560-550 Ma, considering only the Camaquã Basin central portion, it may exist two extensional basins depocentre, such as Santa Bárbara and Guaritas sub-basins (Fig. 30b), being them limited by Caçapava Hill. These sub-basins were already partially filled by coastal deposits at their base, including fluvial and shallow marine sediments, with scarce volcanic contribution and U-Pb age of 601 Ma (Maricá Group). On these rocks, is an unconformity named as Bom Jardim Group, composed of volcanic rocks at the base (Hilário Formation) and sediments at the top. On these rocks, in disconformity, are volcanic rocks of the basaltic and rhyolitic composition (Acampamento Velho). According to Almeida et al (2005, 2007), the generated magma (of Acampamento Velho) at some point initiated its ascension. At a certain stage, this magma separated into two fractions: a mafic portion and another one, enriched in crustal component. Between 560-550 Ma, after the magmatic chamber formation as well as the separation of the magma into two fractions, both fraction magmas rise and mafic flow manifestations (lower mafic association) took place around 553 Ma.

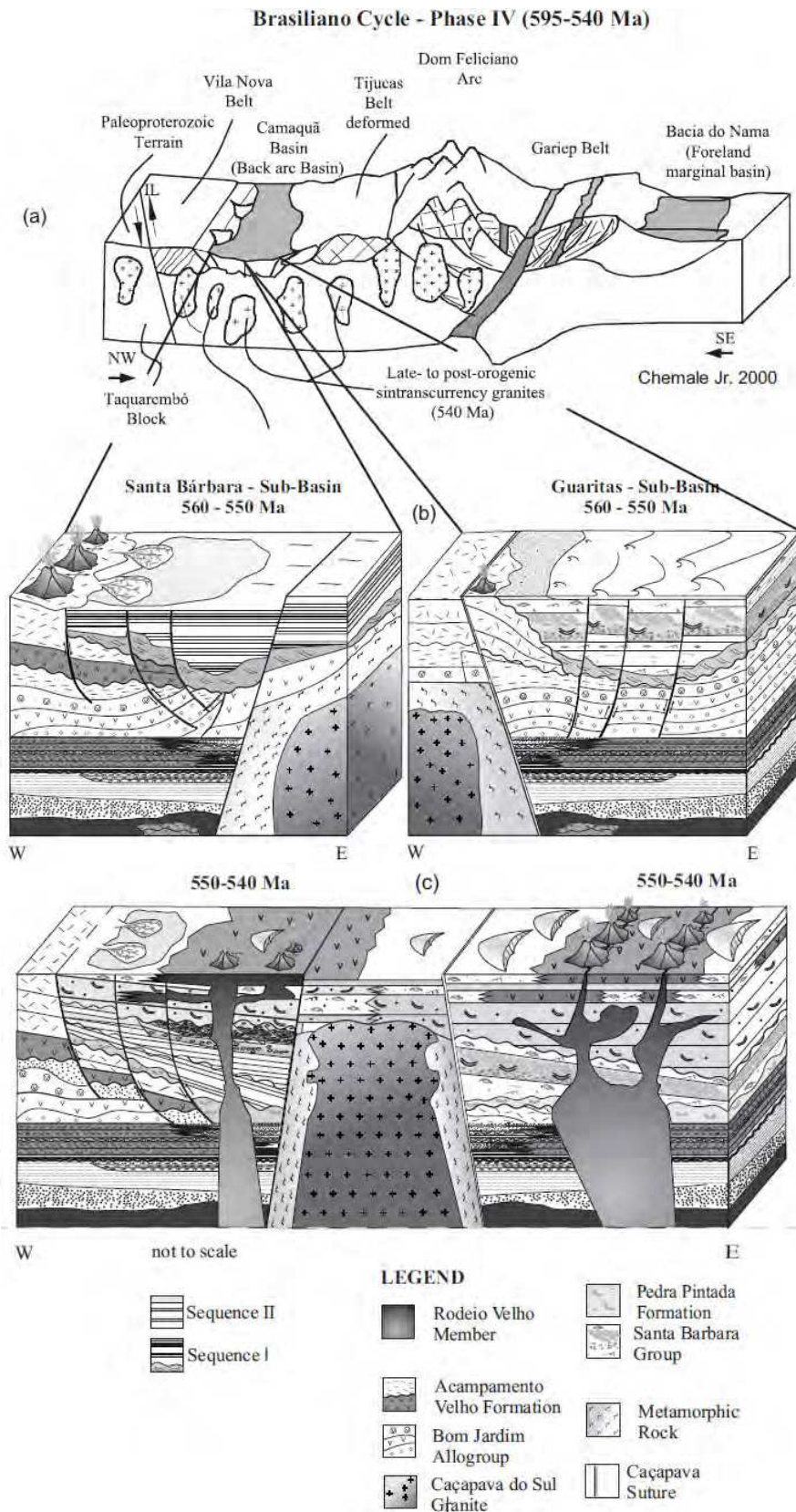


Fig. 30. Schematic diagram block showing the position of the different rock units in the: (a) Santa Bárbara and (b) Guaritas sub-basins between 560-550 Ma and 550-540 Ma. These sub-basins were generated during the Phase IV of Brasiliana Orogeny established by Chemale Jr. (2000).

The other magma fraction underwent through a significant enrichment in crustal component. This viscous magma slowly rise around 549 Ma revealing itself in a first phase as pyroclastic rhyolitic rock (tuff, lapillitic tuff and welded tuff) and afterwards as a rhyolitic flow (the upper felsic association).

In the range of 547-535 Ma (Fig. 30c), an alkaline mantelic magma may ascend in the last magmatism stages by the deep faults during an intra-plate mechanic extensional event, generating the Rodeio Velho Member event (Fig.30c). The Rodeio Velho Member volcanic manifestations took place as flows interbedded which sometimes show interactions of the lava with sediments poorly consolidated, and correspond to the Pedra Pintada Formation eolian deposits from Guaritas Group. We can observe these features at Santa Bárbara and Guaritas sub-basins.

8. Acknowledgements

Delia del Pilar M. de Almeida gratefully acknowledges the fellowship (151477/2007-8 process) granted by Conselho Nacional de Desenvolvimento Científico e Tecnológico-CNPq (Brazil), which made this work possible and feasible. The authors are grateful to the Universidade Federal do Pampa (UNIPAMPA) for the scholarship granted to the undergraduate students Taís Regina Cordeiro de Oliveira and Igo Silva de Almeida that collaborated in the figures edition and text formatting.

9. References

- Almeida, F. (1969). Diferenciação Tectônica da Plataforma Brasileira. In: *Congr. Bras. Geol.*, 1, Salvador, pp. 29-46.
- Almeida, F.; Hasui, Y. & Brito Neves, B. (1976). The Upper Precambrian of South America. *Boletim IG/USP*, Vol.7, pp.45-80.
- Almeida, F.; Hasui, Y.; Brito Neves, B. & Fuck R. (1981). Brazilian structural provinces: an introduction. *Earth Science Ver*, Vol.17, pp.1-29.
- Almeida, D. del P.; Pereira, V.; Machado, A.; Zeffass, H. & Freitas, R. (2007). Late Sodic Metasomatism evidences in bimodal Volcanic Rocks of the Acampamento Velho Alloformation, Neoproterozoic III, Southern Brazil. *Anais da Academia Brasileira de Ciências*, Vol.79, Nº4, pp.1-13, ISSN 001-3765.
- Almeida, D.del P.; Conceição, R.; Chemale Jr. F.; Koester, E.; Borba, A. & Petry, K. (2005). Evolution of heterogeneous Mantle in the Acampamento Velho and Rodeio Velho volcanic events, Camaquã Basin, Southern Brazil. *Gondwana Research*, Vol.8, Nº4, pp.479-492, ISSN 1342-937X.
- Almeida, D.del P.; Zeffass, H.; Basei, M. & Lopes, R. C. (2003a). Eventos vulcânicos alcalinos na Bacia do Camaquã: o vulcanismo Neoproterozoico III Acampamento Velho e o magmatismo Meso-Ordoviciano (?) Rodeio Velho. In: *Caracterização e Modelamento de Depósitos Minerais*, Ronchi, L.H., Althoff, F., (Eds.), 325-350, Universidade do Vale do Rio dos Sinos, São Leopoldo, Brazil.
- Almeida, D. del P.; Hansen, M; Fernsterseifer H.; Petry K. & Lima L.. (2003b). Petrology of a subduction-related caldera and post-collisional, extesion-related volcanic cones from the Early Cambrian and Middle Ordovician (?) of the Camaquã Basin, southern Brazil. *Gondwana Research*, Vol.6, Nº3, pp.541-552, ISSN 1342-937X.

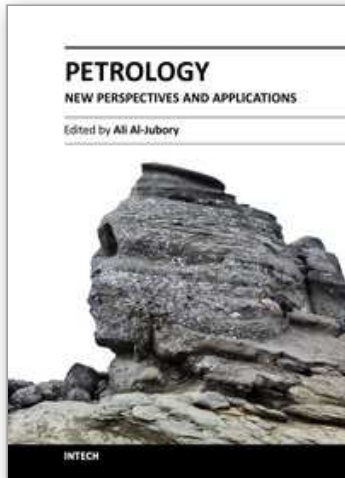
- Almeida, D. del P.; Zerfass, H.; Basei, M.; Petry, K. & Gomes, C. (2002). The Acampamento Velho Formation, a Lower Cambrian bimodal volcanic package: geochemical and stratigraphic studies from the Cerro do Bugio, Perau and Serra de Santa Bárbara (Caçapava do Sul, Rio Grande do Sul, RS – Brazil). *Gondwana Research*, Vol.5, Nº3, pp. 721-733, ISSN 1342-937X.
- Almeida, D. del P.; Lopes R. C.; Lima L. & Gomes, C. (2000). Petrography and Geochemistry of the Volcanic Rocks of the Rodeio Velho Member, Ordovician of the Camaquã Basin (Rs-Brazil): Preliminary Results. *Revista Brasileira de Geociências*, Vol.30, Nº4, pp.23-34, ISSN 0375-7536.
- Almeida, D. del P.; Lima L. & Gomes, C. (1999). Região de Vista Alegre-Lavras do Sul/RS: Uma Zona Tipo da Formação Hilário. *1 Simposio sobre Vulcanismo e Ambientes Associados, Gramado – RS*. Vol.1,pp.56.
- Babinski, M.; Chemale Jr. F.; Hartmann, L.; Van Schmus, W. & Silva, L. (1996). Juvenile accretion at 750-700 Ma in Southern Brazil, *Geology*, Vol.24, Nº5, ISSN 0091-7613.
- Basei M.; Siga J.; Masquelin H.; Harara M.; Reis Neto, J. & Preciozzi P. (2000). The Dom Feliciano Belt of Brazil and Uruguay and Its Foreland Domain, the Rio de La Plata Craton. *Tectonic Evolution of South America*, Cordani, U.G. et al. (Eds.), pp. 311-334, Rio de Janeiro, Brazil.
- Borba, A.; Mizusaki, A. M.; Santos, J.; McNaughton, N.; Onoe, A. & Hartmann, L. (2008). U-Pb zircon and ^{40}Ar - ^{39}Ar K-feldspar dating of syn-sedimentary volcanism of the Neoproterozoic Maricá Formation: constraining the age of foreland basin inception and inversion in the Camaquã Basin of southern Brazil. *Basin Research*, Vol. 20, pp 359-375, ISSN 0950-091X.
- Borba, A., Maraschin, A. & Mizusaki, A. M. (2004). Stratigraphic analysis and depositional evolution of the Neoproterozoic Marica Formation (southern Brazil): constraints from field data and sandstone petrography. *Gondwana Res.*, Vol. 7 Nº 3, pp. 871-886, ISSN 1342-937X.
- Borba, A. & Mizusaki, A. M. (2003). Santa Bárbara Formation (Caçapava do Sul, southern Brazil): depositional sequences and evolution of an Early Paleozoic post-collisional basin. *Journal of South America Earth Sciences*, Vol.16, Nº5, pp.365-380, ISSN 0895-9811.
- Borba, A., Vignol-Lelarge, M.L., Mizusaki, A. M. (2002). Uplift and denudation of the Caçapava do Sul granitoids (southern Brazil) during Late Paleozoic and Mesozoic: constraints from apatite fission-track data. *Journal of South American Earth Sciences*, Vol. 15, pp. 683-692, ISSN 0895-9811.
- Bonhomme, M. & Ribeiro, M. (1983). Datações K-Ar das argilas associadas a mineralização de cobre da Mina Camaquã e de suas encaixantes. In: *1 Simpósio Sul-Brasileiro de Geologia*, Vol. 1, pp. 82-88.
- Chemale Jr., F. (2000). Evolução geológica do Escudo Sul-rio-grandense. *Geologia do Rio Grande do Sul*, Holz, M. & De Ros, L.F. (Eds.), pp. 13-52, Universidade Federal do Rio Grande do Sul, Porto Alegre, Brazil.
- Cordani, U.; Halpern, M. & Berenholc, M. (1974). Comentários sobre as determinações da Folha de Porto Alegre. In: DNPM, Carta Geológica do Brasil ao Milionésimo, texto explicativo da Folha de Porto Alegre e Lagoa Mirim, pp.70-84.
- Costa A. (1997). Teste e modelagem geofísica da estruturação das associações litotectônicas Pré-cambrianas no Escudo Sul-rio-grandense. Tese de Doutorado, Instituto de Geociências, Universidade Federal do Rio Grande do Sul Brazil, 291 pp.

- Cullers, R. & Graf, J. (1984). Rare earth elements in igneous rocks of the continental crust: predominantly basic and ultrabasic rocks. In: *Rare earth Element Geochemistry*, P. Anderson (ed.), 237-274, Amsterdam.
- Fambrini G.; Janikian L; Paes de Almeida, R. & Fragoso-César, A. R. (2005). O Grupo Santa Bárbara (Ediacarano) na Sub-Bacia Camaquã Central, RS: estratigrafia e sistemas deposicionais. *Revista Brasileira de Geociências*, Vol.35, Nº2, pp.227-238, ISSN 0375-7536.
- Fragoso-Cesar, A. R.; Fambrini, G.; Almeida, R.; Pelosi, A. P.; Janikian, L.; Nogueira, A. & Riccomini, C. (2001). As Coberturas do Escudo Gaúcho no Rio Grande do Sul: Revisão e Síntese (Abst.). *XI Congreso Latinoamericano de Geología e III Congreso Uruguayo de Geologia*, Uruguay.
- Fragoso-César, A. R.; Fambrini, G.; Paes de Almeida, R.; Pelosi, A.; Janikian, L.; Riccomini, C.; Machado, R.; Nogueira, A. & Saes G. (2000). The Camaquã extensional basin: Neoproterozoic to early Cambrian sequences in southernmost Brazil, *Revista Brasileira de Geociências*, Vol.30, pp.438-441, ISSN 0375-7536.
- Fragoso-Cesar, A. R., Faccini, U., Paim, P., Lavina, E. & Flores, J. (1985). Revisão na estratigrafia das molassas do Ciclo Brasileiro no Rio Grande do Sul. *2 Simpósio Sulbrasil. Geol.*, pp. 477-491.
- Fragoso-Cesar, A. R., Lavina, E., Paim, P. & Faccini, U. (1984) A antefossa molássica do cinturão Dom Feliciano no Escudo do Rio Grande do Sul. *33 Congresso Brasileiro de Geologia*, pp. 3272-3283.
- Fragoso-Cesar, A. R. (1982). Associações petrotectônicas do Cinturão Dom Feliciano (SE da Plataforma Sul-Americana) (ext. abst.), *1 Congresso Brasileiro de Geologia*, Vol. 1, pp.1-12, Salvador, Brazil.
- Goñi, J.; Goso, H. & Issler R. (1962). Estratigrafia e Geologia Económica do Pré-Cambriano e Eo-Paleozóico uruguaio e sul-Riograndense. Avulso da Escola de Geologia, UFRGS, Vol.3, pp.1-105.
- Gresse, P.; Chemale Jr., F.; Silva, L.; Walraven, F. & Hartmann, L. (1996) Late- to post-orogenic basins of the Pan-African- Brasileiro collision orogen in southern Africa and southern Brazil. *Basin Research*, Vo.8, pp.157-171, ISSN 0950-091X.
- Hartmann, L.; Santos, J. & McNaughton, N. (2008). Detrital zircon U-Pb age data, and Precambrian provenance of the Paleozoic Guaritas Formation, Southern Brazilian Shield. *International Geology Review*, Vol. 50, pp. 364-374, ISSN 0020-6814.
- Hartmann, L.; Silva, L.; Remus, M.; Leite, A. & Philipp R. (1998). Evolução Geotectônica do sul do Brasil e Uruguai entre 3,3 Ga e 470 Ma. *2 Congreso Uruguayo de Geologia*, pp.277-284.
- Horbach, R.; Kuck, L; Marimon, R.; Moreira, H. L.; Fuck, G.; Moreira, M.; Marimon, M.; Pires, J.; Vivian, O.; Marinho, D. & Teixeira, W. (1986). Geologia Folha Sh. 22 (Porto Alegre) e parte das folhas Sh. 21 (Uruguaiana E Si. 22 (Lagoa Mirim). Vol. 33, pp. 29-312, Rio de Janeiro, IBGE.
- Janikian, L.; Almeida, R.; Ferreira da T.; Fragoso-Cesar, A. R.; Souza D'A., M.; Dantas, E. & Tohver, E. (2008). The continental Record of Ediacaran volcano-sedimentary successions in southern Brazil and their global implications. *Terra Nova*, Vol. 20, pp. 259-266, Publ. Online - doi: 10.1111/j.1365-3121.2008.00814.x, ISSN 0954-4879.
- Janikian, L.; Almeida, R.; Fragoso-Cesar, A. R. & Fambrini, G. (2003). Redefinição do Grupo Bom Jardim (Neoproterozóico III) em sua área tipo: litoestratigrafia, evolução

- paleoambiental e contexto tectônico. *Revista Brasileira de Geociências*, Vol.33, No 4, pp. 349-362, ISSN 0375-7536.
- Leinz, V.; Barbosa, A. F. & Teixeira, E. (1941). Mapa Geológico Caçapava-Lavras. Boletim 90, Secretaria da Agricultura, Indústria e Comércio, RS.
- Leite, J.; Hartmann, L.; McNaughton, N. & Chemale Jr., F. (1998). SHRIMP U/Pb zircon geochronology of Neoproterozoic juvenile and crustal-reworked terranes in southernmost Brazil. *International Geology Review*, Vol. 40, No 8, pp. 688-705, ISSN 0020-6814.
- Leite, J. (1997). A origem dos Harzburgitos da Sequência Cerro Mantiqueiras e implicações tectônicas para o desenvolvimento do Neoproterozóico no Sul do Brasil. Unpublished, PhD Thesis, Universidade Federal do Rio Grande do Sul, 243 p.
- Leite, J.; McNaughton, N.; Hartmann, L. & Chemale Jr., F. (1995). Age and tectonic setting of metabasalts and metagranitoids from the Cerro Mantiqueiras region: evidences from SHRIMP U/Pb zircon dating and Pb/Pb. In: *5 Simpósio Nacional de Estudos Tectônicos*, Vol. 1, pp. 389-390.
- Leites, S.; Lopes, R. C.; Wildner, W.; Porcher, C. & Sander, A. (1990). Divisão litofaciológica da Bacia do Camaquã na folha Passo do Salsinho, Caçapava do Sul, RS, e sua interpretação paleoambiental. *36 Congresso Brasileiro de Geologia*, pp.300-312.
- Lima, L.; Almeida, D. del P.; Collao, S. (2001). El distrito Minero de Camaquã: Um ejemplo de mineralizaciones tipo epi-mesotermales alojadas em rocas sedimentarias. *Acta Geologica Leopoldensia*, Vol.23 No 51, pp.85-102, ISSN 0102-1249
- Lima, E. & Nardi, L. (1998). The Lavras do Sul Shoshonitic Association: implications for origin and evolution of Neoproterozoic Shoshonitic magmatism in southernmost Brazil, *Journal of South American Earth Sciences*, Vol.11, pp.67-77, ISSN 0895-9811.
- Lima, E.; Wildner W.; Lopes R.C., Sander, A. & Sommer C. (1995). Vulcanismo Neoproterozóico associado às bacias do Camaquã e Santa Bárbara - RS: Uma revisão, *VI Simp. Sul-Brasileiro de Geologia / I Encontro de Geologia do Cone Sul*, pp. 197-199.
- Lopes, R. C.; Wildner, W.; Sander, A. & Camozzato, E. (1999). Alogrupo Guaritas: aspectos gerais e considerações sobre o posicionamento do vulcanismo Rodeio Velho (encerramento do Ciclo Brasileiro ou instalação da Bacia do Paraná) (Abst.), *1 Simpósio Sobre Vulcanismo e Ambientes Associados*, pp. 17, Gramado, Brazil.
- Nardi, L. & Lima, E. (1985). A associação shoshonítica de Lavras do Sul, RS. *Revista Brasileira de Geociências*, Vol.15, pp.139-146, ISSN 0375-7536.
- Nakamura, N. (1977). Determination of REE, Ba, Fe, Mg, Na and K in carbonaceous and ordinary chondrites. *Acta Geochimica et Cosmochimica*, Vol.38, pp.757-775.
- Paim, P.; Chemale Jr., F. & Lopes, R. C. (2000). A Bacia do Camaquã. *Geologia do Rio Grande do Sul*, Holz, M., De Ros, L.F. (Eds.), 231-274, Universidade Federal do Rio Grande do Sul, Porto Alegre, Brazil.
- Pearce, J. & Norry, M. (1979). Petrogenetic Implications of Ti, Zr, Y, and Nb Variations in Volcanic Rocks. *Contributions to Mineral and Petrology*, Vol.69, pp.3-47, ISSN 0010-7999.
- Petry, K. (2006). Feições de interação vulcano-sedimentares: seu uso como indicadores de contemporaneidade no Magmatismo rodeio Velho (Meso-Ordoviciano) e no vulcanismo Serra Geral (Cretáceo inferior), Unpublished, Dissertação de Mestrado, Universidade do Vale do Rio dos Sinos (UNISINOS), 91pp.

- Remus, M.; McNaughton, M.; Hartmann, L. & Fletcher, I. (1999). Gold in the Neoproterozoic juvenile Bossoroca Volcanic Arc of southernmost Brazil: isotopic constraints on timing and sources, *Journal of South American Earth Sciences*, Vol. 12, pp. 349-366, ISSN 0895-9811.
- Remus, M.; McNaughton, N.; Hartmann, L. & Fletcher, I. (1997). Zircon SHRIMP dating and Nd isotope data of granitoids of the São Gabriel Block, southern Brazil: evidence for an Archean Paleoproterozoic basement. II International Symposium on Granites and Associated Mineralization (pp. 271-272). II ISGAM, Salvador, BA, Brazil, SME-BA.
- Remus, M.; McNaughton, N.; Hartmann, L. & Groves, D. (1996). SHRIMP U/Pb zircon dating at 2448 Ma of the oldest igneous rock in southern Brazil: identification of the westernmost border of the Dom Feliciano Belt. 1 *Symposium on Archean Terranes of the South American Platform*, Vol, 1, pp. 67-70.
- Ribeiro, M. & Fantinel, L. (1978). Associações petrotectônicas do Escudo Sul-rio-grandense: I-Tabulação e distribuição das associações petrotectônicas do Rio Grande do Sul, *Inheringia, Série Geológica*, Vol.5, pp.19-54, ISSN 0073-4705.
- Ribeiro, M. & Teixeira, C. (1970). Datações de rochas do Rio Grande do Sul e sua influência nos conceitos estratigráficos e geotectônicos locais. *Inheringia, Série Geológica*, Vol. 3, pp. 109-120, ISSN 0073-4705.
- Ribeiro, M.; Bocchi, P.; Figueiredo Filho, P. & Tessari, R. (1966). Geologia da Quadrícula de Caçapava do Sul, Rio Grande do Sul - Brasil. Divisão de Fomento da Produção Mineral, Boletim 127.
- Robertson, J. (1966). Revision of Stratigraphy and nomenclature of rock units in Caçapava-Lavras Region. IG-UFRGS, *Notas e Estudos*, Vol.1, Nº2, pp.41-54, Porto Alegre, Brazil.
- Sartori, P. (1978). Petrologia do Complexo Granítico São Sepé, RS. Ph.D. thesis, São Paulo University, 195 p.
- Sartori, P. & Kawashita, K. (1985). Petrologia e geocronologia do Batólito Granítico de Caçapava do Sul, RS. 2 *Simpósio Sul-Brasileiro de Geologia*, Vol. 1, pp. 102-115.
- Silva Fº, W.; Fragoso-Cesar, A. R.; Machado, R.; Sayeg, H.; Fambrini, G. & Ribeiro de Almeida, T. (1996). O magmatismo Rodeio velho e a Formação Guaritas no eopaleozóico do Rio Grande do Sul: Uma revisão (ext. abst.). 39 *Congresso Brasileiro de Geologia*, Vol. 5, pp. 433-435, Salvador, Brazil.
- Simon, E; Jackson, S.; Pearson A.; Griffina W.; Belousova E. (2004). The application of laser ablation-inductively coupled plasma-mass spectrometry to in situ U-Pb zircon geochronology. *Chemical Geology*, Vol. 211, pp. 47-69, ISSN 0009-2541.
- Soliani Jr., E.; Koester, E. & Fernandes, L. (2000). Geologia isotópica do Escudo Sul-rio-grandense, parte II: os dados isotópicos e interpretações petrogenéticas. *Geologia do Rio Grande do Sul*, Holz, M. & De Ros, L.F. (Eds.), 175-230, Universidade Federal do Rio Grande do Sul, Porto Alegre, Brazil.
- Soliani Jr., E.; Fragoso-Cesar, A. R.; Teixeira, W. & Kawashita, K. (1984). Panorama geocronológico da porção meridional do Escudo Atlântico. 33 *Congresso Brasileiro de Geologia*, Vol. 5, pp. 2435-2449.
- Sommer, C.; Lima, E.; Nardi, L.; Figueiredo, A. & Pierosan, R. (2005). Potassic and low- and high-Ti mildly alkaline volcanism in the Neoproterozoic Ramada Plateau, southernmost Brazil. *Journal of South American Earth Sciences*, Vol.18, Nº3, pp.237-254, ISSN 0895-9811.

- Sommer, C.; Lima, E.; Nardi, L. (2000) . Evolução Do Vulcanismo Alcalino da Porção Sul do Platô do Taquarembó, Dom Pedrito, RS. *Revista Brasileira de Geociências*, Vol. 29, Nº 2, pp. 245-254, ISSN 0375-7536.
- Stacey, J.S., Kramers, J.D., 1975. Approximation of terrestrial lead isotope evolution by a two-stage model. *Earth and Planetary Science Letters* 26 207-221.
- Sun, S. & McDonough, W. (1989). Chemical and isotopic systematics of oceanic basalts: implications for mantle composition and process. In: *Magnetism in the ocean basins. Geological Society, Special Publication*, Vol.42, pp.313-345, ISSN 0305-8749.
- Takehara, L.; Babinski, M.; Toniolo, J.; Chemale Jr., F.; Borba, M. & Guadagnin, F. (2010). Pb-Pb isotope signature of Cu deposits in the Sul-Rio-Grandense Shield, *VII South American Symposium on Isotope Geology*, pp 441-444.
- Teixeira, W. (1982). Folhas SH.22-Porto Alegre, SI.22-Lagoa Mirim e SH.21-Uruguaiana: interpretação dos dados radiométricos e evolução geocronológica. Projeto RADAMBRASIL, Florianópolis, Brazil.
- Wernick, E.; Hasui, Y. & Brito Neves, B. (1978). As regiões de dobramentos nordeste e sudeste (ext. abst.). *Congresso Brasileiro de Geologia*, Vol. 6, pp. 2493-2506.
- Wildner, W.; Lima, E.; Nardi, L. & Sommer, C. (2002). Volcanic cycles and setting in the Neoproterozoic III to Ordovician Camaquã Basin succession in southern Brazil: characteristic of post-collisional magmatism. *Journal of Volcanic and Geothermal Research*, Vol.118, pp.261-283, ISSN 0377-0273.
- Wildner W. & Nardi, L. (1999). Características geoquímicas e petrogenéticas do vulcanismo neoproterozóico do sul do Brasil - Platô do Taquarembó - RS. In: 1 *Simp. Vulcanismo e Ambientes Associados*, pp.30.
- Winchester, J. & Floyd, P. (1977). Geochemical discrimination of different magma series and their differentiation products using immobile elements. *Chemical Geology*, Vol. 20, pp. 325-343, ISSN 0009-2541.
- Wood, D. (1980). The application of a Th-Hf-Ta diagram to problems of tectonomagmatic classification and to establishing the nature of crustal contamination of basaltic lavas of the British Tertiary volcanic province. *Earth and Planetary Science Letters*, Vol. 50, pp.11-30, ISSN 0084-6597.
- Zerfass, H. & Almeida, D. del P. (1997). Mapa geológico da região dos cerros Bugio e Perau, Município de Caçapava do Sul, RS. *Acta Geologica Leopoldensia*, Série Mapas 3, Vol. XX, Nº3, pp.1-15, ISSN 0102-1249.
- Zerfass, H.; Almeida, D. del P. & Gomes, C. (2000). Faciologia of the Acampamento Velho Formation volcanic rocks (Camaquã Basin) in the region of Serra de Santa Bárbara, Cerro do Perau and Cerro do Bugio (Municipality of Caçapava do Sul - RS). *Revista Brasileira de Geociências*, Vol.30, No3, pp.375-379, ISSN 0375-7536.
- Zerfass, H.; Almeida, D. del P. & Petry, K. (2001). Mapa Geológico da Serra de Santa Bárbara, Caçapava do Sul (RS): uma contribuição ao conhecimento da Bacia do Camaquã. *Acta Geologica Leopoldensia*, Série Mapas 5, Vol. XXIV, Nº5, pp.3-16, ISSN 0102-1249.
- Zindler, A. & Hart, S. (1986). Chemical geodynamics. *Earth Planetary Science Letter*, Vol.14, pp.493-571, ISSN 0084-6597.



Petrology - New Perspectives and Applications

Edited by Prof. Ali Al-Juboury

ISBN 978-953-307-800-7

Hard cover, 224 pages

Publisher InTech

Published online 13, January, 2012

Published in print edition January, 2012

Petrology, New Perspectives and Applications is designed for advanced graduate courses and professionals in petrology. The book includes eight chapters that are focused on the recent advances and application of modern petrologic and geochemical methods for the understanding of igneous, metamorphic and even sedimentary rocks. Research studies contained in this volume provide an overview of application of modern petrologic techniques to rocks of diverse origins. They reflect a wide variety of settings (from South America to the Far East, and from Africa to Central Asia) as well as ages ranging from late Precambrian to late Cenozoic, with several on Mesozoic/Cenozoic volcanism.

How to reference

In order to correctly reference this scholarly work, feel free to copy and paste the following:

Delia del Pilar Montecinos de Almeida, Farid Chemale Jr. and Adriane Machado (2012). Late to Post-Orogenic Brasiliano-Pan-African Volcano-Sedimentary Basins in the Dom Feliciano Belt, Southernmost Brazil, *Petrology - New Perspectives and Applications*, Prof. Ali Al-Juboury (Ed.), ISBN: 978-953-307-800-7, InTech, Available from: <http://www.intechopen.com/books/petrology-new-perspectives-and-applications/late-to-post-orogenic-brasiliano-pan-african-volcano-sedimentary-basins-in-the-dom-feliciano-belt-so>

INTECH
open science | open minds

InTech Europe

University Campus STeP Ri
Slavka Krautzeka 83/A
51000 Rijeka, Croatia
Phone: +385 (51) 770 447
Fax: +385 (51) 686 166
www.intechopen.com

InTech China

Unit 405, Office Block, Hotel Equatorial Shanghai
No.65, Yan An Road (West), Shanghai, 200040, China
中国上海市延安西路65号上海国际贵都大饭店办公楼405单元
Phone: +86-21-62489820
Fax: +86-21-62489821

© 2012 The Author(s). Licensee IntechOpen. This is an open access article distributed under the terms of the [Creative Commons Attribution 3.0 License](#), which permits unrestricted use, distribution, and reproduction in any medium, provided the original work is properly cited.

IntechOpen

IntechOpen